

Invited review

Cretaceous sea-surface temperature evolution: Constraints from TEX₈₆ and planktonic foraminiferal oxygen isotopes

Charlotte L. O'Brien^{a,*,1}, Stuart A. Robinson^a, Richard D. Pancost^{b,c}, Jaap S. Sinninghe Damsté^{d,e}, Stefan Schouten^{d,e}, Daniel J. Lunt^{c,f}, Heiko Alsenz^g, André Bornemann^{h,i,2}, Cinzia Bottini^j, Simon C. Brassell^k, Alexander Farnsworth^{c,f}, Astrid Forster^d, Brian T. Huber^l, Gordon N. Inglis^{b,c}, Hugh C. Jenkyns^a, Christian Linnert^{m,3}, Kate Littler^{m,4}, Paul Markwickⁿ, Alison McAnena^{o,5}, Jörg Mutterlose^p, B. David A. Naafs^{b,c}, Wilhelm Püttmann^g, Appy Sluijs^e, Niels A.G.M. van Helmond^e, Johan Vellekoop^{e,6}, Thomas Wagner^{o,7}, Neil E. Wrobelⁿ

^a Department of Earth Sciences, University of Oxford, South Parks Road, Oxford, OX1 3AN, United Kingdom

^b Organic Geochemistry Unit, School of Chemistry, University of Bristol, Cantock's Close, Bristol, BS8 1TS, United Kingdom

^c Cabot Institute, University of Bristol, Bristol, BS8 1UJ, United Kingdom

^d NIOZ Royal Netherlands Institute of Sea Research, Department of Marine Microbiology and Biogeochemistry and Utrecht University, 1790 AB Den Burg, Texel, The Netherlands

^e Department of Earth Sciences, Faculty of Geosciences, Utrecht University, Budapestlaan 4, 3584 CD Utrecht, Netherlands

^f BRIDGE, School of Geographical Sciences, University of Bristol, University Road, Bristol BS8 1SS, United Kingdom

^g Institute of Atmospheric and Environmental Sciences, Department of Environmental Analytical Chemistry, Goethe-University, Altenhöferallee 1, 60438 Frankfurt am Main, Germany

^h Scripps Institution of Oceanography, University of California, San Diego, Geosciences Research Division, 9500 Gilman Drive, La Jolla, CA 92093–0244, United States

ⁱ Institut für Geophysik und Geologie, Universität Leipzig, Talstraße 35, D-04103 Leipzig, Germany

^j Department of Earth Sciences, Università degli Studi di Milano, 20133 Milan, Italy

^k Department of Geological Sciences, Indiana University, 1001 East 10th Street, Bloomington, IN 47405-1405, United States

^l Smithsonian National Museum of Natural History, Washington, DC, United States

^m Department of Earth Sciences, University College London, London WC1E 6BT, United Kingdom

ⁿ Getech Plc, Leeds LS8 2LJ, United Kingdom

^o School of Civil Engineering and Geosciences, Newcastle University, Newcastle Upon Tyne NE1 7RU, United Kingdom

^p Institut für Geologie, Mineralogie und Geophysik, Ruhr-Universität Bochum, 44801 Bochum, Germany

ARTICLE INFO

Keywords:

Cretaceous
Sea-surface temperatures
Glycerol dialkyl glycerol tetraethers
TEX₈₆
Organic geochemistry
 $\delta^{18}\text{O}$
Planktonic foraminifera
Geochemical proxies
Palaeoclimate
Greenhouse climate

ABSTRACT

It is well established that greenhouse conditions prevailed during the Cretaceous Period (~145–66 Ma). Determining the exact nature of the greenhouse-gas forcing, climatic warming and climate sensitivity remains, however, an active topic of research. Quantitative and qualitative geochemical and palaeontological proxies provide valuable observational constraints on Cretaceous climate. In particular, reconstructions of Cretaceous sea-surface temperatures (SSTs) have been revolutionised firstly by the recognition that clay-rich sequences can host exceptionally preserved planktonic foraminifera allowing for reliable oxygen-isotope analyses and, secondly by the development of the organic palaeothermometer TEX₈₆, based on the distribution of marine archaeal membrane lipids. Here we provide a new compilation and synthesis of available planktonic foraminiferal $\delta^{18}\text{O}$ ($\delta^{18}\text{O}_{\text{pl}}$) and TEX₈₆-SST proxy data for almost the entire Cretaceous Period. The compilation uses SSTs recalculated from published raw data, allowing examination of the sensitivity of each proxy to the calculation method (e.g., choice of calibration) and places all data on a common timescale. Overall, the compilation shows

* Corresponding author.

E-mail address: charlotte.obrien@yale.edu (C.L. O'Brien).

¹ Present address: Department of Geology and Geophysics, Yale University, New Haven, CT 06520, United States of America.

² Present address: Bundesanstalt für Geowissenschaften und Rohstoffe (Federal Institute of Geosciences and Natural Resources), Stillweg 2, D-30655 Hannover, Germany.

³ Present address: Institut für Geologie, Mineralogie und Geophysik, Ruhr-Universität Bochum, 44801 Bochum, Germany.

⁴ Present address: Camborne School of Mines, University of Exeter, Penryn Campus, Cornwall TR10 9FE, United Kingdom.

⁵ Present address: ICE Publishing, Institution of Civil Engineers, One Great George Street, London SW1P 3AA, United Kingdom.

⁶ Present address: Geo-instituut, KU Leuven, Celestijnenlaan 200E, B-3001 Leuven-Heverlee, Belgium.

⁷ Present address: Lyell Centre for Earth and Marine Science and Technology, School of Energy, Geoscience, Infrastructure and Society, Heriot-Watt University, Edinburgh EH14 4AS, United Kingdom.

many similarities with trends present in individual records of Cretaceous climate change. For example, both SST proxies and benthic foraminiferal $\delta^{18}\text{O}$ records indicate maximum warmth in the Cenomanian–Turonian interval. Our reconstruction of the evolution of latitudinal temperature gradients (low, $< \pm 30^\circ$, minus higher, $> \pm 48^\circ$, palaeolatitudes) reveals temporal changes. In the Valanginian–Aptian, the low-to-higher mid-latitudinal temperature gradient was weak (decreasing from ~ 10 – 17°C in the Valanginian, to ~ 3 – 5°C in the Aptian, based on TEX_{86} -SSTs). In the Cenomanian–Santonian, reconstructed latitudinal temperature contrasts are also small relative to modern ($< 14^\circ\text{C}$, based on low-latitude TEX_{86} and $\delta^{18}\text{O}_{\text{pl}}$ SSTs minus higher latitude $\delta^{18}\text{O}_{\text{pl}}$ SSTs, compared with $\sim 20^\circ\text{C}$ for the modern). In the mid-Campanian to end-Maastrichtian, latitudinal temperature gradients strengthened (~ 19 – 21°C , based on low-latitude TEX_{86} and $\delta^{18}\text{O}_{\text{pl}}$ SSTs minus higher latitude $\delta^{18}\text{O}_{\text{pl}}$ SSTs), with cooling occurring at low-, middle- and higher palaeolatitude sites, implying global surface-ocean cooling and/or changes in ocean heat transport in the Late Cretaceous. These reconstructed long-term trends are resilient, regardless of the choice of proxy (TEX_{86} or $\delta^{18}\text{O}_{\text{pl}}$) or calibration. This new Cretaceous SST synthesis provides an up-to-date target for modelling studies investigating the mechanics of extreme climates.

1. Introduction

1.1. Cretaceous climate

The Cretaceous Period (145–66 Ma) is widely understood to have had a warm-hot, greenhouse climate (e.g., Huber et al., 2002; Littler et al., 2011; Friedrich et al., 2012), characterized by weak latitudinal temperature gradients (e.g., Barron, 1983; Huber et al., 1995; Littler et al., 2011) and relatively high atmospheric CO_2 concentrations (Freeman and Hayes, 1992; Bice and Norris, 2002; Bice et al., 2006; Sinninghe Damsté et al., 2008; Barclay et al., 2010; Wang et al., 2014). This climatic warmth is qualitatively evidenced by the presence of thermophilic floras and faunas at high latitudes in the Cretaceous (Nathorst, 1890; Frakes et al., 1992; Francis and Frakes, 1993; Tarduno et al., 1998). Concurrently, eustatic sea level during the Cretaceous was on average 75–250 m higher than present-day mean sea level (Miller et al., 2005; Haq, 2014) and there was an absence of large, quasi-permanent ice sheets (e.g., Huber et al., 2002; Miller et al., 2005; MacLeod et al., 2013), although small-scale glaciation events have been proposed for both the Early and Late Cretaceous (e.g., Bornemann et al., 2008; Price and Nunn, 2010). In general, $p\text{CO}_2$ levels are thought to have been relatively high throughout the Cretaceous (typically > 500 ppm, Wang et al., 2014, and references therein) but were generally lower in the Early Cretaceous, highest in the mid-Cretaceous (reaching ~ 1000 – 2000 ppm, Royer et al., 2012) and then declined during the Late Cretaceous (> 500 ppm) (Wang et al., 2014). Under greenhouse conditions, intermediate to deep ocean waters were warm, at times $> 20^\circ\text{C}$ (summarized in a global benthic foraminiferal oxygen-isotope ($\delta^{18}\text{O}_{\text{b}}$) compilation; Friedrich et al., 2012), while low-latitude surface waters reached temperatures $> 32^\circ\text{C}$ (Huber et al., 2002; Norris et al., 2002; Schouten et al., 2003; Bice et al., 2006; Forster et al., 2007a; Forster et al., 2007b; Bornemann et al., 2008; Littler et al., 2011). Reconstructions of terrestrial mean annual temperature (MAT) and palaeobotanical temperature estimates also indicate Cretaceous climate warmth (e.g., Herman and Spicer, 1996; Amiot et al., 2004; Poole et al., 2005). Against a background of greenhouse conditions, the Earth's climate and oceans underwent significant changes and perturbations during the Cretaceous including oceanic anoxic events (OAEs; Schlanger and Jenkyns, 1976; Schlanger et al., 1987; Wilson and Norris, 2001; Jenkyns, 2010; Jenkyns et al., 2017) and oceanic gateway reorganisation (e.g., opening of the Equatorial Atlantic Gateway; Wagner and Pletsch, 1999; Friedrich and Erbacher, 2006), with substantial consequences for ocean circulation (e.g., Poulsen et al., 2003; Robinson and Vance, 2012; Jung et al., 2013; Murphy and Thomas, 2013; Voigt et al., 2013).

Understanding global temperatures in the Cretaceous, both in terms of absolute magnitude and spatial and temporal variation, is vital to elucidating the exact nature of greenhouse-gas forcing, climate sensitivity and ocean circulation at this time (e.g., Friedrich et al., 2012; PALEOSENS Project Members, 2012; Royer et al., 2012; Wang et al.,

2014). Terrestrial MAT estimates from, for example, plant macrofossils, palynomorphs and $\delta^{18}\text{O}$ of vertebrate tooth enamel (e.g., Askin, 1989; Wolf, 1990; Herman and Spicer, 1996; Amiot et al., 2004; Poole et al., 2005; Upchurch et al., 2015), provide important constraints on temperatures of continental interiors and high palaeolatitudes and in some cases information on seasonality (e.g., Herman and Spicer, 1996; Poole et al., 2005). In the marine realm, Cretaceous ocean sediments are host to valuable palaeotemperature proxy archives, offering considerable spatial and temporal coverage. Recent $\delta^{18}\text{O}_{\text{b}}$ compilations (e.g., Cramer et al., 2009; Friedrich et al., 2012) have provided important insights into the evolution of intermediate to deep-ocean temperature conditions, often assumed to reflect variations in global temperature, during the middle to Late Cretaceous. However, intermediate to deep-water temperature trends can differ between ocean basins depending on the influences of source waters with different temperatures, such that the relationship between surface and benthic temperatures depends on ocean circulation. Upper mixed-layer temperatures can provide more precise constraints on climate because of the direct contact between the atmosphere and the surface ocean. Thus, estimating the global evolution of Cretaceous sea surface temperature remains a prime objective of palaeoclimate research.

1.2. Cretaceous surface-ocean palaeotemperature proxies: planktonic $\delta^{18}\text{O}$ and TEX_{86}

Much of our understanding of Cretaceous surface-ocean temperatures comes from either calcitic (planktonic foraminifera) or organic (marine Thaumarchaeota) fossil remains in sediments. Planktonic foraminiferal oxygen-isotope ($\delta^{18}\text{O}_{\text{pl}}$) palaeothermometry is the conventional tool for reconstructing Cretaceous surface-ocean temperatures, providing information on calcification (growth) temperature when the $\delta^{18}\text{O}$ composition of seawater ($\delta^{18}\text{O}_{\text{sw}}$) can be independently estimated. More recently, the TEX_{86} (TetraEther index of tetraethers composed of 86 carbon atoms) temperature proxy has been widely applied in Cretaceous settings (e.g., Schouten et al., 2003; Jenkyns et al., 2004; Dumitrescu et al., 2006; Forster et al., 2007a; Littler et al., 2011; Jenkyns et al., 2012; Alsenz et al., 2013; McAnena et al., 2013; Linnert et al., 2014). The TEX_{86} proxy is based on the distribution of isoprenoidal glycerol dialkyl glycerol tetraether lipids (isoGDGTs; Schouten et al., 2002; Kim et al., 2010), which in open-marine settings appear to predominantly be derived from pelagic Thaumarchaeota. These archaeal isoGDGT lipids vary in structure, containing 0–4 cyclopentane moieties. Thaumarchaeota also produce crenarchaeol, which contains 4 cyclopentane moieties and an additional cyclohexane moiety, as well as a regioisomer (crenarchaeol'). The number of cyclopentane moieties has been found to increase with growth temperature (Schouten et al., 2002; Wuchter et al., 2004; Schouten et al., 2007), enabling isoGDGT-derived estimates of sea-surface temperature (SST).

Both $\delta^{18}\text{O}_{\text{pl}}$ palaeothermometry and the TEX_{86} palaeothermometer can provide estimates of SST, but each technique is subject to several

proxy-specific caveats (see Sections 3.2 and 3.4 for detailed discussion). For example, $\delta^{18}\text{O}_{\text{pl}}$ values can be compromised by preservation and/or diagenetic alteration (e.g., Schrag et al., 1995; Pearson et al., 2001), the carbonate ion effect (e.g., Spero et al., 1997; Zeebe, 2001), and

uncertainties related to the $\delta^{18}\text{O}$ of seawater in which the foraminifer calcified (e.g., Poulsen et al., 1999; Zhou et al., 2008). Indeed, earlier research using $\delta^{18}\text{O}_{\text{pl}}$ values to reconstruct Cretaceous surface-ocean conditions suggested that tropical SSTs were similar or cooler than

Table 1

Sites from which Cretaceous raw GDGT data/TEX₈₆ indices were compiled.

Site	Location	Palaeolatitude	Reference	Lab
DSDP 249	Mozambique Ridge	50.9°S (Barr.) 51.7°S (Haut.) 53.9°S (Val.) 59.1°S (Berr.)	Littler et al. (2011)	University College London
DSDP 367	Cape Verde Basin	8.6°N (Cen.)	Forster et al. (2007b) Schouten et al. (2003)	NIOZ NIOZ
DSDP 398	Proto-North Atlantic	33.5°N (Apt.)	Naafs and Pancost (2016)	University of Bristol
DSDP 463	Mid-Pacific Mountains	17.2°S (Apt.)	Schouten et al. (2003)	NIOZ
DSDP 511	Falkland Plateau	49.1°S (Apt.) 49.6°S (Barr.)	Jenkyns et al. (2012)	NIOZ
DSDP 534	Blake-Bahama Basin	23.4°N (Barr.) 21.5°N (Haut.) 18.8°N (Val.) 10.9°N (Berr.)	Littler et al. (2011)	University College London
DSDP 545	Mazagan Plateau	24.7°N (Alb.) 25.8°N (Apt.)	Hofmann et al. (2008) Wagner et al. (2008) McAnena et al. (2013)	NIOZ NIOZ Newcastle University
DSDP 603B	Eastern North American continental margin	27.1°N (Haut.) 15.0°N (Val.)	Littler et al. (2011)	University College London
ODP 692B	Weddell Sea	54.4°S (Barr.) 52.6°S (Haut.) 54.6°S (Val.) 59.9°S (Berr.)	Littler et al. (2011)	University College London
ODP 693A	Weddell Sea	62.5°S (Alb.) 56.3°S (Apt.)	Jenkyns et al. (2012)	NIOZ
ODP 766	Exmouth Plateau	51.1°S (Barr.) 53.3°S (Haut.) 51.9°S (Val.)	Littler et al. (2011)	University College London
ODP 1049	Blake Nose Plateau	30.0°N (Apt.)	Schouten et al. (2003) Wagner et al. (2008)	NIOZ
ODP 1207	Shatsky Rise	2.6°S (Apt.)	Dumitrescu et al. (2006)	NIOZ
ODP 1258	Demerara Rise	5.4°N (Tur.) 5.4°N (Cen.) 8.2°N (Alb.)	Forster et al. (2007a)	NIOZ
ODP 1259	Demerara Rise	5.7°N (Sant.) 5.6°N (Con.) 5.5°N (Tur.)	Bornemann et al. (2008) Forster et al. (2007a)	NIOZ
ODP 1260	Demerara Rise	5.5°N (Tur.) 5.5°N (Cen.)	Forster et al. (2007b)	NIOZ
ODP 1276	Newfoundland Basin	38.9°N (Tur.) 38.4°N (Cen.)	Sinninghe Damsté et al. (2010)	NIOZ
FL533	Arctic Ocean	80.4°N (Maas.) 80.6°N (Camp.)	Jenkyns et al. (2004)	NIOZ
A39 outcrop	Northwest Germany	40.6°N (Apt.) 39.1°N (Barr.)	Mutterlose et al. (2010)	NIOZ
Gott outcrop	Northwest Germany	39.1°N (Barr.)	Mutterlose et al. (2010)	NIOZ
Moorberg outcrop	Northwest Germany	39.1°N (Barr.) 36.2°N (Haut.)	Mutterlose et al. (2012)	NIOZ
Speeton outcrop	Northeast England	38.2°N (Haut.)	Mutterlose et al. (2012)	NIOZ
Alstätte 1 outcrop	Northwest Germany	40.6°N (Apt.) 38.9°N (Barr.)	Mutterlose et al. (2014)	NIOZ
Cismon core	Italian Southern Alps	24.7°N (Apt.)	Bottini et al. (2015)	NIOZ
Aderet borehole 1	Israel	18.9°N (Maas.) 17.6°N (Camp.)	Alsenz et al. (2013)	Goethe-University
PAMA Quarry outcrop	Israel	18.9°N (Maas.) 17.6°N (Camp.)	Alsenz et al. (2013)	Goethe-University
Shuqalak-Evans borehole	Mississippi, USA	36.2°N (Maas.) 34.9°N (Camp.)	Linnert et al. (2014)	University College London
Bass River borehole, ODP Leg 174AX	New Jersey Shelf, USA	36.5°N (Tur.) 35.7°N (Cen.)	van Helmond et al. (2014)	NIOZ
Brazos River 1 section	Texas, USA	36.3°N (Maas.)	Vellekoop et al. (2014)	Utrecht University
Meirs Farm 1	New Jersey, USA	40.2°N (Maas.)	Vellekoop et al. (2016)	Utrecht University
Wunstorf core	Lower Saxony Basin, northern Germany	47.6°N (Tur.) 47.5°N (Cen.)	van Helmond et al. (2015)	Utrecht University

ODP = Ocean Drilling Program; DSDP = Deep Sea Drilling Project; NIOZ = The Netherlands Institute of Ocean Science; Apt. = Aptian; Camp. = Campanian; Maas. = Maastrichtian; Cen. = Cenomanian; Tur. = Turonian; Berr. = Berriasian; Barr. = Barremian; Con. = Coniacian. Estimates of palaeolatitude are derived using a palaeorotational model provided by Gedge Plc. N.B., University College London laboratory now moved to University of Oxford.

modern tropical ocean conditions (the cool tropics paradox; Sellwood et al., 1994; D'Hondt and Arthur, 1996) even though $\delta^{18}\text{O}_{\text{pl}}$ values from polar regions indicated sub-tropical-like SSTs. It has since been demonstrated that these inferred cool tropical temperatures reflect biased $\delta^{18}\text{O}_{\text{pl}}$ values derived from diagenetically altered, cool-biased planktonic foraminifera (Schrage et al., 1995; Pearson et al., 2001), indicating the importance of selecting only well-preserved foraminifera, i.e. “glassy” foraminifera found in clay-rich sediments. This realization essentially eliminated all published $\delta^{18}\text{O}_{\text{pl}}$ data from carbonate-rich deep ocean settings as reliable indicators for SST.

For the TEX_{86} proxy, the exact mechanism(s) that relates sedimentary GDGT distributions to those produced by Thaumarchaeota in surface waters and therefore to SSTs are not fully understood (Pearson and Ingalls, 2013; Schouten et al., 2013b; Taylor et al., 2013; Tierney, 2014). For example, recent work has suggested that non-temperature factors such as oxygen concentration (Qin et al., 2015), growth phase (Elling et al., 2014), ammonium oxidation rate (Hurley et al., 2016) and other physiological, environmental, and ecological factors (Elling et al., 2015) may play an important role in governing GDGT distributions. Moreover, other factors will govern how the signal generated in surface waters is preferentially exported to sediments, with some work suggesting that TEX_{86} ratios are in fact an integrated signal from the surface and shallow-subsurface (0 to ~250 m; Wakeham et al., 2003; Wuchter et al., 2005; Taylor et al., 2013; Hernández-Sánchez et al., 2014). Recent work has suggested that the TEX_{86} signal is predominantly exported from deeper waters (Ho and Laepple, 2016). However, this assumption is likely flawed because it does not recognize

modern mechanistic studies on TEX_{86} -SST sensitivity and fails to predict SSTs in shallow settings (Tierney et al., 2017).

For both $\delta^{18}\text{O}_{\text{pl}}$ and TEX_{86} palaeothermometry, a number of different calibrations exist for converting proxy data values to estimates of SST (e.g., Erez and Luz, 1983; Bemis et al., 1998). Consequently not all published absolute estimates of Cretaceous SSTs for a given proxy are directly comparable. Furthermore, since publication of earlier Cretaceous TEX_{86} data, constraints on the application of the proxy have appeared, e.g., the Branched and Isoprenoid Tetraether (BIT) index (Hopmans et al., 2004). Hence, data rejection criteria have changed over time (see later discussion, Section 2.1.3). Aside from temperature proxy developments, the most recent Cretaceous time scale has undergone revisions since the publication of several datasets (Gradstein et al., 2004; Gradstein et al., 2012). Thus, given the current body of Cretaceous $\delta^{18}\text{O}_{\text{pl}}$ and TEX_{86} data, it is timely to re-evaluate critically all currently available Cretaceous SST data derived from both of these techniques, assessing their quality as well as their ages. Here we present a global SST compilation for the Cretaceous Period in order to provide new constraints on long-term SST evolution and uncertainty, and to provide a target for modelling studies.

2. Methods

2.1. Data compilation

Original published marine palaeotemperature proxy data, raw GDGT data and planktonic $\delta^{18}\text{O}$ data, were collated from all available

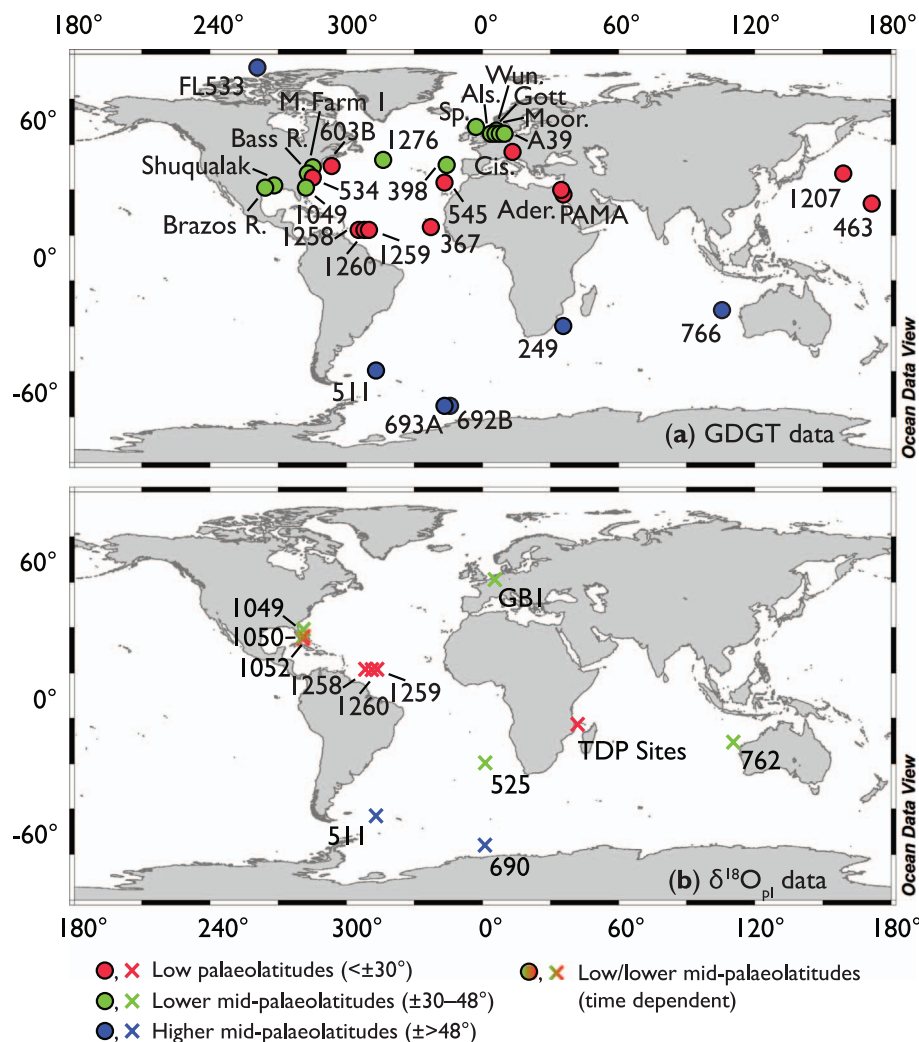


Fig. 1. Map showing the modern-day locations of sites with published Cretaceous (a) GDGT data and (b) planktonic $\delta^{18}\text{O}$ data compiled in this paper. Sites are colour-coded by approximate Cretaceous palaeolatitude, estimated using a palaeorotational model provided by Getech Plc. Abbreviations: Bass R. = Bass River; Brazos R. = Brazos River; Sp. = Speeton; Als. = Alstätte; Moor. = Moorberg; Cis. = Cismon; Ader. = Aderet 1 borehole; PAMA = PAMA Quarry; Wun. = Wunstorf core; M. Farm 1 = Meirs Farm 1. (For interpretation of the references to colour in this figure legend, the reader is referred to the web version of this article.)

locations where these determinations are accepted as primarily reflecting Cretaceous SSTs, as interpreted by the original authors and in subsequent publications. We then apply additional tests to ensure that all data have had the same scrutiny and to incorporate new understanding on proxy biases. While $\delta^{18}\text{O}_{\text{pl}}$ data are reported relative to an international standard, Vienna Pee Dee Belemnite (VPDB), indicating that it is valid to compare data produced in different laboratories, no such standard currently exists for the TEX_{86} proxy. The most recent TEX_{86} inter-laboratory comparison study (Schouten et al., 2013a) of variations in measured TEX_{86} values across different laboratories indicated a range of 0.023–0.053 (equivalent to 1.5–3.5 °C in the TEX_{86} -SST calibration of Schouten et al., 2002), which should be considered when comparing different records generated in different laboratories. However, this variation is typically less than the errors in the temperature calibrations (2.5 to 4.0 °C; Kim et al., 2010) and additionally, ~55% of the GDGT data presented here were generated in one laboratory, namely at the Royal Netherlands Institute for Sea Research (NIOZ; Table 1). For comparison intra-laboratory precision (repeatability) is typically < 1 °C for TEX_{86} (Schouten et al., 2013a) and < 0.08‰ for $\delta^{18}\text{O}_{\text{pl}}$, equivalent to < 0.4 °C (Ravelo and Hillaire-Marcel, 2007).

2.1.1. Compilation of raw GDGT data

Fractional abundances of isoprenoid GDGTs (see structures given in Supplementary Fig. 1) were compiled for locations where published TEX_{86} palaeotemperature proxy data have been generated from Cretaceous sediments. Where possible, we compute and report the fractional abundance of all individual GDGTs. For some datasets, original raw GDGT data were unavailable, and for these locations we rely solely on published TEX_{86} values. In addition, where available, Branched and Isoprenoid Tetraether (BIT) indices, a proxy for input of soil-derived organic matter (Hopmans et al., 2004; Weijers et al., 2006), were either collected or determined (see below). Locations of Cretaceous sediments for which raw GDGT data/ TEX_{86} indices were obtained are shown in Fig. 1a; data references are given in Table 1.

2.1.2. GDGT-based SST indices: TEX_{86} , $\text{TEX}_{86}^{\text{H}}$, and BAYSPAR

We calculate TEX_{86} values using the original definition of Schouten et al. (2002):

$$\text{TEX}_{86} = \frac{[\text{GDGT-2}] + [\text{GDGT-3}] + [\text{Cren}']}{[\text{GDGT-1}] + [\text{GDGT-2}] + [\text{GDGT-3}] + [\text{Cren}']} \quad (1)$$

where GDGT-1, GDGT-2, GDGT-3 and Cren' refer to the structures shown in Supplementary Fig. 1. Several global core-top based calibrations exist for converting TEX_{86} estimates to SSTs. Originally the TEX_{86} -SST relationship was described using a linear calibration (Schouten et al., 2002; Kim et al., 2008). Subsequently, a $1/\text{TEX}_{86}$ expression (Liu et al., 2009) and then a logarithmic relationship (Kim et al., 2010) were applied to better fit the TEX_{86} -SST relationship. Kim et al. (2010) provided two logarithmic calibrations, $\text{TEX}_{86}^{\text{H}}$ and $\text{TEX}_{86}^{\text{L}}$, with the former recommended for reconstructing SSTs > 15 °C, such as those characteristic of the Cretaceous Period. More recently, a Bayesian model approach has been developed to predict SSTs from TEX_{86} values, BAYSPAR (Tierney and Tingley, 2014; Tierney and Tingley, 2015). Motivation for this model arose from observations that the TEX_{86} -temperature relationship appears to vary for different ocean regions and environments (e.g., Trommer et al., 2009; Ho et al., 2014) and that previous calibration models feature structured residuals indicating strong spatially varying trends in the response of TEX_{86} to temperature (Tierney and Tingley, 2014). BAYSPAR model SST predictions are derived using an online graphical use interface (GUI; www.who.edu/bayspar) or directly via the corresponding MatLab code (Tierney, 2014; Tierney and Tingley, 2015). For pre-Quaternary applications, the BAYSPAR model searches modern core-top data (including data from the Red Sea) for TEX_{86} values that are similar to the measured TEX_{86} values in a given dataset and derives linear-regression parameters from

these modern 'analogues'. This analogue approach is not geographically dependent (unlike the Quaternary BAYSPAR approach) and relies only on the assumption that it is reasonable to compare modern and ancient TEX_{86} values, which is little different to assumptions incorporated in traditional TEX_{86} -temperature calibrations (Tierney and Tingley, 2014). Another feature of the BAYSPAR approach versus traditional TEX_{86} -temperature regression models is that the BAYSPAR model fully propagates uncertainties in the core-top data into resulting temperature predictions (Tierney and Tingley, 2014). In addition to TEX_{86} -SST calibrations, there are now TEX_{86} calibrations for deriving shallow subsurface temperatures, 0–200 m water depth, in certain settings (e.g., Kim et al., 2015; Tierney and Tingley, 2015).

Regardless of the choice of TEX_{86} -SST calibration, application of the TEX_{86} proxy in the Cretaceous Period, where TEX_{86} values are frequently high (> 0.8), requires extrapolation of TEX_{86} -SST calibrations above the upper limit of the modern range reflected in the core-top datasets, ~0.72 (excluding data from the Red Sea; Kim et al., 2008; Kim et al., 2010). Thaumarchaeota mesocosm studies at high temperature, 30–46 °C (e.g., Wuchter et al., 2004; Schouten et al., 2007; Pitcher et al., 2010) provide support for extrapolation of temperatures above the modern calibration datasets, but do not yield an alternative calibration due to an unusually low abundance of the crenarchaeol regio-isomer. However, Pitcher et al. (2010) record a TEX_{86} value of 0.99 at an incubation temperature of 46 °C for a Thaumarchaeote suggesting an upper limit for the maximum SST estimate the TEX_{86} proxy can yield.

Depending on the TEX_{86} -SST relationship, different core-top-derived calibrations produce a different maximum SST estimate; for the $1/\text{TEX}_{86}$ calibration (Liu et al., 2009), a linear calibration (Kim et al., 2008) and the $\text{TEX}_{86}^{\text{H}}$ calibration (Kim et al., 2010) the maximum SSTs that can be computed, i.e. when $\text{TEX}_{86} = 1$, are 34.1 °C, 45.4 °C and 38.6 °C, respectively. For the BAYSPAR model, the nature of the regression is dependent on the core-top analogues selected, as such the corresponding SST estimate when $\text{TEX}_{86} = 1$ is not fixed. The maximum computable TEX_{86} -SST estimate derived using the $1/\text{TEX}_{86}$ calibration of Liu et al. (2009) is significantly lower than for the other calibrations discussed here and is least consistent with other evidence of greenhouse conditions where maximum SSTs may well have been higher than this limit. As such, we herein convert TEX_{86} values to SSTs using three calibrations: (1) the $\text{TEX}_{86}^{\text{H}}$ calibration and (2) a new TEX_{86} -Linear calibration, both based on the global core-top dataset (see below; Kim et al., 2010), and (3) a BAYSPAR model approach (Tierney and Tingley, 2014; Tierney and Tingley, 2015).

$\text{TEX}_{86}^{\text{H}}$ -derived SSTs were computed using the temperature equations of Kim et al. (2010). Similar to the original TEX_{86} relationship (Schouten et al., 2002), $\text{TEX}_{86}^{\text{H}}$ is calculated from the fractional abundances of GDGT-1, GDGT-2, GDGT-3 and the regio-isomer of crenarchaeol, Cren', and is defined as:

$$\text{TEX}_{86}^{\text{H}} = \log(\text{TEX}_{86}) \quad (2)$$

$\text{TEX}_{86}^{\text{H}}$ is correlated to SST using a global core-top calibration (Kim et al., 2010) that excludes data from the (sub)polar oceans and the Red Sea:

$$\text{TEX}_{86}^{\text{H}}\text{-derived SST (°C)} = 68.4 \times (\text{TEX}_{86}^{\text{H}}) + 38.6; (\text{calibration error } \pm 2.5^\circ\text{C}) \quad (3)$$

For comparison, we generated a modified version of the linear TEX_{86} -SST calibration presented in Kim et al. (2010), designed for application in warm Cretaceous climates (Supplementary Fig. 2):

$$\text{TEX}_{86}\text{-linear} = 0.017 \times \text{SST} + 0.19; (\text{calibration error: } \pm 2.0^\circ\text{C}) \quad (4)$$

A similarly derived high temperature TEX_{86} calibration for the Cretaceous was previously presented in Schouten et al. (2003). This newly modified TEX_{86} linear calibration excludes all data from the Red Sea and also all data for which satellite-derived mean annual SSTs are < 15 °C. The maximum SST that can be derived using this

calibration (when $\text{TEX}_{86} = 1$) is 42.7 °C.

We also compute Cretaceous SSTs from GDGT data using BAYSPAR (Tierney and Tingley, 2014; Tierney and Tingley, 2015). Here, we apply the default settings of the BAYSPAR “Deep-Time” model (Tierney and Tingley, 2014; Tierney and Tingley, 2015), inputting all Cretaceous TEX_{86} data into the BAYSPAR model as one whole dataset. This approach allows us to generate a single, Bayesian-derived Global Regression ($\text{BAY}_{\text{GlobR}}$) in order to predict Cretaceous SSTs, $\text{BAY}_{\text{GlobR}}\text{-SSTs}$. This single ‘global’ approach maintains the original inter-site distribution of the TEX_{86} data, avoiding potentially artificial inter-site relative shifts introduced by generating a specific regression for each dataset.

We note that we do not apply the $\text{TEX}_{86}^{\text{L}}$ calibration proposed by Kim et al. (2010). Designed for reconstructing SSTs across all temperature ranges (−3–30 °C; Kim et al., 2010), the $\text{TEX}_{86}^{\text{L}}$ calibration differs from other TEX_{86} calibrations since it only employs GDGT-1, GDGT-2 and GDGT-3, removes GDGT-3 from the numerator and excludes the crenarchaeol regio-isomer entirely; moreover, it is not mathematically related to ring number, thereby removing the inferred physiological foundation of GDGT-based temperature proxies (Schouten et al., 2002). Application of $\text{TEX}_{86}^{\text{L}}$ alongside other TEX_{86} calibrations, namely $\text{TEX}_{86}^{\text{H}}$, in the Cretaceous and Palaeogene has highlighted significant offsets between the two calibrations in a range of different settings (Taylor et al., 2013; Inglis et al., 2015), including the western proto-North Atlantic (Early Cretaceous; Littler et al., 2014), the western North Atlantic Shelf (Late Cretaceous; Linnert et al., 2014), the New Jersey Coastal Plain (Palaeocene; Taylor et al., 2013) and the southwest Pacific (middle Palaeocene to middle Eocene; Hollis et al., 2012; Bijl et al., 2013). Recent work has illustrated that it is the $\text{TEX}_{86}^{\text{L}}$ calibration that is particularly sensitive to GDGT export depth issues, due to the vertical variation of GDGT-2/GDGT-3 ratios in the water column (Hernández-Sánchez et al., 2014; Villanueva et al., 2014; Kim et al., 2015; Kim et al., 2016), rendering the calibration inaccurate (see Inglis et al., 2015). Indeed, the $\text{TEX}_{86}^{\text{L}}$ calibration can underestimate SST in some settings, e.g., in tropical Eocene settings, yielding SSTs lower than modern despite greenhouse conditions (Sluijs et al., 2014; Inglis et al., 2015) and, even in subpolar and polar regions the $\text{TEX}_{86}^{\text{L}}$ calibration does not perform substantially better than $\text{TEX}_{86}^{\text{H}}$ (Ho et al., 2014). As such, we focus on other indices and calibrations, e.g., $\text{TEX}_{86}^{\text{H}}$, $\text{TEX}_{86}^{\text{Linear}}$ and $\text{BAY}_{\text{GlobR}}$ here.

2.1.3. GDGT preservation and secondary effects

GDGT distributions can be potentially influenced by secondary, non-thermal effects including oxic degradation, thermal alteration, terrestrial inputs and methanogenesis. Diagenetic alteration of GDGT distributions related to oxic degradation of GDGTs, either in the water column or in sediments, could potentially modify primary TEX_{86} values. However, studies suggest that TEX_{86} appears to neither be significantly nor systematically influenced by degree of oxidation/diagenesis (Schouten et al., 2004; Huguet et al., 2008; Huguet et al., 2009; Kim et al., 2009; Lengger et al., 2013). Van Helmond et al. (2015) found preferential preservation of brGDGTs over isoGDGTs relative to %Total Organic Carbon in Cretaceous sediments, similar to observations from organic matter-rich turbidites affected by post-depositional oxidation (e.g., Huguet et al., 2008; Lengger et al., 2013). This preferential preservation in Cretaceous sediments was also reflected by higher BIT values when TEX_{86} values were lower (van Helmond et al., 2015), thus, in addition to identifying samples biased by inputs of terrestrially derived isoGDGTs, the BIT index (see later discussion, Section 2.1.4) may help identify samples biased by preferential preservation. Another concern is the potential for thermal alteration, particularly in older, i.e. Mesozoic sediments (e.g., Bottini et al., 2015) which can bias TEX_{86} values to cooler SST estimates (Schouten et al., 2004). However, the degree of sediment thermal maturity can be relatively straightforwardly assessed by evaluating homohopanoide isomer compositions (e.g., van Duin et al., 1997; Schouten et al., 2004). There is also some evidence for small, consistent differences in TEX_{86} from interbedded lithologies

of similar Cretaceous age (Littler et al., 2014). These sedimentary TEX_{86} offsets were interpreted to represent ecological differences in Thaumarchaeotal populations, spatial distribution or seasonality preferences, emphasizing the importance of careful sample selection (Littler et al., 2014). In addition to diagenesis and sampling biases, the primary marine TEX_{86} signal can be modified by the introduction of additional GDGTs either from terrestrial (soil-derived) sources (Weijers et al., 2006) or synthesizing sedimentary methanogenic and methanotrophic Archaea (Blaga et al., 2009; Zhang et al., 2011; Sinninghe Damsté et al., 2012). Further details and methods to identify these additional GDGT sources are described below.

2.1.4. GDGT-based indices for assessing secondary effects

To screen sedimentary GDGT distributions for potential secondary influences on TEX_{86} , we utilize a number of proposed and/or established GDGT indices: the BIT index (Hopmans et al., 2004; Weijers et al., 2006), %GDGT-0 (Blaga et al., 2009; Sinninghe Damsté et al., 2012), the Methane Index (Zhang et al., 2011), and the Ring Index (Zhang et al., 2016). We also propose a new ratio, the fraction of crenarchaeol regio-isomer to total crenarchaeol, $f_{\text{Cren}':\text{Cren}'} + \text{Cren}'$, to screen, tentatively, for ‘anomalous’ versus ‘warm’ GDGT distributions.

To examine the influence of soil-derived GDGT input on TEX_{86} values, we apply the BIT index. The ratio of branched GDGTs to crenarchaeol in marine sediments is a function of soil and riverine organic-matter input (and to a minor extent in situ production of brGDGTs also; Peterse et al., 2009), and is expressed as the BIT index (Hopmans et al., 2004):

$$\text{BIT} = \frac{([\text{I}] + [\text{II}] + [\text{III}])}{([\text{I}] + [\text{II}] + [\text{III}] + [\text{Cren}])} \quad (5)$$

where I, II, III and Cren refer to the structures shown in Supplementary Fig. 1. TEX_{86} estimates associated with BIT indices > 0.3, indicative of a potential soil-derived GDGT signal influence, should not be used for SST reconstruction (Weijers et al., 2006). However, this value may be conservative in some settings (e.g., certain Eocene sediments, Inglis et al., 2015) or overly inclusive in others (e.g., Wunstorf core, northern Germany, van Helmond et al., 2015). In addition, measured BIT values vary dramatically across different laboratories (based on findings from interlaboratory comparison studies; Schouten et al., 2009; Schouten et al., 2013a) such that a BIT threshold may be reached by one laboratory but not at another. A way to circumvent this issue is to cross-correlate each data set internally, i.e. BIT values with TEX_{86} values, as an additional control (e.g., van Helmond et al., 2015).

Sedimentary methanogenic Archaea can synthesize GDGT-0 and, in lesser quantities, GDGT-1, -2 and -3 (Koga et al., 1993; Weijers et al., 2006). To assess sedimentary GDGT production qualitatively we compute %GDGT-0 (Sinninghe Damsté et al., 2012), an expression of the contribution of sedimentary archaeal methanogen-synthesized GDGTs to the sedimentary GDGT pool:

$$\% \text{GDGT-0} = \left(\frac{[\text{GDGT-0}]}{[\text{GDGT-0}] + [\text{Cren}]} \right) * 100 \quad (6)$$

where %GDGT-0 exceeds a threshold value > 67 an additional source of GDGT-0, i.e. sedimentary GDGT production via methanogenesis, and by extension potentially also GDGT-1, -2 and -3, is implied. This threshold is based on the range of %GDGT-0 values observed in enrichment cultures of Thaumarchaeota (Blaga et al., 2009; Sinninghe Damsté et al., 2012; Elling et al., 2015).

To distinguish the relative input of methanotrophic Euryarchaeota (which produce predominantly GDGT-0, -1, -2; Pancost et al., 2001; Wakeham et al., 2003) versus ammonia-oxidizing Thaumarchaeota (Cren and Cren'; N.B. GDGT-1, -2 and -3 are also produced by non-methanotrophic marine Thaumarchaeota) and further deduce whether Cretaceous depositional conditions are characterized by anaerobic oxidation of methane (AOM) in either gas hydrates, methane-rich deep-

sea environments and/or continental shelves characterized by diffusive methane flux (Weijers et al., 2011), we apply the Methane Index (MI; Pancost et al., 2001; Wakeham et al., 2003; Blumenberg et al., 2004; Zhang et al., 2011):

$$MI = \left(\frac{[GDGT-1] + [GDGT-2] + [GDGT-3]}{[GDGT-1] + [GDGT-2] + [GDGT-3] + [Cren] + [Cren']} \right) \quad (7)$$

High MI values, > 0.5 , could reflect hydrate-impacted sediments and by extension indicate that corresponding TEX_{86} values should be excluded, whereas low values, < 0.3 , suggest no appreciable contribution from AOM Archaea to the sedimentary GDGT pool.

In the modern realm, the TEX_{86} -SST proxy has been found to deviate from the general TEX_{86} -SST relationship in certain ocean regions including the Red Sea and the Mediterranean Sea (e.g., Kim et al., 2008; Kim et al., 2010; Kim et al., 2015), suggesting additional environmental controls on the TEX_{86} proxy in these settings. TEX_{86} values recorded in Red Sea core-top sediments translate into much warmer TEX_{86}^H SSTs than measured values by up to $\sim 8^\circ\text{C}$ (Trommer et al., 2009). As a result, Kim et al. (2008, 2010) excluded GDGT data from the Red Sea in their global core-top calibration dataset. However, core-top GDGT data from the Red Sea are included in the BAYSPAR calibration dataset (Tierney and Tingley, 2014; Tierney and Tingley, 2015). Similarly, in both the Mediterranean Sea (also a restricted basin) and along the Portuguese continental margin, TEX_{86}^H values do not correlate well with annual mean SST (Kim et al., 2015; Kim et al., 2016). Kim et al. (2015) discovered a deep-water derived GDGT influence on TEX_{86}^H values recorded in Mediterranean Sea sediments, which had been previously argued to occur in various settings on the basis of GDGT-2/GDGT-3 ratios (Taylor et al., 2013). Using both surface sediments and suspended particulate matter collected at < 1000 m water depth in the Mediterranean Sea, Kim et al. (2015) found that proportions of GDGT-2 and also crenarchaeol regio-isomer increased with water depth. This phenomenon resulted in warm-biased TEX_{86}^H -temperature estimates from sub-surface derived isoGDGTs. At greater water depths, > 1000 m, surface sediment TEX_{86}^H values no longer correlate with water depth, instead exhibiting a strong relationship with annual mean SSTs (Kim et al., 2015). Similarly, Kim et al. (2016) observed a strong positive relationship between water depth and surface-sediment TEX_{86}^H values (and also suspended particulate matter TEX_{86}^H values) along the Portuguese continental margin. Phylogenetic analyses revealed that Thaumarchaeota populations identified at 1 m and 50 m water depth were different from those residing at 200 m and 1000 m water depth, leading to the suggestion that high surface-sediment TEX_{86}^H values could be due to the increasing contribution of isoGDGTs from the deep-water population of Thaumarchaeota. Together, these studies suggest (1) a water-depth control on TEX_{86}^H values – and by extrapolation, other TEX-based indices – in certain settings (Taylor et al., 2013; Kim et al., 2015; Kim et al., 2016), potentially due to the effect of deep-water Thaumarchaeotal communities on sedimentary isoGDGT distributions (Kim et al., 2016), and (2) a statistically different TEX_{86}^H -temperature correlation from the general global correlation in certain > 1000 m water-depth settings (Kim et al., 2015).

To explore anomalous GDGT distributions in Cretaceous sediments we evaluate variations in the relative abundance of the crenarchaeol regio-isomer in such deposits using a new ratio:

$$f_{Cren':Cren'+Cren} = \left(\frac{[Cren']}{[Cren] + [Cren']} \right) \quad (8)$$

Produced by non-methanotrophic marine Thaumarchaeota, a significant enhancement in the proportion of the crenarchaeol regio-isomer relative to crenarchaeol, $f_{Cren':Cren'+Cren}$, i.e. a substantial deviation from values observed in the modern core-top dataset (Kim et al., 2010) could be indicative of a non-temperature control, potentially water depth (Kim et al., 2015), on isoGDGT fractional abundances. This

ratio does not include GDGT-0, GDGT-1, or GDGT-2, which could have additional sources from methanotrophic Euryarchaeota (see earlier discussion).

We also apply the Ring Index to help distinguish samples that could have been influenced by non-thermal factors and/or deviate from modern analogues (Zhang et al., 2016). The Ring Index (RI) is a weighted average of the ring numbers in GDGT compounds:

$$RI = 0 \times \left(\frac{[GDGT-0]}{\Sigma GDGT} \right) + 1 \times \left(\frac{[GDGT-1]}{\Sigma GDGT} \right) + 2 \times \left(\frac{[GDGT-2]}{\Sigma GDGT} \right) + 3 \times \left(\frac{[GDGT-3]}{\Sigma GDGT} \right) + 4 \times \left(\frac{[Cren]}{\Sigma GDGT} \right) + 4 \times \left(\frac{[Cren']}{\Sigma GDGT} \right) \quad (9)$$

where $\Sigma GDGT = [GDGT-0] + [GDGT-1] + [GDGT-2] + [GDGT-3] + [Cren] + [Cren']$. In the modern core-top dataset, RI is significantly correlated ($R^2 = 0.87$; $n = 531$) with TEX_{86} (Zhang et al., 2016); this relationship is expressed by the following quadratic regression:

$$RI_{TEX} = -0.77(\pm 0.38) \times TEX_{86} + 3.32(\pm 0.34) \times (TEX_{86})^2 + 1.59(\pm 0.10) \quad (10)$$

The TEX_{86} -RI relationship appears insensitive to shifts in GDGT production (related to depth and/or seasonality), transportation and changes in archaeal community structure, provided that temperature remains the dominant control on GDGT distributions (Zhang et al., 2016). Zhang et al. (2016) suggest that geological samples cannot confidently be used for palaeothermometry if they deviate from the modern TEX_{86} -RI relationship:

$$\Delta RI = RI_{TEX} - RI_{sample} \quad (11)$$

ΔRI values $> |0.3|$ are thought to represent samples for which GDGT distributions reside outside the modern TEX_{86} -RI relationship, based on the 95% confidence interval (2σ) of the modern regression, reflecting properties distinct from the modern production of GDGTs (Zhang et al., 2016). Using this approach, the Ring Index can help determine samples influenced by either soil-derived isoprenoidal GDGT inputs or methanotrophic archaeal communities and identify samples with atypical GDGT distributions probably impacted by non-thermal factors, e.g., Mediterranean Sea samples from < 1000 m water depth (Kim et al., 2015; Zhang et al., 2016).

2.1.5. Compilation of raw planktonic $\delta^{18}\text{O}$ data

Original published raw planktonic $\delta^{18}\text{O}$ data were collected from locations where palaeotemperature proxy data were of sufficient number and quality (see below) to offer accurate information on Cretaceous climate. Locations of Cretaceous sediments for which raw planktonic $\delta^{18}\text{O}$ data were obtained are shown in Fig. 1b; data references are given in Table 3.

2.1.6. Conversion of planktonic $\delta^{18}\text{O}$ values to sea-surface temperature

Planktonic $\delta^{18}\text{O}$ values were converted to palaeotemperatures using the equation of Bemis et al. (1998). Similar to the TEX_{86} proxy, temperature calibrations for $\delta^{18}\text{O}_{\text{pl}}$ in modern seawater or culture studies are somewhat limited beyond a maximum of approximately 30°C (for review see Pearson, 2012). However, synthetic calcite studies (e.g., Kim and O'Neil, 1997) provide support for extrapolation of $\delta^{18}\text{O}_{\text{pl}}$ culture studies beyond 30°C , akin to SSTs indicated for the Cretaceous oceans. Assuming that foraminiferal calcite was precipitated in isotopic equilibrium with Cretaceous seawater, we use a $\delta^{18}\text{O}_{\text{sw}}$ value of -1.0‰ standard mean ocean water (VSMOW) to represent the mean isotopic composition of seawater in a non-glacial world (Shackleton and Kennett, 1975), which corresponds to a $\delta^{18}\text{O}_{\text{sw}}$ value of -1.27‰ (PDB) in the temperature equation (Hut, 1987):

$$T(^{\circ}\text{C}) = 16.5 - 4.8(\delta^{18}\text{O}_{\text{pl}} - \delta^{18}\text{O}_{\text{sw}}); \text{ calibration error: } \pm 0.7^{\circ}\text{C} \quad (12)$$

A $\delta^{18}\text{O}_{\text{sw}}$ value of -1.0‰ (VSMOW) lies within the range of more recent estimates for isotopic ice-free conditions, $-1.11 \pm 0.03\text{‰}$

(Lhomme et al., 2005) and $-0.89 \pm 0.02\text{‰}$ (Cramer et al., 2011), implying an overall range in uncertainty of $\sim 0.28\text{‰}$ equating to $\sim 1.4^\circ\text{C}$, although this figure does not account for any temporal variation during the Cretaceous, i.e. deviation from ice-free conditions. Reconstructions of Cretaceous $\delta^{18}\text{O}_{\text{sw}}$ from clumped isotope measurements on marine macrofossils indicate a $\delta^{18}\text{O}_{\text{sw}}$ value of -1.0‰ (VSMOW) in the Late Cretaceous (late Campanian–Maastrichtian, Dennis et al., 2013). For the Early Cretaceous, however, estimates of $\delta^{18}\text{O}_{\text{sw}}$ from two studies measuring clumped isotopes in belemnites suggest values of -0.1 to $+1.2\text{‰}$ (VSMOW, Bernasconi et al., 2011) and -1.1 to $+0.1\text{‰}$ (average -0.7‰), -1.8 to -0.4‰ (average -1.0‰) and -0.2 to $+0.9\text{‰}$ (average -0.4‰) for the Berriasian, early Valanginian and late Valanginian, respectively (Price and Passey, 2013). These $\delta^{18}\text{O}_{\text{sw}}$ reconstructions from clumped isotope measurements span a range of latitudes and hence $\delta^{18}\text{O}_{\text{sw}}$ values. If episodes of glaciation occurred during the Cretaceous (see later discussion, Section 4.4.3), $\delta^{18}\text{O}_{\text{sw}}$ would have been higher, leading to an underestimation of SSTs if a constant $\delta^{18}\text{O}_{\text{sw}}$ value of -1.0‰ (VSMOW) were assumed. Underestimation of SSTs during periods of ice growth would result in an overestimation of the temporal variability between glaciated and non-glaciated climate phases.

In addition, we also convert $\delta^{18}\text{O}_{\text{pl}}$ values to temperature with an added adjustment for differences in the oxygen-isotopic composition of local seawater ($\delta^{18}\text{O}_{\text{sw}}$) owing to changes in site palaeolatitude – the “salinity effect”. In the modern surface ocean, $\delta^{18}\text{O}_{\text{sw}}$ varies significantly (~ -0.5 to $+1.25\text{‰}$) because local variations in precipitation versus evaporation coupled with fractionation between water and water vapour result in an increase in $\delta^{18}\text{O}_{\text{sw}}$ and salinity with enhanced evaporation (see Pearson, 2012, for review). Average latitudinal variations in $\delta^{18}\text{O}_{\text{sw}}$ can be predicted for Cretaceous palaeolatitudes by analogy with modern oceans (Zachos et al., 1994). Adjusting Cretaceous $\delta^{18}\text{O}_{\text{pl}}$ values for differences in latitude and hence changes in precipitation versus evaporation is thought to reduce the error in Cretaceous $\delta^{18}\text{O}_{\text{pl}}$ -SST reconstructions, assuming that latitudinal variations in $\delta^{18}\text{O}_{\text{sw}}$ in the Cretaceous were not significantly different from modern. This assumption disagrees with model predictions of meridional $\delta^{18}\text{O}_{\text{sw}}$ for the mid-Cretaceous (e.g., Poulsen et al., 1999; Zhou et al., 2008). However, currently available model views of $\delta^{18}\text{O}_{\text{sw}}$ only provide information for certain time slices of the Cretaceous, e.g., the Cenomanian (Zhou et al., 2008). As such, we still apply the latitudinal $\delta^{18}\text{O}_{\text{sw}}$ correction of Zachos et al. (1994), based on analogy with modern latitudinal gradients in $\delta^{18}\text{O}$ in the surface ocean:

$$\text{Local } \delta^{18}\text{O}_{\text{sw}} (\text{‰}, \text{VSMOW}) = 0.576 + 0.041L - 0.0017L^2 + 0.0000135L^3 \quad (13)$$

Estimates of palaeolatitude, L , for each site were extracted from global palaeorotations provided by Gtech Plc. We use the model of Gtech Plc to be consistent with modelling efforts (Ingliš et al., 2015; Lunt et al., 2016), but we recognize that there are other available tools for generating estimates of Cretaceous palaeolatitudes (van Hinsbergen et al., 2015).

2.2. Data quality

In compiling all available planktonic $\delta^{18}\text{O}$ data for the Cretaceous, we undertook an initial screening of the data. We only include published planktonic $\delta^{18}\text{O}$ data from reportedly well-preserved, i.e. good-to-exceptionally preserved specimens. We acknowledge that, by focusing on $\delta^{18}\text{O}_{\text{pl}}$ data from well-preserved foraminifera present in clay-rich lithologies, the resulting datasets are skewed to sites proximal to the continents. Thus, even sparse SST data obtained from well-preserved carbonate at open-ocean sites, e.g., Maastrichtian $\delta^{18}\text{O}$ data from remarkably well-preserved metastable carbonate from the carbonate platform of Wodejebato Guyot in the western equatorial Pacific (Wilson and Opdyke, 1996), are of particular value. In addition, we have not included planktonic $\delta^{18}\text{O}$ data from older sites that have since

been re-drilled using newer coring systems and subsequently sampled with improved recovery. For example, for Demerara Rise we do not include published planktonic $\delta^{18}\text{O}$ data from Deep Sea Drilling Project Site 144 which was spot-cored but instead include data from the re-cored site, Ocean Drilling Program Site 1257, which recovered a far more complete sample of the stratigraphic record (Shipboard Scientific Party, 2004). Likewise, for Blake Plateau we include published planktonic $\delta^{18}\text{O}$ data from ODP Site 1049 but not DSDP Site 390 (Shipboard Science Party, 1998).

Raw GDGT data from sediments reported to be strongly affected by thermally mature allochthonous organic-matter input, which can lower SST estimates substantially, were also excluded from our compilation: approximately 50% of the sample set from the Cismon core in northern Italy (Bottini et al., 2015). Other tests to screen GDGT data, e.g., the BIT index and the Ring Index, are discussed in the ‘Results’ section. Owing to a great many differences between the TEX_{86} and $\delta^{18}\text{O}_{\text{pl}}$ temperatures proxies, e.g. their very definitions and their duration in use (TEX_{86} being relatively younger), our discussion of potential secondary effects on TEX_{86} (Section 3.2) is somewhat more extensive than that of $\delta^{18}\text{O}_{\text{pl}}$ (Section 3.4) with Pearson, 2012 providing a detailed review of the latter topic.

2.3. Age control

All TEX_{86} indices and $\delta^{18}\text{O}$ values are reported relative to Geological Time Scale 2012 (GTS 2012; Gradstein et al., 2012). Age control typically relies on biostratigraphic datum levels but in some cases also magnetostratigraphy (e.g. Berriasian–Barremian and Campanian–Maastrichtian intervals) and carbon-isotope stratigraphy (e.g., OAE 2).

3. Results

3.1. Cretaceous TEX_{86} values

Raw TEX_{86} values for Cretaceous sediments range between 0.51 and 0.96 ($n = 1146$; Figs. 2a, 3a), with a substantial number of these data being higher than any value observed in modern ocean sediments outside of the Red Sea (0.72; Fig. 3b; Kim et al., 2010). There is a significant ‘time gap’ during the late Aptian–Albian, ca. 114–105 Ma, for which no GDGT data currently exist. TEX_{86} values > 0.9 are recorded for the time intervals 100–87 Ma (encompassing the Cenomanian–Turonian), ~ 125 Ma (earliest Aptian) and also 139–130 Ma (Valanginian–Hauterivian). These high TEX_{86} values generally correspond to low palaeolatitude sites, although not during all time intervals: for example, in the Campanian–Maastrichtian, ~ 83 –67 Ma, TEX_{86} values from the Shuqualak–Evans borehole located in Mississippi at 34 – 36°N palaeolatitude are similar to or warmer than TEX_{86} values from PAMA Quarry and the Aderet borehole 1, located in Israel at ~ 17 – 19°N palaeolatitude. For some time intervals, data exist only for a small range of palaeolatitudes, precluding observations of latitudinal variations in TEX_{86} -derived SSTs. The lowest TEX_{86} values are generally recorded at the highest palaeolatitudes ($> \pm 39^\circ$). However, data from high-palaeolatitude locations ($> \pm 48^\circ$) are only available for the Valanginian to Late Aptian, 138–114 Ma, and one Arctic Ocean site dated as early Maastrichtian, ca. 71 Ma (Jenkyns et al., 2004).

3.2. Critical evaluation of GDGT data

Application of the TEX_{86} -palaeothermometer is complicated by factors influencing GDGT distributions other than sea-surface temperature (e.g., Weijers et al., 2006; Zhang et al., 2011; Sinningh-Damsté et al., 2012; Zhang et al., 2016) and the fact that TEX_{86} values for the Cretaceous Period commonly lie outside of the upper range of TEX_{86} values for the modern core-top datasets (e.g., Kim et al., 2008; Kim et al., 2010). Here we employ a variety of GDGT distribution

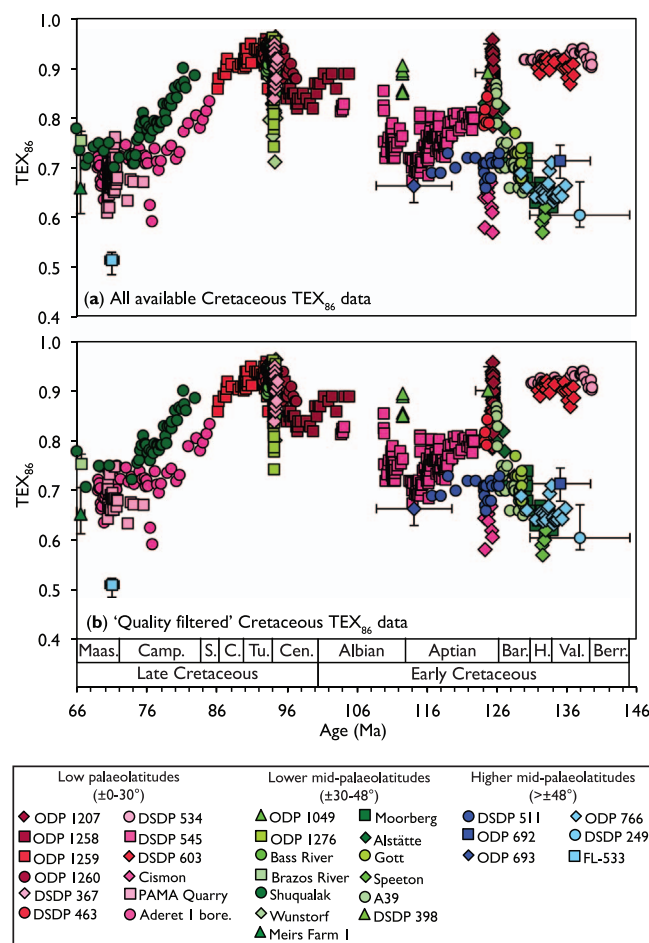


Fig. 2. (a) Compiled published raw TEX₈₆ values for the Cretaceous ($n = 1143$). (b) Compiled published raw TEX₈₆ values for the Cretaceous after quality screening filtering for potentially problematic samples ($n = 993$); exclusion criteria are summarized in Table 2. For individual datasets where only a few datapoints exist and/or the data span a very narrow temporal window (e.g., Brazos River, Meirs Farm 1 and FL-533), or age uncertainties are large (e.g., ODP 692, ODP 693 and DSDP 249) only the mean is plotted with full ranges of the datasets represented by horizontal and vertical bars. For Meirs Farm 1 and Brazos River horizontal bars are obscured since they lie within the areas of the respective mean datapoints.

parameters (BIT, %GDGT-0, MI, $f_{\text{Cren}^{\text{Cren}} + \text{Cren}}$, ΔRI) to investigate potential secondary controls on Cretaceous GDGT data and identify any samples that are problematic. We note that this exercise is only possible for samples where BIT values ($n = 540$) and/or fractional abundances

of individual GDGTs (GDGT-1, GDGT-2, GDGT-3, crenarchaeol and the crenarchaeol regio-isomer; $n = 810$; or $n = 678$ for samples where GDGT-0 was also included) are available, not just TEX₈₆ ($n = 1143$). We then explore the suitability of the TEX₈₆-Linear (this study), TEX₈₆^H, (Kim et al., 2010) and BAYSPAR (Tierney and Tingley, 2014; Tierney and Tingley, 2015) calibrations for reconstructing Cretaceous SSTs.

3.2.1. Terrestrial input

BIT indices were reported for approximately 47% of the Cretaceous TEX₈₆ dataset. For BIT indices > 0.3, we exclude the corresponding TEX₈₆ data points from our temperature reconstructions. In the case of the Wunstorf core, in line with the original published data (van Helmond et al., 2015), TEX₈₆ data with BIT indices of 0.15–0.3 were also excluded due to additional concerns that these samples were affected by post-depositional oxidation. In total we exclude 29 data points, 2.5% ($n = 1143$) of the TEX₈₆ dataset. Given the range of depositional settings and the total number of datasets, it is surprising that so few BIT indices have values > 0.3. One issue is that the BIT threshold of 0.3 was based on a mixing model of the Congo River, an intermediate temperature site (Weijers et al., 2006). Under extreme warmth (such as the Cretaceous) an increase in the fractional abundance of crenarchaeol could produce lower BIT values, potentially shifting the threshold indicated by the Congo mixing model (Weijers et al., 2006).

3.2.2. Archaeal methanogenesis and methanotrophy

Sedimentary Euryarchaeota involved in anaerobic oxidation of methane (AOM) either at active cold seeps or in many continental shelf settings can synthesize isoprenoidal GDGTs containing 0–3 cyclopentane moieties (Pancost et al., 2001; Aquilina et al., 2010; Weijers et al., 2011; Zhang et al., 2011), potentially altering marine sediment TEX₈₆ values and subsequent climate interpretation (Blaga et al., 2009; Zhang et al., 2011; Weijers et al., 2011). Methanogenic Archaea also synthesize small quantities of isoprenoidal GDGTs, specifically GDGT-0, and, to a lesser extent, GDGT-1 and -2 (Koga et al., 1993; Weijers et al., 2006). Although present in marine sediments, these methanogens to date only appear to affect TEX₈₆ values in lacustrine settings (Blaga et al., 2009; Powers et al., 2010; Sinninghe Damsté et al., 2012), not marine settings (Inglis et al., 2015).

Cretaceous %GDGT-0 values range between 2 and 79 (Fig. 4), with a mean value of 19 ($n = 678$, $\sigma = 15.5$) suggesting that methanogenic contributions of GDGT-0 are relatively minor. Only two data points, from the Aderet borehole 1, Israel (Alsenz et al., 2013), have %GDGT-0 values > 67, indicating that associated TEX₈₆ values are potentially compromised by an additional, potentially methanogenic, source of GDGT-0. Cretaceous %GDGT-0 values exhibit a greater range than observed for the modern core-top dataset, 9–65 ($n = 426$; $\sigma = 12.5$; Fig. 4), but are narrower in span than %GDGT-0 values for the Eocene,

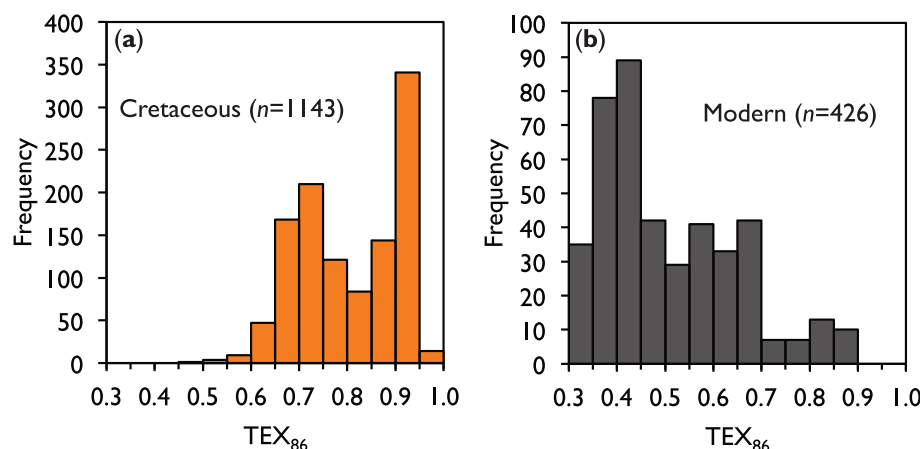


Fig. 3. Distribution of all (a) compiled published raw Cretaceous TEX₈₆ data ($n = 1143$) and (b) modern core-top TEX₈₆ data ($n = 426$; Kim et al., 2010). Cretaceous TEX₈₆ values are commonly high, > 0.7, in comparison to modern TEX₈₆ values and also exceed the maximum values recorded in the modern core-top data, > 0.9.

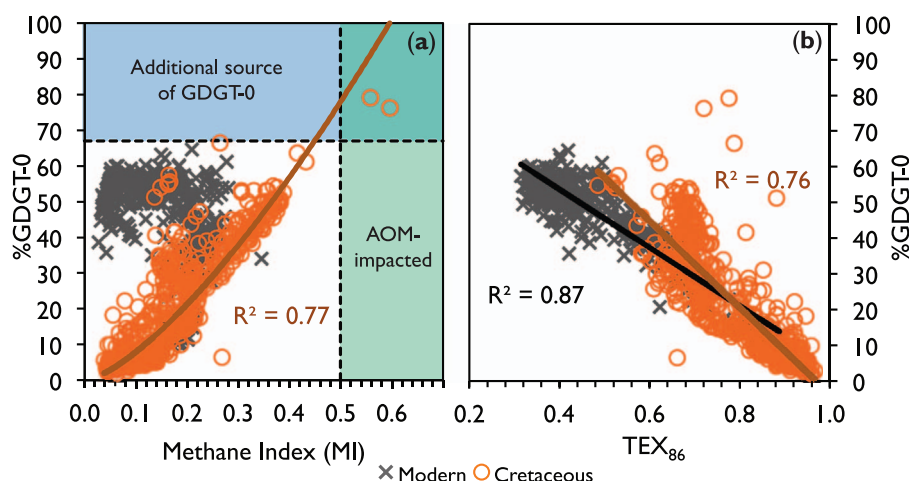


Fig. 4. (a) %GDGT-0 versus MI values from the core-top dataset (Trommer et al., 2009; Kim et al., 2010) and Cretaceous sediments. Dashed lines indicate limits above which samples have an additional source of GDGT-0 (horizontal) and/or are impacted by anaerobic oxidation of methane (vertical). (b) %GDGT-0 versus TEX_{86} from Cretaceous sediments.

5–97 ($n = 641$; $\sigma = 17.3$; Inglis et al., 2015). The average %GDGT-0 for the Cretaceous, 19, is substantially lower than the %GDGT-0 mean for the modern core-top data and the Eocene compilation, which possess similar values of 45 and 42, respectively. To a first order, a low fractional abundance is likely due to the much higher temperatures of the study interval, as derived from this and previous studies (Schouten et al., 2002). As such, for %GDGT-0 to exceed 67% would require a substantial methanogen contribution, and it is likely harder to resolve this influence in warm settings and time intervals, such as the Cretaceous and Eocene. At lower TEX_{86} values, ~ 0.6 – 0.7 , %GDGT-0 values are higher and more variable relative to the modern core-top dataset (Fig. 4b). This result derives from lower abundances of crenarchaeol when TEX_{86} values are lower (temperatures are cooler) such that contributions from GDGT-0 are more dominant, while increased variability reflects the range of spatial and temporal depositional settings.

Cretaceous methane indices, where computed, range from 0.04 to 0.60 and average 0.18 ($n = 810$; $\sigma = 0.09$), generally suggesting a relatively small input of methanogens and methanotrophs ($MI < 0.3$; Fig. 4a). This average is similar to that for the modern dataset 0.15 ($n = 426$; $\sigma = 0.07$), where MI values range between 0.03 and 0.35, exceeding 0.3 in $< 1\%$ of samples. In Cretaceous samples, MI values exceed 0.3 for $\sim 8\%$ of the dataset, although these values are associated solely with samples from PAMA quarry and Aderet borehole 1, Israel (Alsenz et al., 2013). Only two samples from Aderet borehole 1 (Alsenz et al., 2013) have MIs > 0.5 ; these same samples also have high, $> 67\%$, %GDGT-0 values and are hence excluded from our Cretaceous temperature reconstructions.

In combination, MI and %GDGT-0 values indicate that Cretaceous sediments are unlikely to have been subjected to appreciable sedimentary GDGT input via archaeal methanogenesis and/or archaeal methanotrophy sufficient to compromise TEX_{86} values.

3.2.3. Anomalous GDGT distributions

We apply the $f_{Cren':Cren' + Cren}$ ratio and ΔRI to investigate anomalous GDGT distributions in ancient sediments (Fig. 5a). Cretaceous $f_{Cren':Cren' + Cren}$ values ($n = 810$) mostly range between 0.03 and 0.24, which is broadly similar to the range observed in the modern core-top sediments 0.00–0.16 with the inclusion of $f_{Cren':Cren' + Cren}$ values from the modern Red Sea (Fig. 5a). Similar to the modern core-top dataset, $f_{Cren':Cren' + Cren}$ in Cretaceous sediments increases with TEX_{86} , suggesting that most Cretaceous sediments have a similar GDGT distribution-temperature relationship as the modern. There are some exceptions to these patterns; some Cretaceous samples deviate from the overall $f_{Cren':Cren' + Cren}$ - TEX_{86} relationship, displaying $f_{Cren':Cren' + Cren}$ values > 0.25 (Fig. 5a). These outliers are from Aderet borehole 1, Israel and DSDP 463, Mid-Pacific mountains. The enhanced contribution of the crenarchaeol regio-isomer, Cren', in these few outlier sediments could indicate a potential warm bias in corresponding TEX_{86} values and/or a different TEX_{86} -temperature response; therefore, sediments with $f_{Cren':Cren' + Cren}$ values > 0.25 are excluded from our Cretaceous SST compilation. Overall though, the $f_{Cren':Cren' + Cren}$ values indicate that conditions in the Cretaceous were very warm. This exercise for Cretaceous sediments (Fig. 5a) suggests that this approach could be a valuable tool for identifying anomalous GDGT distributions

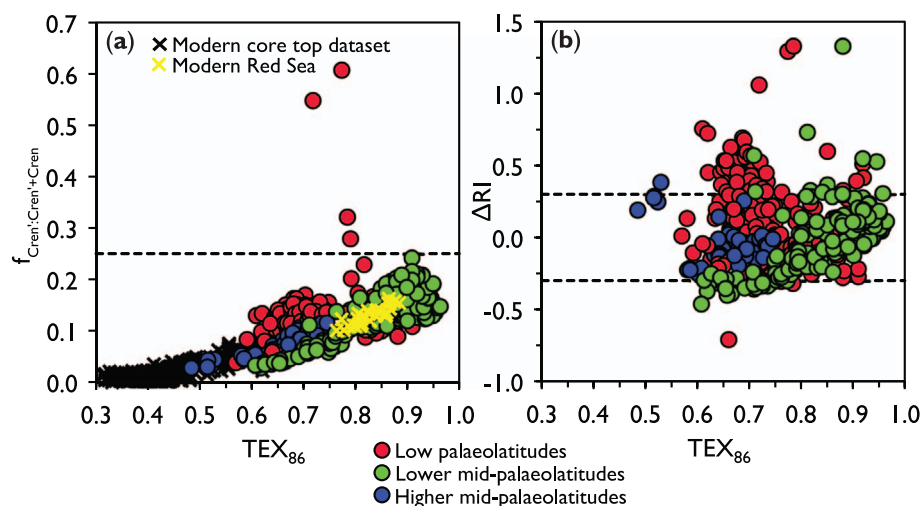


Fig. 5. (a) Proportion of Cren' relative to Cren, $f_{Cren':Cren' + Cren}$, in Cretaceous sediments, categorized by palaeolatitude. $f_{Cren':Cren' + Cren}$ values for the modern core-top dataset, including the Red Sea, are also shown. (b) ΔRI values for Cretaceous samples, categorized by palaeolatitude.

in other investigations, i.e. increased proportions of the crenarchaeol regio-isomer could indicate a potential depth influence, similar to that observed in modern Mediterranean Sea and Portuguese continental margin sediments (Kim et al., 2015; Kim et al., 2016).

Δ RI values calculated for Cretaceous GDGT data range between -0.71 and 1.33 (Fig. 5b). Of the Cretaceous GDGT distributions evaluated ($n = 678$), 128 samples have Δ RI values $> |0.30|$, indicating a significant deviation from modern analogues and/or an influence from non-thermal factors. The Ring Index is designed to identify spurious data, including those that would likely be detected by computing MIs and/or BIT indices. The application of the Ring Index here identifies substantially more anomalous/problematic samples than all other indices — BIT index, MI, %GDGT-0 and $f_{\text{Cren}':\text{Cren}'} + \text{Cren}$ — combined (33 samples total). However, the majority of the Cretaceous Δ RI values $> |0.30|$, 80 samples, are from one location, PAMA quarry, Israel. Of the remaining 48 samples with Δ RI values $> |0.3|$ (1049, $n = 1$; 463, $n = 1$; 534, $n = 3$; FL533, $n = 1$; 1207, $n = 2$; 1258, $n = 1$; Shuqualak, $n = 10$; Aderet borehole 1, $n = 6$; Bass River, $n = 2$; Wunstorff, $n = 4$; DSDP 398, $n = 4$; Meirs Farm 1, $n = 12$; Brazos River, $n = 1$), 9 were also identified as potentially influenced by non-temperature factors based on one or more other indices. The observation that $> 76\%$ of the Cretaceous GDGT data from PAMA quarry ($n = 105$) are identified as spurious by Δ RI, suggests a strong influence from non-thermal factors undetected by the other indices employed here. Given that BIT indices and hopane isomers (maturity indicators) are unavailable for these sediments, which were deposited in the centre of an upwelling system (Edelman-Furstenberg, 2009; Ashckenazi-Polivoda et al., 2011; Schneider-Mor et al., 2012), we exclude all data from all samples with Δ RI values $> |0.30|$ from our SST compilation and interpret the rest of the data from the PAMA quarry with caution. We also exclude data from all other locations with Δ RI values $> |0.30|$. In general, these data represent a small proportion of the total samples at any given site, suggesting that if Δ RI is detecting influences from non-thermal factors they were not persistent.

Having undertaken screening of Cretaceous GDGT data using a variety of GDGT distribution parameters (BIT, %GDGT-0, MI, $f_{\text{Cren}':\text{Cren}'} + \text{Cren}$, Δ RI), we chose to exclude a small portion (13%) of the GDGT data from our SST compilation (compare Fig. 2a with Fig. 2b; 150 samples total; exclusion criteria summarized in Table 2) based on potential secondary controls, specifically significant terrestrial influences, methanogenesis, anomalously high $f_{\text{Cren}':\text{Cren}'} + \text{Cren}$ values (> 0.25) and/or high Δ RI values (> 0.30).

3.3. Cretaceous planktonic foraminifer $\delta^{18}\text{O}$ data

The new planktonic oxygen-isotope ($\delta^{18}\text{O}_{\text{pl}}$) compilation ($n = 3843$) indicates that $\delta^{18}\text{O}_{\text{pl}}$ values for the Cretaceous (120–66 Ma) range between 1.2 and -5.4‰ (Fig. 6a). Lowest $\delta^{18}\text{O}_{\text{pl}}$ values occur during the Cenomanian–Turonian (MacLeod et al., 2013), highest $\delta^{18}\text{O}_{\text{pl}}$ values are recorded in the Late Aptian and Late Maastrichtian, although $\delta^{18}\text{O}_{\text{pl}}$ data are unavailable prior to ca. 120 Ma owing to a lack of published records due to a combination of low planktonic foraminiferal abundances, small test sizes, and poor skeletal calcite preservation in Lower Cretaceous sediments.

3.4. Critical evaluation of planktonic $\delta^{18}\text{O}$ data

3.4.1. Secondary controls on planktonic foraminifer $\delta^{18}\text{O}$ -SSTs in the Cretaceous

Although the primary controls on $\delta^{18}\text{O}_{\text{pl}}$ values are temperature and ice volume, several secondary factors influence Cretaceous $\delta^{18}\text{O}_{\text{pl}}$ values including depth of foraminiferal habitat, seasonality, test preservation, changes in surface-water $\delta^{18}\text{O}$ ($\delta^{18}\text{O}_{\text{sw}}$) due to variations in the evaporation–precipitation balance, and carbonate ion concentration.

3.4.2. Planktonic foraminifer species, depth of habitat and seasonality

The range in $\delta^{18}\text{O}_{\text{pl}}$ -values and consequently $\delta^{18}\text{O}_{\text{pl}}$ -SST estimates for any given site partly reflects the variety of planktonic species from which the data were generated. For most Cretaceous $\delta^{18}\text{O}_{\text{pl}}$ -SST datasets, $\delta^{18}\text{O}_{\text{pl}}$ values are derived from more than one planktonic foraminiferal species. Importantly, as is observed in the modern ocean, for most sites, e.g., North Atlantic ODP Site 1050 (Ando et al., 2009), planktonic species can represent a combination of annual and/or seasonal mixed-layer dwellers and potentially also some (sub)thermocline species, with peaks in seasonal abundance varying for different taxa. Further complicating temperature–depth-related signals, foraminifera can vary their depth habitat over a life cycle (e.g., Hemleben et al., 1989). In the modern ocean, many planktonic foraminiferal species migrate through the mixed layer (Bijma and Hemleben, 1994; Schiebel and Hemleben, 2005), typically secreting gametogenic calcite in the upper thermocline. For extinct Cretaceous species, foraminiferal calcification regimes are less well understood (Houston et al., 1999; Bornemann and Norris, 2007).

It is problematic to exclude Cretaceous planktonic $\delta^{18}\text{O}_{\text{pl}}$ data on the basis of seasonality or depth habitat because of the limited understanding of planktonic foraminiferal ecology in the Cretaceous Period. Paired $\delta^{13}\text{C}_{\text{pl}}$ and $\delta^{18}\text{O}_{\text{pl}}$ measurements can potentially be used to evaluate foraminiferal habitats and seasonal preferences since $\delta^{13}\text{C}_{\text{pl}}$ reflects $\delta^{13}\text{C}$ of dissolved inorganic carbon in the ambient seawater, which will vary both vertically and seasonally. However, Cretaceous foraminiferal $\delta^{18}\text{O}_{\text{pl}}$ and $\delta^{13}\text{C}_{\text{pl}}$ gradients are commonly insufficient to separate planktonic species on account of depth, i.e. foraminiferal $\delta^{13}\text{C}_{\text{pl}}$ reflects multiple factors (e.g., Pearson et al., 2001), resulting in a potential bias towards inclusion of only the lowest (warmest) $\delta^{18}\text{O}_{\text{pl}}$ values. Hence, we include all Cretaceous $\delta^{18}\text{O}_{\text{pl}}$ data with the understanding that they represent upper-ocean conditions, but not exclusively the surface ocean.

3.4.3. Foraminiferal calcite preservation

Foraminiferal tests can undergo alteration via dissolution, recrystallization and/or the addition of calcite overgrowths, all of which have the potential to compromise $\delta^{18}\text{O}_{\text{pl}}$ values (e.g., Pearson et al., 2001). In general, our compilation presents published $\delta^{18}\text{O}_{\text{pl}}$ data from foraminifera of good-to-exceptional preservation, ideally demonstrated by ‘glassy’ tests. However, diagenetic micro-recrystallization, whereby modification occurs but the structure of the shell, e.g., wall pores, is maintained so as to appear unaltered under a scanning electron microscope, could explain some of the high $\delta^{18}\text{O}_{\text{pl}}$ values derived from some Cretaceous sediments (Pearson et al., 2001). Diagenetic recrystallization produces higher $\delta^{18}\text{O}_{\text{pl}}$ values in planktonic foraminiferal calcite equating to lower palaeotemperatures (Pearson et al., 2001; Sexton et al., 2006), a result of the precipitation of diagenetic calcite from relatively cold bottom waters or pore waters below the sea floor and the fast rate of carbonate recrystallization (Rudnicki et al., 2001; Schrag et al., 1995). This process has the potential to exert the

Table 2
Summary of TEX₈₆ sample exclusion criteria.

Index	Threshold for TEX ₈₆ data exclusion	References
Branched and Isoprenoid Tetraether (BIT) Index	BIT > 0.3	Hopmans et al. (2004) Weijers et al. (2006)
%GDGT-0	%GDGT-0 $> 67\%$	Sinninghe Damsté et al. (2012)
Methane Index (MI)	MI > 0.5	Zhang et al. (2011)
Δ Ring Index (RI)	Δ RI $> 0.3 $	Zhang et al. (2016)
$f_{\text{Cren}':\text{Cren}'} + \text{Cren}$	$f_{\text{Cren}':\text{Cren}'} + \text{Cren} > 0.25$	This study

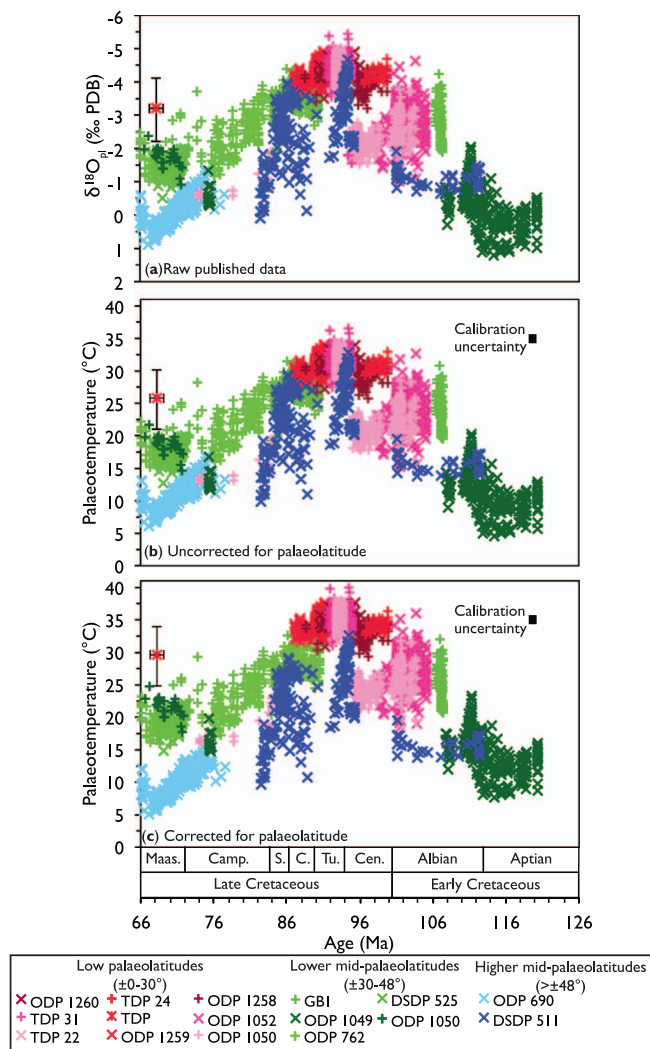


Fig. 6. Compiled $\delta^{18}\text{O}_{\text{pl}}$ temperature reconstructions for the Cretaceous Period ($n = 3789$). (a) Published raw $\delta^{18}\text{O}_{\text{pl}}$ values. (b) $\delta^{18}\text{O}_{\text{pl}}$ -derived sea-surface temperature estimates using the palaeotemperature equation (1) of Bemis et al. (1998) and assuming ice-free conditions, ($\delta w = -1\text{‰}$ (VSMOW); Shackleton and Kennett, 1975; Hut, 1987). (c) Same as previous but with the addition of a $\delta^{18}\text{O}_{\text{sw}}$ correction for changes in palaeolatitude (Zachos et al., 1994). Estimates of palaeolatitude are derived using a palaeorotational model provided by Getech Plc. In the case of site TDP, all data pertain to one sample and so instead the mean is plotted with full ranges of the dataset represented by horizontal and vertical bars. In panels (b) and (c) the black bar represents the palaeotemperature calibration uncertainty ($\pm 0.7\text{ °C}$, Bemis et al., 1998).

most significant influence on $\delta^{18}\text{O}_{\text{pl}}$ values of planktonic foraminifera from low-latitude sites, where temperature differences between surface waters and pore waters are greatest.

Comments on planktonic foraminiferal preservation for each Cretaceous $\delta^{18}\text{O}_{\text{pl}}$ dataset are provided in Table 3. The majority of Cretaceous $\delta^{18}\text{O}_{\text{pl}}$ datasets report either exceptional ‘glassy’ preservation or excellent/very good/good preservation (Table 3). We interpret exceptional/excellent preservation to reflect foraminiferal tests with no diagenetic alteration and very good/good preservation to imply minimal diagenetic effects on planktonic $\delta^{18}\text{O}_{\text{pl}}$ values, i.e. foraminiferal wall microstructures are visible via SEM, suggesting that primary temperature trends are preserved (Pearson et al., 2001). Evidence of more substantial diagenetic alteration (and correspondingly high $\delta^{18}\text{O}_{\text{pl}}$ values) is reported for two sites, ODP Site 1049 and ODP Site 1050. Highest $\delta^{18}\text{O}_{\text{pl}}$ values (and lowest $\delta^{18}\text{O}_{\text{pl}}$ palaeotemperatures) are reconstructed for the late Aptian North Atlantic (Fig. 6a; ODP 1049; Huber et al., 2011). Huber et al. (2011) identified diagenetic overprinting of upper Aptian samples from ODP Site 1049

associated with high $\delta^{18}\text{O}_{\text{pl}}$ values, $> 0\text{‰}$, which in some cases were greater than corresponding benthic $\delta^{18}\text{O}$ ($\delta^{18}\text{O}_{\text{b}}$) values from the same sample set. Manifestly, diagenesis provides one explanation for the high $\delta^{18}\text{O}_{\text{pl}}$ values, although early diagenesis cannot fully explain the highest $\delta^{18}\text{O}_{\text{pl}}$ values if the benthic values are taken as the diagenetic end-member. In Albian–Cenomanian sediments from North Atlantic ODP Site 1050, Ando et al. (2009, 2010) also found foraminifera from certain intervals had undergone some diagenetic recrystallization impacting $\delta^{18}\text{O}_{\text{pl}}$ values (Huber et al., 2002; Petrizzo et al., 2008; Ando et al., 2009), although $\delta^{18}\text{O}_{\text{pl}}$ values are much lower than for the upper Aptian North Atlantic (ODP 1049; Huber et al., 2011). Based on our assessment of preservation, we exclude these problematic $\delta^{18}\text{O}_{\text{pl}}$ data from ODP 1049 and ODP 1050 from our Cretaceous SST compilation.

3.4.4. Changes in surface-water $\delta^{18}\text{O}$

Differences in surface-water $\delta^{18}\text{O}$ patterns, $\delta^{18}\text{O}_{\text{sw}}$, in the Cretaceous Period relative to the present day likely influenced $\delta^{18}\text{O}_{\text{pl}}$ values and corresponding palaeotemperatures on a regional scale. Although we adjust Cretaceous $\delta^{18}\text{O}_{\text{pl}}$ values for differences in latitude and hence changes in precipitation versus evaporation (Zachos et al., 1994), this approach assumes that latitudinal variations in $\delta^{18}\text{O}_{\text{sw}}$ in the Cretaceous were not significantly different from modern. This supposition is likely to hold true for some locations, such as low-latitude open-ocean sites. However, this approach is rather simplistic because it does not account for regional variations in $\delta^{18}\text{O}_{\text{sw}}$ due to both mixing and surface hydrological processes (e.g., Poulsen et al., 1999; Zhou et al., 2008), temporal variations in precipitation/evaporation patterns (Haq, 2014 and references therein), short-term freshening events including those linked with OAEs, e.g., surface water freshening in the north Atlantic during the onset of OAE 1b (Erbacher et al., 2001; Wagner et al., 2008), or uncertainties in the effective fractionation between seawater and exported water vapour, i.e. the slope of $\delta^{18}\text{O}_{\text{sw}}$ versus salinity (Zhou et al., 2008; Huber et al., 2011). Indeed, a high evaporative fractionation factor ($\delta^{18}\text{O}_{\text{sw}}/\text{salinity}$) producing higher $\delta^{18}\text{O}_{\text{sw}}$ at elevated salinities in the early Albian North Atlantic, i.e. an accelerated hydrological cycle (Ufnar et al., 2004), is used by Huber et al. (2011) to explain why $\delta^{18}\text{O}_{\text{pl}}$ values are exceptionally high at ODP 1049 in the early Albian and thereby yield unreasonably cool temperatures for the mid-Cretaceous ($\sim 10\text{--}16\text{ °C}$ cooler than modern; Fig. 6).

3.4.5. Kinetic effects - changes in carbonate ion chemistry

Cretaceous $\delta^{18}\text{O}_{\text{pl}}$ values may have a cool bias owing to relatively low activity of the carbonate ion in a high $p\text{CO}_2$ ocean (Spero et al., 1997; Zeebe, 2001; Tyrrell and Zeebe, 2004). Royer et al. (2004) suggested a 3 to 5 °C cool bias in shallow-water carbonate $\delta^{18}\text{O}$ palaeotemperature estimates for the Cretaceous. However, subsequent studies (e.g., Beck et al., 2005; Uchikawa and Zeebe, 2010) indicate that the nature of oxygen-isotope fractionation within the carbonic acid system is less systematic than previously thought; for example, thermodynamic theory predicts a much greater change in the $\delta^{18}\text{O}$ of the dissolved inorganic carbon species per unit pH between pH 6 and 8 than between pH 8 and 9 (Uchikawa and Zeebe, 2010), although it is not known if the same trend of $\delta^{18}\text{O}$ versus pH applies to the $\delta^{18}\text{O}$ of foraminiferal calcite (Zeebe, 1999; Uchikawa and Zeebe, 2010). Indeed, a culturing study by De Nooijer et al. (2009) demonstrated that planktonic foraminifera could regulate intracellular pH during calcification. Even for the modern day, comparisons between planktonic foraminiferal $\delta^{18}\text{O}$ values and local SSTs frequently reveal under- or over-estimations in reconstructed SSTs, presumably due to $\delta^{18}\text{O}$ -disequilibrium related to physiological and ecological effects (Niebler et al., 1999; Mohtadi et al., 2011), despite parameters such as salinity, $\delta^{18}\text{O}_{\text{sw}}$ and the carbonate system itself (e.g., Hönisch et al., 2013). Given these uncertainties, we make no formal adjustment to $\delta^{18}\text{O}_{\text{pl}}$ data for kinetic effects associated with past changes in ocean pH but note that the effect of lowering seawater pH under high $p\text{CO}_2$ conditions likely leads to an under-estimation of Cretaceous SSTs (e.g., Zeebe, 2001; Royer et al., 2004;

Table 3Sites from which Cretaceous planktonic $\delta^{18}\text{O}$ data were compiled.

Site	Location	Palaeolatitude	Reference	Preservation notes
DSDP 511	Falkland Plateau	48.7°S (Apt.) 52.3°S (Alb.) 54.3°S (Cen.) 54.3°S (Tur.) 54.4°S (Con.) 54.4°S (Sant.) 54.3°S (Camp.)	Huber et al. (1995) Fassell and Bralower (1999) Bice et al. (2003)	Excellent preservation (Turonian–Santonian to Upper Campanian), minor recrystallization (upper Cenomanian and upper Albian; Huber et al., 1995). Hollow tests with minimal secondary calcite (Albian; Fassell and Bralower, 1999). Samples from below 480 mbsf (upper Aptian–lower Albian) were poorly preserved, reflected in highly negative $\delta^{18}\text{O}$ values, -3 to -6‰ (Fassell and Bralower, 1999), these data are excluded entirely from this study. Exceptionally well-preserved, 'glassy', to excellent preservation (Bice et al., 2003).
DSDP 525	Walvis Ridge	37.9°S (Camp.) 37.7°S (Maas.)	Friedrich et al. (2009)	Very good to good preservation, most tests appear 'glassy' when wet (Friedrich et al., 2009).
ODP 690	Maud Rise	62.3°S (Camp.) 64.1°S (Maas.)	Barrera and Huber (1990) Barrera and Savin (1999) Wilf et al. (2003) Friedrich et al. (2009)	Microstructure alteration (secondary calcite); however, no obvious associated modification of foraminifer original isotopic and elemental chemistries (Barrera and Huber, 1990). Appear well-preserved, evidence of minor to moderate recrystallization of the wall structure (Barrera and Savin, 1999). Good to very good preservation, most tests appearing 'glassy' when wet (Friedrich et al., 2009).
ODP 762	Exmouth Plateau	44.2°S (Tur.) 44.1°S (Con.) 44.4°S (San.) 44.3°S (Camp.) 45.3°S (Maas.)	Falzone et al. (2016)	We include data from foraminifera reported to have 'very good' or 'good' preservation (Falzone et al., 2016). Isotopic data from foraminifera with 'moderate' or 'poor' preservation (Cenomanian data) are excluded (Falzone et al., 2016).
ODP 1049	Blake Nose Plateau	30.0°N (Apt.) 30.3°N (Camp.)	Erbacher et al. (2001) Huber et al. (2002) Huber et al. (2011)	'Glassy' shells with preserved surface ornamentation and without infilling calcite, Albian* (Erbacher et al., 2001). Well-preserved, Campanian (Huber et al., 2002). Well-preserved, nearly all samples contain specimens that appear to be 'glassy', early Albian* (Huber et al., 2011). Upper Aptian shells exhibit moderate to good preservation*.
ODP 1050	Blake Nose Plateau	28.3°N (Alb.) 26.5°N (Cen.) 29.4°N (Camp.) 30.5°N (Maas.)	Huber et al. (2002) Petrizzo et al. (2008) Ando et al. (2009)	Well-preserved, uppermost Albian–Maastrichtian (Huber et al., 2002). Excellent to good preservation in late Albian to early Cenomanian (Petrizzo et al., 2008). Some diagenetic recrystallisation of Cenomanian tests causing discernable diagenetic shifts from primary $\delta^{18}\text{O}$ * (Ando et al., 2009; Ando et al., 2010).
ODP 1052	Blake Nose Plateau	27.8°N (Alb.) 26.0°N (Cen.)	Petrizzo et al. (2008)	Excellent to good preservation (Petrizzo et al., 2008).
ODP 1258	Demerara Rise	8.2°N (Alb.) 5.4°N (Cen.) 5.4°N (Tur.) 5.5°N (Con.)	Bice and Norris (2005) Moriya et al. (2007) Friedrich et al. (2008)	Generally excellent to good preservation (Bice and Norris, 2005). Exceptionally well-preserved, 'glassy', (Moriya et al., 2007). Generally extremely well-preserved, 'glassy', lacking internal cements and recrystallization (Friedrich et al., 2008).
ODP 1259	Demerara Rise	5.6°N (Con.) 5.5°N (Cen.) 5.5°N (Tur.)	Bornemann et al. (2008)	'Glassy' appearance and pristine, well-preserved wall textures (Bornemann and Norris, 2007; Bornemann et al., 2008).
ODP 1260	Demerara Rise	5.5°N (Tur.) 5.5°N (Cen.)	Forster et al. (2007b)	Exceptionally well-preserved, 'glassy', free of secondary calcite chamber infillings (Forster et al., 2007b).
TDP	Tanzania	26.5°S (Cen.) 22.3°S (Maas.)	Pearson et al. (2001)	Exceptionally well-preserved, 'glassy' (Pearson et al., 2001).
TDP 22	Tanzania	25.0°S (Tur.)	MacLeod et al. (2013)	Exceptionally well-preserved, 'glassy' (MacLeod et al., 2013).
TDP 24	Tanzania	27.0°S (Cen.)	Ando et al. (2015)	Exceptionally well-preserved, 'glassy' (Ando et al., 2015).
TDP 31	Tanzania	27.0°S (Cen.) 25.4°S (Tur.)	MacLeod et al. (2013)	Exceptionally well-preserved, 'glassy' (MacLeod et al., 2013).
GB1 core	Saxony Basin, Northwest Germany	43.5°N (Alb.)	Erbacher et al. (2011)	Outstanding (glassy) to very well-preserved (Erbacher et al., 2011).

ODP = Ocean Drilling Program; DSDP = Deep Sea Drilling Program; TDP = Tanzania Drilling Project. *Data excluded from our Cretaceous SST compilation due to either poor preservation or potential salinity influences/exceptionally low $\delta^{18}\text{O}_{\text{pl}}$ values. Estimates of palaeolatitude are derived using a palaeorotational model provided by Getech Plc.

Uchikawa and Zeebe, 2010).

Our evaluation of potential secondary controls on $\delta^{18}\text{O}_{\text{pl}}$ values suggests that most available Cretaceous $\delta^{18}\text{O}_{\text{pl}}$ data are supposed to reflect surface temperatures or underestimate SSTs owing to kinetic and/or diagenetic effects biasing $\delta^{18}\text{O}_{\text{pl}}$ values to higher values (this potential underestimation of SSTs equates to an uncertainty on the order of ~ 3 to 5°C). There are also some notable data outliers; based on our assessment: for example, we exclude ODP 1049 Aptian–Albian data from our temperature compilation owing to exceptionally high $\delta^{18}\text{O}_{\text{pl}}$ values: potentially due to a combination of salinity influences and variable preservation and similarly exclude data from ODP 1050 in cases where samples were reported to suffer from preservation issues.

4. Discussion

4.1. Comparison of $\text{TEX}_{86}^{\text{H}}$, $\text{TEX}_{86}^{\text{Linear}}$ and $\text{BAY}_{\text{GlobR}}$ -SSTs for the Cretaceous

Compiled TEX_{86} -derived SSTs for the Cretaceous Period range

between $18.8 \pm 2.5^\circ\text{C}$ and $37.5 \pm 2.5^\circ\text{C}$ ($\text{TEX}_{86}^{\text{H}}$; Fig. 7a), or $18.8 \pm 2.0^\circ\text{C}$ and $45.1 \pm 2.0^\circ\text{C}$ ($\text{TEX}_{86}^{\text{Linear}}$; Fig. 7b), or 16.3°C and 44.8°C ($\pm \sim 7\text{--}9^\circ\text{C}$ 90% confidence; $\text{BAY}_{\text{GlobR}}$; Fig. 7c), depending on the choice of calibration. The differences in maximum values arise from the fact that a significant proportion of the data exceed the highest TEX_{86} value in the calibration dataset ($\text{TEX}_{86} = 0.72$ or $\text{TEX}_{86} = 0.89$ if Red Sea data are included, which is relevant for $\text{BAY}_{\text{GlobR}}$; Kim et al., 2010, Tierney and Tingley, 2015), requiring us to project the calibration outside of its modern range. Furthermore, such high TEX_{86} values are near the limit of the calibration ($\text{TEX}_{86} = 1$, $\text{TEX}_{86}^{\text{H}}\text{-SST} = 38.6^\circ\text{C}$; Fig. 7).

When TEX_{86} values lie between ~ 0.45 and 0.70 , the $\text{TEX}_{86}^{\text{H}}$, $\text{TEX}_{86}^{\text{Linear}}$ and $\text{BAY}_{\text{GlobR}}$ calibrations all yield similar SST estimates (Fig. 7). However, once TEX_{86} values exceed ~ 0.7 , SST estimates for the logarithmic versus linear approaches diverge, with the linear-regression approaches, $\text{TEX}_{86}^{\text{Linear}}$ and $\text{BAY}_{\text{GlobR}}$, yielding markedly warmer temperature estimates than the $\text{TEX}_{86}^{\text{H}}$ calibration. This difference is because the logarithmic $\text{TEX}_{86}^{\text{H}}$ calibration yields only small increases in SST as TEX_{86} increases above 0.7 . A linear response of TEX_{86} to

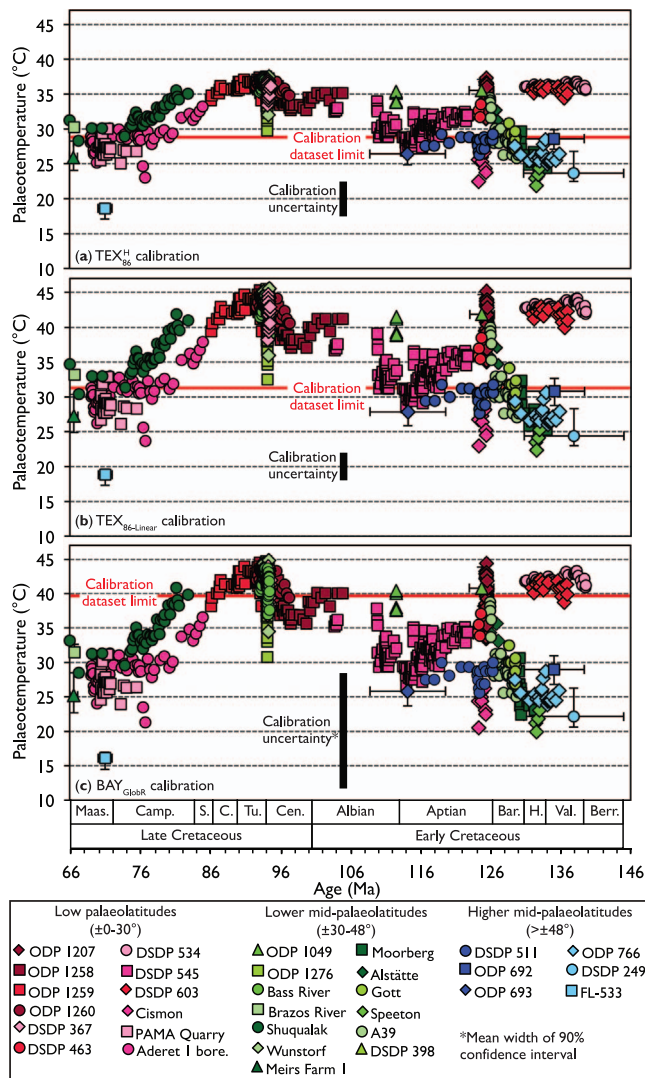


Fig. 7. Compiled TEX_{86} temperature reconstructions for the Cretaceous ($n = 993$). (a) SST estimates derived using the $\text{TEX}_{86}^{\text{H}}$ -SST calibration (Kim et al., 2010). (b) SST estimates derived using a linear TEX_{86} -SST calibration, $\text{TEX}_{86}\text{-Linear}$, based on “warmer” ocean data, $> 15^\circ\text{C}$, from the global core-top calibration of Kim et al. (2010) and excluding data from the Red Sea (see Supplementary Fig. 2 and text for further details). (c) SST estimates derived using a Bayesian global core-top regression ($\text{BAY}_{\text{GlobR}}$; Tierney and Tingley, 2015). The red horizontal lines indicate the upper limits of the modern $\text{TEX}_{86}^{\text{H}}$, $\text{TEX}_{86}\text{-Linear}$ and $\text{BAY}_{\text{GlobR}}$ -SST calibration datasets. The black bar in each panel represents the uncertainty in the corresponding paleotemperature calibration. In the case of $\text{BAY}_{\text{GlobR}}$, since the calibration uncertainty is expressed as confidence intervals for each individual TEX_{86} datapoint, we approximate the $\text{BAY}_{\text{GlobR}}$ uncertainty to the mean ($n = 993$) width of the 90% confidence interval. As in Fig. 2, for individual datasets where only a few datapoints exist and/or the data span a very narrow temporal window or age uncertainties are large, only the mean is plotted with full ranges of the datasets represented by horizontal and vertical bars. (For interpretation of the references to colour in this figure legend, the reader is referred to the web version of this article.)

temperature, even near 40°C (Schouten et al., 2007), is supported by experimental mesocosm evidence, suggesting that the non-linear $\text{TEX}_{86}^{\text{H}}$ calibration model may be underestimating Cretaceous warmth. Moreover, the logarithmic $\text{TEX}_{86}^{\text{H}}$ calibration has structured residuals at high temperatures (elements of variation which are unexplained by the fitted model) that make it particularly problematic when applied beyond the calibration range (Tierney and Tingley, 2014). However, maximum SSTs predicted by $\text{TEX}_{86}\text{-Linear}$ and $\text{BAY}_{\text{GlobR}}$ are exceptionally warm, $> 40^\circ\text{C}$, to the extent these temperatures raise questions regarding the maximum heat stress Cretaceous plants and mammals could have tolerated (e.g., Hay and Floegel, 2012). Given the different

strengths and weaknesses of the TEX_{86} calibrations, we present and discuss compiled Cretaceous TEX_{86} -SSTs derived using both the $\text{TEX}_{86}^{\text{H}}$ -SST calibration and also a linear approach, $\text{TEX}_{86}\text{-Linear}$, the latter yielding SSTs very similar to those using $\text{BAY}_{\text{GlobR}}$.

4.2. Cretaceous planktonic foraminifer $\delta^{18}\text{O}$ -SSTs

Cretaceous $\delta^{18}\text{O}_{\text{pl}}$ -SSTs vary between $4.6 \pm 0.7^\circ\text{C}$ and $36.6 \pm 0.7^\circ\text{C}$ (Fig. 6b) and between $5.6 \pm 0.7^\circ\text{C}$ and $40.0 \pm 0.7^\circ\text{C}$ corrected for palaeolatitude (Fig. 6c). The two $\delta^{18}\text{O}_{\text{pl}}$ -SST reconstructions (Fig. 6b, c) exhibit very similar long-term trends with warmest surface-ocean conditions occurring during the Cenomanian–Turonian interval at both low palaeolatitude and higher mid-palaeolatitude locations. Application of a $\delta^{18}\text{O}_{\text{sw}}$ palaeolatitude correction (Eq. (13)) results in greater offsets in $\delta^{18}\text{O}_{\text{pl}}$ -SSTs between different sites, e.g., between low-palaeolatitude and higher mid-palaeolatitude locations through the Albian to Coniacian ($\sim 6\text{--}9^\circ\text{C}$ versus $\sim 3\text{--}5^\circ\text{C}$ offset) and between lower mid-latitude and higher mid-latitude sites in the Campanian–Maastrichtian ($\sim 6^\circ\text{C}$ versus $\sim 3^\circ\text{C}$ offset, Fig. 6b, c). Aside from the long-term trends, $\delta^{18}\text{O}_{\text{pl}}$ -SST estimates are often highly variable at any given site (Figs. 6b, c, 7). This variability is unlikely to be strongly driven by preservation since (a) we have only included data derived from good to excellently preserved planktonic foraminiferal specimens, and (b) this variability exists within individual core datasets. Instead, this likely reflects some combination of habit depth, species variety, seasonality, local and regional fluctuations in $\delta^{18}\text{O}_{\text{sw}}$ resulting from changes in oceanic circulation, source water, continental runoff and the hydrologic cycle, and short-term climate variability driven by orbital cyclicity.

4.3. Comparison of $\text{TEX}_{86}^{\text{H}}$, $\text{TEX}_{86}\text{-Linear}$ and $\delta^{18}\text{O}_{\text{pl}}$ -SSTs for the Cretaceous

$\text{TEX}_{86}^{\text{H}}/\text{TEX}_{86}\text{-Linear}$ -SSTs and $\delta^{18}\text{O}_{\text{pl}}$ -SSTs indicate similar thermal evolutionary histories of the Cretaceous surface ocean with warmest temperatures occurring during the Cenomanian–Turonian, followed by cooling in the Campanian–Maastrichtian intervals (Fig. 8). By comparison with $\text{TEX}_{86}^{\text{H}}/\text{TEX}_{86}\text{-Linear}$ -SST reconstructions, $\delta^{18}\text{O}_{\text{pl}}$ -SSTs display greater variability in Cretaceous sediments and generally indicate significantly cooler surface-ocean conditions (Fig. 8): a discrepancy that is obviously greater for the $\text{TEX}_{86}\text{-Linear}$ calibration (and likewise the $\text{BAY}_{\text{GlobR}}$ calibration). For sites where contemporaneous $\text{TEX}_{86}^{\text{H}}/\text{TEX}_{86}\text{-Linear}$ and $\delta^{18}\text{O}_{\text{pl}}$ -SSTs exist, namely the low-latitude ODP Sites 1258, 1259 and 1260, $\text{TEX}_{86}^{\text{H}}$ -SSTs indicate maximum Cretaceous SSTs, $37\text{--}38 \pm 2.5^\circ\text{C}$ that are similar to maximum $\delta^{18}\text{O}_{\text{pl}}$ -SSTs (corrected for palaeolatitude) but record slightly higher minimum temperature estimates, $33\text{--}34 \pm 2.5^\circ\text{C}$ compared with $29\text{--}32 \pm 0.7^\circ\text{C}$, although these temperature offsets are typically within associated proxy errors (Fig. 8a). By comparison, both maximum and minimum $\text{TEX}_{86}\text{-Linear}$ -SSTs at ODP Sites 1258, 1259 and 1260 are warmer than corresponding $\delta^{18}\text{O}_{\text{pl}}$ -SSTs by $\sim 7\text{--}8^\circ\text{C}$ (Fig. 8b). These observations are similar to those for the Eocene where (i) temporal trends in TEX_{86} , $\text{TEX}_{86}^{\text{H}}$ and $\delta^{18}\text{O}_{\text{pl}}$ -SSTs are similar but (ii) absolute $\delta^{18}\text{O}_{\text{pl}}$ -SST estimates are similar or lower than those of TEX_{86} and $\text{TEX}_{86}^{\text{H}}$ -SSTs (Zachos et al., 2006; Pearson et al., 2007; Hollis et al., 2012).

For the Cretaceous mid-latitudes, offsets between $\text{TEX}_{86}^{\text{H}}/\text{TEX}_{86}\text{-Linear}$ and $\delta^{18}\text{O}_{\text{pl}}$ -SSTs are more apparent (Fig. 8). Indeed, although $\delta^{18}\text{O}_{\text{pl}}$ data from DSDP Site 525 ($\sim 38^\circ\text{S}$), ODP 762 ($\sim 44\text{--}45^\circ\text{S}$), ODP 1049 ($\sim 30^\circ\text{N}$) and ODP 1050 ($\sim 30^\circ\text{N}$) represent four lower mid-palaeolatitude settings, these data give considerably lower SST estimates than $\text{TEX}_{86}^{\text{H}}/\text{TEX}_{86}\text{-Linear}$ -derived SST estimates from other lower mid-latitude locations for the Campanian–Maastrichtian, namely the Shuqualak–Evans Borehole ($35\text{--}36^\circ\text{N}$) and Brazos River ($\sim 36^\circ\text{N}$). Similarly, $\delta^{18}\text{O}_{\text{pl}}$ -SST estimates from ODP Site 690 ($\sim 62\text{--}64^\circ\text{S}$ palaeolatitude) give cooler SST estimates than $\text{TEX}_{86}^{\text{H}}/\text{TEX}_{86}\text{-Linear}$ -SST values from a higher palaeolatitude location (FL533; $\sim 80^\circ\text{N}$), although in this case

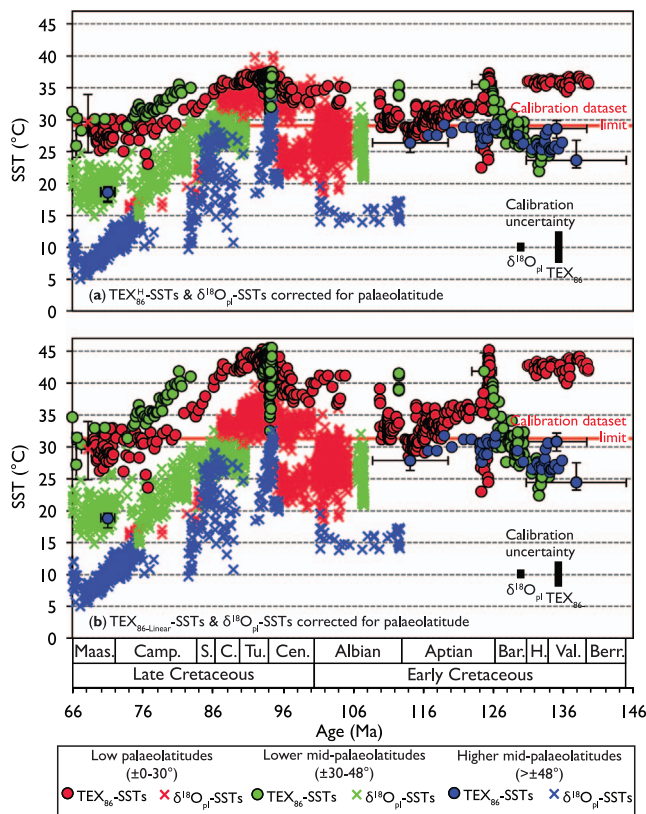


Fig. 8. Compiled TEX_{86} ($n = 993$) and $\delta^{18}\text{O}_{\text{pl}}$ ($n = 3789$) SST estimates for the Cretaceous Period derived from (a) $\text{TEX}_{86}^{\text{H}}$ and $\delta^{18}\text{O}_{\text{pl}}$, (b) $\text{TEX}_{86}^{\text{Linear}}$ and $\delta^{18}\text{O}_{\text{pl}}$. $\delta^{18}\text{O}_{\text{pl}}$ -SST estimates include a $\delta^{18}\text{O}_{\text{sw}}$ correction for changes in palaeolatitude (Zachos et al., 1994). The red horizontal lines indicate the upper limits of the modern $\text{TEX}_{86}^{\text{H}}$ - and $\text{BAY}_{\text{Global}}$ -SST calibration datasets. The black bars in each panel represent the corresponding paleotemperature calibration uncertainties. As in Figs. 2 and 6, for individual datasets where only a few datapoints exist and/or data span a very narrow temporal window or age uncertainties are large, or all data pertain to the same sample, only the mean is plotted with full ranges of the datasets represented by horizontal and vertical bars. (For interpretation of the references to colour in this figure legend, the reader is referred to the web version of this article.)

the two proxy records are from different hemispheres. Cretaceous $\delta^{18}\text{O}_{\text{pl}}$ estimates offer better agreement with $\text{TEX}_{86}^{\text{H}}/\text{TEX}_{86}^{\text{Linear}}$ -SST estimates when a palaeolatitude $\delta^{18}\text{O}_{\text{sw}}$ adjustment is applied. However, in several cases (including both lower mid-palaeolatitude and higher mid-palaeolatitude records), $\delta^{18}\text{O}_{\text{pl}}$ -SST estimates are still significantly lower than $\text{TEX}_{86}^{\text{H}}/\text{TEX}_{86}^{\text{Linear}}$ -SST estimates, suggesting that either assumptions regarding changes in $\delta^{18}\text{O}_{\text{sw}}$ are inaccurate and/or other controls on foraminiferal $\delta^{18}\text{O}_{\text{pl}}$ are important; alternatively, the TEX_{86} proxy may be overestimating SST, particularly at higher palaeolatitudes, as suggested for the early Eocene (Hollis et al., 2012). Unfortunately, current Cretaceous TEX_{86} - and $\delta^{18}\text{O}_{\text{pl}}$ -SST data are insufficient to determine how well these proxies agree at high latitudes.

Data from several high-resolution events are included in this compilation (Figs. 6, 7, 8): namely, datasets for OAE 1a (early Aptian, ~125 Ma) and OAE 2 (Cenomanian–Turonian boundary, ~94 Ma) and also a high-resolution $\delta^{18}\text{O}_{\text{pl}}$ dataset from the Albian of the Lower Saxony Basin (~107 Ma). The high-resolution datasets indicate changes in SSTs, both $\delta^{18}\text{O}_{\text{pl}}$ - and TEX_{86} -SSTs, over relatively short periods of time, on the order of 0.1–1 Myr. Again, the variability is greater for the $\delta^{18}\text{O}_{\text{pl}}$ proxy than for the TEX_{86} proxy, such that the latter yields SSTs that are higher but less variable across the entire data set. These differences imply that either $\delta^{18}\text{O}_{\text{pl}}$ variability is driven by more than simple orbital cyclicity, e.g., seasonality, depth of habitat and variations in local $\delta^{18}\text{O}_{\text{sw}}$, or that the TEX_{86} proxy is less sensitive

to these short-term variations.

4.3.1. Possible reasons for disagreement between TEX_{86} and $\delta^{18}\text{O}_{\text{pl}}$ -SSTs

One major difference between the $\delta^{18}\text{O}_{\text{pl}}$ and TEX_{86} proxies is the way in which the water column represented by the proxy is treated and interpreted. The $\delta^{18}\text{O}_{\text{pl}}$ palaeothermometer is based on the calibration of $\delta^{18}\text{O}_{\text{pl}}$ values with growth temperature in laboratory culture studies (e.g., Bemis et al., 1998) or, alternatively, via modern core-top calibrations (e.g., Mulitza et al., 2004). However, as discussed earlier, the data likely reflect a range of different growth (and hence temperature) depths (e.g., Mohtadi et al., 2011; Hönisch et al., 2013). By contrast, the TEX_{86} proxy is based on calibration of TEX_{86} values in core-top sediments with overlying SST and therefore assumes that the depth of export of the TEX_{86} signal is predominantly from the upper mixed-layer and that this was the same in the past as it is today (e.g., Schouten et al., 2013b). This assumption has been questioned (Hernández-Sánchez et al., 2014; Kim et al., 2015) but it is partially incorporated into the calibration uncertainty along with seasonality, unlike the $\delta^{18}\text{O}_{\text{pl}}$ proxy. However, what remains unclear is how these export processes vary spatially and temporally, resulting in deviations from the modern core-top calibrations (Taylor et al., 2013; Kim et al., 2015), i.e. to what extent signal depth and seasonality in the Cretaceous was analogous to modern. Another likely reason for disagreement between the $\delta^{18}\text{O}_{\text{pl}}$ and TEX_{86} proxies is the uncertainty in $\delta^{18}\text{O}_{\text{pl}}$ values related to the combined effects of salinity and variations in carbonate ion concentration. It is likely that these factors are important, particularly as regards kinetic effects that can potentially lower $\delta^{18}\text{O}_{\text{pl}}$ -SST estimates on the order of ~3–5 °C (Crowley and Zachos, 2000; Royer et al., 2004; Uchikawa and Zeebe, 2010). Unfortunately, it remains difficult to assess the extent of these influences on $\delta^{18}\text{O}_{\text{pl}}$ values as these variables differ both temporally and spatially and are relatively poorly constrained for the Cretaceous Period.

4.4. Evolution of Cretaceous SSTs

4.4.1. Cretaceous climate maxima

For over a decade, climate reconstructions of the Cretaceous greenhouse have yielded palaeotemperature estimates that encompass the highest (> 35 °C) proxy data-based SST estimates of the last 150 Myr ‘super greenhouse’ conditions, with the most pronounced warming in the late Cenomanian–Turonian (e.g., Jenkyns et al., 1994; Huber et al., 1995; Norris and Wilson, 1998; Clarke and Jenkyns, 1999; Wilson et al., 2002; Schouten et al., 2003; Voigt et al., 2004; Forster et al., 2007a; Forster et al., 2007b; Bornemann et al., 2008; Jarvis et al., 2011; MacLeod et al., 2013; van Helmond et al., 2014). The specific timing of this thermal maximum, whether at the Cenomanian–Turonian stage boundary or in the early or late Turonian, is still debated (e.g., Voigt et al., 2004). This pronounced warming is also reflected in palaeotemperature estimates from brachiopods of temperate conditions in mid-latitude shelf seas (Voigt et al., 2004). Our data compilation (Fig. 8) indicates that during most of the Cretaceous Period, temperatures of the warmest surface waters were significantly greater than the maximum surface temperatures recorded in the modern ocean (~28–30 °C). Maximum SSTs did not drop below 30 °C until the late Santonian (~84 Ma, $\delta^{18}\text{O}_{\text{pl}}$) or early Campanian (~80 Ma, TEX_{86}) during global cooling that started in the Coniacian, ~88 Ma. Our compilation (Figs. 6, 7, 8) indicates that warmest Cretaceous surface-ocean palaeotemperatures (> 35 °C) occurred from the late Cenomanian to Turonian in the equatorial Atlantic ($\delta^{18}\text{O}_{\text{pl}}$ & $\text{TEX}_{86}^{\text{H}}/\text{TEX}_{86}^{\text{Linear}}$; ODP Sites 1258, 1259 and 1260, DSDP Sites 367 and 603), mid-latitude North Atlantic ($\text{TEX}_{86}^{\text{H}}/\text{TEX}_{86}^{\text{Linear}}$; Bass River and ODP Site 1276) and offshore Tanzania ($\delta^{18}\text{O}_{\text{pl}}$; Tanzania Drilling Project, TDP, drill cores 22 and 31) sites. In addition, SST estimates of ≥ 35 °C ($\text{TEX}_{86}^{\text{H}}/\text{TEX}_{86}^{\text{Linear}}$; Figs. 7a, b, 8) are recorded in the proto-North Atlantic during the end-Berriasian to early Barremian (DSDP Site 534 and DSDP Site 603) and the mid-Aptian (ODP Site 1049), and also in

the central equatorial Pacific (ODP Site 1207) during the early Aptian OAE 1a. Following the onset of global cooling in the Coniacian, low-latitude SSTs continued to cool for the remainder of the Cretaceous, with values ranging between 17 °C and 36 °C (Fig. 8). This trend agrees with Earth system model zonal mean SSTs that, along with SST proxy data from a range of sources (not only GDGTs and planktonic foraminifera but also fish tooth enamel, mollusks, bivalves, brachiopods and belemnite rostra), together confirm that Late Cretaceous SST cooling was widespread (Tabor et al., 2016).

4.4.2. Cretaceous climate minima

Mean global minimum Cretaceous surface-ocean temperatures are less well constrained than maximum global mean SSTs because of critical gaps in proxy temperature data from higher latitudes ($> \text{ca. } 48^\circ$ palaeolatitude; Fig. 8) relative to data from low latitudes ($< \text{ca. } 30^\circ$ palaeolatitude). In particular, SST estimates are provided solely by the TEX_{86} proxy prior to 114 Ma (this limitation applies for the low-latitude data also), whereas after this time SST estimates for higher latitudes are almost exclusively provided by $\delta^{18}\text{O}_{\text{pl}}$ data, with the exception of a small dataset from the lower Maastrichtian of the Arctic Ocean (Jenkyns et al., 2004). Interpreting each proxy separately, $\text{TEX}_{86}^{\text{H}}$ and $\text{TEX}_{86}^{\text{Linear}}$ from higher mid-latitude locations ($> \pm 48^\circ$ palaeolatitude) suggest minimum SSTs $> 22^\circ\text{C}$ ($\text{TEX}_{86}^{\text{H}}/\text{TEX}_{86}^{\text{Linear}}$) in the Early Cretaceous and SSTs of $\sim 19^\circ\text{C}$ ($\text{TEX}_{86}^{\text{H}}/\text{TEX}_{86}^{\text{Linear}}$) for the early Maastrichtian. $\delta^{18}\text{O}_{\text{pl}}$ data from higher mid-latitude locations ($> \pm 48^\circ$ palaeolatitude) suggest minimum SSTs $> 13^\circ\text{C}$ in the Albian ($\delta^{18}\text{O}_{\text{pl}}$) and $> 20^\circ\text{C}$ ($\delta^{18}\text{O}_{\text{pl}}$) in the Turonian, while later in the Cretaceous minimum SSTs were $\sim 10^\circ\text{C}$ ($\delta^{18}\text{O}_{\text{pl}}$) and $\sim 5^\circ\text{C}$ ($\delta^{18}\text{O}_{\text{pl}}$) in the early and late Maastrichtian, respectively. Clumped-isotope palaeothermometry estimates from high-latitude belemnites indicate marine temperatures of $10\text{--}20^\circ\text{C}$ in the sub-Arctic ($60\text{--}65^\circ\text{N}$) for the Berriasian to late Valanginian, 145–134 Ma (Price and Passey, 2013). These temperatures derived from sub-Arctic nekto-benthonic organisms are broadly consistent with the lower palaeolatitude estimates of SSTs from TEX_{86} (Price and Passey, 2013).

The lowest SSTs during the Cretaceous are not observed at the higher latitude sites. In the Early Cretaceous, $\sim 133\text{--}124$ Ma, the lowest SSTs are in fact recorded at lower mid-latitude sites plus one low-latitude palaeolocation. In the late Valanginian to early Aptian ($135\text{--}124$ Ma), TEX_{86} proxy data from sites in England (Speeton), Germany (Gott and Moorberg) and Italy (Cismon) yield similar or slightly cooler minimum SSTs, $\sim 21\text{--}22^\circ\text{C}$, compared with higher latitude sites ($\sim 25\text{--}27^\circ\text{C}$, ODP Site 766 and DSDP Site 511). Similarly, in the Late Cretaceous, Campanian to late Maastrichtian ($83\text{--}69$ Ma), low-palaeolatitude TEX_{86} data from the Southern Tethys margin (Aderet borehole 1 and PAMA quarry, Israel; only the datapoints which were not excluded after screening) indicate cooler temperatures than contemporaneous TEX_{86} data from a lower mid-palaeolatitude site, the Shuqualak-Evans borehole (Fig. 7). This difference may reflect the Southern Tethys oceanographic setting, namely, a high-productivity upwelling system (Alsenz et al., 2013). Modern SST reconstructions based on TEX_{86} values in suspended organic matter from the Santa Barbara Basin, an upwelling area, and also the Benguela upwelling system, were suggested to reflect mainly cooler, deeper water temperatures (Huguet et al., 2007; Lee et al., 2008; Seki et al., 2012). For the Cismon core, given that some of the sediments (excluded here) are known to have been strongly affected by thermally mature allochthonous organic matter input (Bottini et al., 2015), it is more likely that TEX_{86} data from the lowest maturity Cismon sediments are also affected by allochthonous input, producing cooler SST estimates, rather than upwelling or cold surface currents.

4.4.3. Evidence for glaciation in the Cretaceous

The occurrence of cooler episodes and/or ephemeral ice sheets at times in the Cretaceous has been proposed and debated in numerous studies (e.g., Kemper and Schmitz, 1981; Stoll and Schrag, 1996; Price,

1999; Stoll and Schrag, 2000; Miller et al., 2005; Bornemann et al., 2008; Price and Passey, 2013; Ladant and Donnadieu, 2016). Below we discuss evidence for glaciation in the Cretaceous in light of our Cretaceous SST compilation.

4.4.3.1. Evidence for glaciation in the Early Cretaceous. Evidence for cooler episodes during the Early Cretaceous was originally provided by a variety of mineralogical findings including the presence of glendonites (e.g., Kemper and Schmitz, 1981; Kemper, 1987; Price and Nunn, 2010; Rogov and Zakharov, 2010; Grasby et al., 2017), putative tillites and dropstones (Frakes and Francis, 1988; Frakes et al., 1995) and supposed glacial diamictite (Alley and Frakes, 2003) at various high-latitude locations, including Arctic Canada and Australia. Possible cold phases in the Early Cretaceous have also been inferred from $\delta^{18}\text{O}$ values measured in fish teeth enamels (Puc  at et al., 2003; Barbarin et al., 2012), belemnites (Pirrie et al., 1995; Pirrie et al., 2004; Price and Mutterlose, 2004; McArthur et al., 2007; Bodin et al., 2015), carbonate concretions from fluvial sediments (Ferguson et al., 1999), reptile remains (Amiot et al., 2011) and hydrothermal zircon (Yang et al., 2013), as well as bipolar distribution patterns of calcareous nannofossils (Mutterlose et al., 2003; Mutterlose et al., 2009) and the presence of steryl alkyl ethers (Brassell, 2009). Although suggestive of (local) cooler phases, not all of these findings necessarily provide definitive evidence for glaciation, or at least the spatial extent of it. Glendonites, for example, can form in marine and continental bottom waters of up to 4°C and 7°C , respectively (De Lurio and Frakes, 1999, and references therein), but potentially also higher temperatures, in association with methane seeps (Teichert and Luppold, 2013). Dropstones can derive from a number of rafting agents including vegetation (e.g. driftwood), kelp, corals and pumice, vertebrates (via ingestion), as well as icebergs, sea and lake ice (Bennett and Doyle, 1996). Indeed, Lower Cretaceous glendonites and dropstones have been mainly found in epicontinental/shelf seas indicating a potential terrestrial origin (e.g., Kemper, 1987; Frakes and Francis, 1988).

Since most available Cretaceous SST proxy data derive from locations $< \pm 54^\circ$ palaeolatitude, inferences about conditions at polar latitudes rely on extrapolation of these data. The persistence of very warm, $\sim 30\text{--}35^\circ\text{C}$, (sub)tropical surface waters in the Cretaceous does not preclude the presence of ice at the highest latitudes (and/or at high altitudes), but would require an exceptionally steep Pole–Equator thermal gradient at higher latitudes in order to achieve sustained freezing temperatures. Indeed, clumped-isotope palaeotemperature estimates from belemnites for the Berriasian to late Valanginian imply generally warm ($10\text{--}20^\circ\text{C}$) polar ($60\text{--}65^\circ\text{N}$) conditions consistent with a greenhouse climate punctuated by cooler intervals when transient polar ice was possible, particularly at high altitudes (Price and Passey, 2013). Such equable conditions (at least for $\pm 0\text{--}54^\circ$ palaeolatitude) in the Early Cretaceous likely occurred in combination with a hydrosphere significantly different from today, with implications for moisture transport and potential cryosphere development at high southern latitudes (Fl  gel et al., 2011). The current paucity of high-latitude, $> 70^\circ\text{S}$, climate data for the Early Cretaceous along with a lack of detailed understanding of the elevation history of Antarctica implies that, for now, evidence for an Early Cretaceous icehouse from available ‘cool temperature’ proxy data remains equivocal (Jenkyns et al., 2012).

4.4.3.2. Evidence for a Late Aptian ‘cold snap’. On shorter timescales in the Early Cretaceous, micropalaeontological and sedimentological studies (Kemper, 1987; Mutterlose et al., 2009) along with TEX_{86} -derived SSTs from the subtropical Atlantic (McAnena et al., 2013) suggest that episodic (< 2 Myr) interludes of global cooling may have occurred in the Aptian–Albian, in particular a late Aptian ‘cold snap’ ~ 114 Ma during prolonged cooling in the late Aptian (Bodin et al., 2015; Erba et al., 2015). In further support of this contention, Herrle et al. (2015) found glendonite beds in upper Aptian to lower Albian sediments of the Polar Sea, $\sim 118\text{--}112$ Ma, interpreted to reflect the

presence of cool shelf waters in the High Arctic at this time, but not necessarily ice.

4.4.3.3. Evidence for glaciation in the Middle–Late Cretaceous. In the mid-Cretaceous, an interval of glaciation has been reported for the mid-Turonian based on discrete parallel shifts in both planktonic and benthic oxygen-isotope records and sea-level fluctuations (Miller et al., 2004; Bornemann et al., 2008; Galeotti et al., 2009). However, recent $\delta^{18}\text{O}$ temperature reconstructions from Turonian shelf sediments of Tanzania ($\sim 25^\circ\text{S}$ palaeolatitude; MacLeod et al., 2013) indicate stable, hot temperatures, suggesting that the mid-Turonian excursion may not be a global feature (Stoll and Schrag, 2000). An effectively ice-free mid-Cretaceous climate is consistent with our compiled estimates of exceptional low-palaeolatitude and lower mid-palaeolatitude warmth during this time ($\sim 15\text{--}40^\circ\text{C}$, both TEX_{86} and $\delta^{18}\text{O}_{\text{pl}}$ proxy estimates; Fig. 8). Some modelling approaches have indicated that ice growth is possible in the mid-Cretaceous under specific circumstances, i.e. when $p\text{CO}_2$ is < 800 ppm (e.g., Barron et al., 1995; Tabor et al., 2016). However, a recent mixed resolution modelling study suggests that the palaeogeography of the Cenomanian–Turonian renders the Earth System resilient to the inception of Antarctic glaciation under CO_2 concentrations as low as 420 ppm (Ladant and Donnadieu, 2016). Furthermore, at such low $p\text{CO}_2$, modelling studies also indicate that SSTs in extra-tropical regions will not be $> \sim 30^\circ\text{C}$ (e.g., Bice and Norris, 2002). In the Upper Cretaceous, planktonic and benthic oxygen-isotope records show a discrete positive shift in the early Maastrichtian (e.g., Barrera and Savin, 1999; Huber et al., 2002; Friedrich et al., 2009; Friedrich et al., 2012). This excursion may reflect a short-lived glaciation event (e.g., Barrera and Savin, 1999; Miller et al., 1999) and/or cooling of ocean bottom waters associated with a reorganisation of intermediate- to deep-water sources (e.g., Barrera et al., 1997; Friedrich et al., 2009).

In summary, our SST compilation (Fig. 8) documents very warm global Cretaceous SSTs, particularly during the middle to late Aptian and the Cretaceous Thermal Maximum (Cenomanian–Turonian). Under such conditions of global warmth, episodes of sustained continental glaciation seem improbable, at least until the latest Cretaceous.

4.4.4. Latitudinal SST gradients during the Cretaceous

Available evidence suggests that latitudinal temperature gradients were lower in the Cretaceous Period compared with the present day (e.g., Barron, 1983; Huber et al., 1995; Barrera and Savin, 1999; Bice and Norris, 2002; Huber et al., 2002; Littler et al., 2011). This conventionally accepted view is confirmed by our Cretaceous SST compilation, that indicates, regardless of the choice of proxy, TEX_{86} or $\delta^{18}\text{O}_{\text{pl}}$, generally low latitudinal SST gradients between low- and higher mid-palaeolatitude sites, with small SST differences ($\Delta\text{SST} = 3\text{--}17^\circ\text{C}$ prior to the late Campanian; Figs. 8, 9a, b). This observation stands even if the most extreme calibration comparison is made, higher latitude $\delta^{18}\text{O}_{\text{pl}}$ -SSTs with low-latitude $\text{TEX}_{86\text{-Linear}}$ or $\text{BAY}_{\text{GlobR}}$ -SSTs (Fig. 9b).

Our compilation allows examination of the temporal evolution of higher/higher mid- versus low-latitude SST conditions. We compute the SST gradient (low–higher mid, ΔSST) based on compiled $\text{TEX}_{86}^{\text{H}}$ and $\delta^{18}\text{O}_{\text{pl}}$ higher mid-palaeolatitude ($48\text{--}54^\circ\text{S}$ palaeolatitude, with the addition of a small amount of data from Arctic Ocean Core FL533, $\sim 80^\circ\text{N}$ palaeolatitude) and low-palaeolatitude ($< \pm 30^\circ$) SST estimates, separately fitted with a LOESS smooth function, span = 0.5, using the PAST software package (Hammer et al., 2001; Fig. 9a). Note, in general there is little difference if the Cretaceous latitudinal SST gradient is calculated with $\text{TEX}_{86\text{-Linear}}$ SST data rather than $\text{TEX}_{86}^{\text{H}}$ SST data (Fig. 9b) or solely $\delta^{18}\text{O}_{\text{pl}}$ SST data (Supplementary Fig. 3), the resulting latitudinal SST gradient reconstructions often overlap. Uncertainty envelopes ($\pm 95\%$ confidence band) for the curves were calculated using an inbuilt bootstrap method based on 999 random replicates (Fig. 9a, b). LOESS curves were interpolated at 1.0 Myr resolution in order to compute the gradient. Limitations of the SST proxy

data (e.g., signal depth; see earlier discussion) mean that temporal trends are likely more robust than absolute SST estimates using this approach. Importantly, we regard our ΔSST reconstruction for the Early Cretaceous (Fig. 9c) as tentative since a crucial caveat of the available data is that Early Cretaceous ΔSST s are based on TEX_{86} -SST estimates only, whereas ΔSST s for the middle to Late Cretaceous are generated from low-palaeolatitude TEX_{86} and $\delta^{18}\text{O}_{\text{pl}}$ data minus higher palaeolatitude $\delta^{18}\text{O}_{\text{pl}}$ proxy data, with the exception of a few TEX_{86} values for the Arctic Ocean (Jenkyns et al., 2004). This comparison implies that a low-palaeolatitude minus higher palaeolatitude TEX_{86} gradient would tend to give lower ΔSST s compared with a TEX_{86} and $\delta^{18}\text{O}_{\text{pl}}$ minus

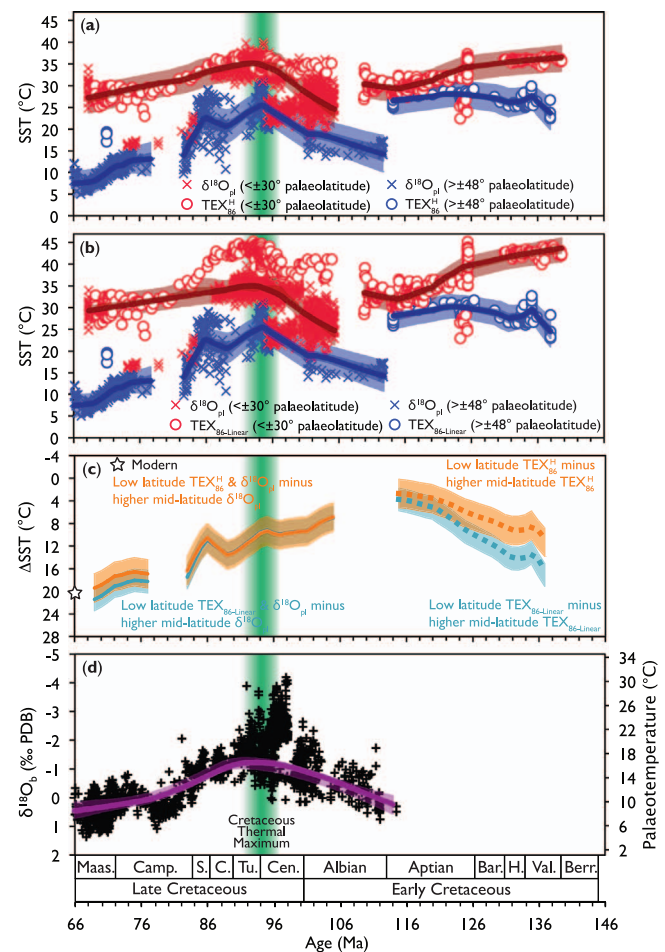


Fig. 9. Evolution of the latitudinal SST gradient during the Cretaceous Period. Smoothed SST estimates, (a) $\text{TEX}_{86}^{\text{H}}$ and $\delta^{18}\text{O}_{\text{pl}}$ and (b) $\text{TEX}_{86\text{-Linear}}$ and $\delta^{18}\text{O}_{\text{pl}}$, for low ($< \pm 30^\circ$; red smoothed line) and higher middle ($> \pm 48^\circ$; blue smoothed line) palaeolatitude settings for the Cretaceous. Low and higher mid-palaeolatitude temperature data were smoothed using a LOESS function (span = 0.5; thick red and blue lines). (c) Latitudinal SST temperature gradient (thick lines) based on the difference between LOESS smoothed low, $< \pm 30^\circ$, and higher mid-, $> \pm 48^\circ$, palaeolatitude $\text{TEX}_{86}^{\text{H}}$ (orange)/ $\text{TEX}_{86\text{-Linear}}$ (light blue) and $\delta^{18}\text{O}_{\text{pl}}$ SST estimates, after interpolating at 1 Myr resolution. Dashed lines represent 'tentative' latitudinal SST temperature gradient reconstructions for the Early Cretaceous, calculated in the same way as for the middle–Late Cretaceous but only using $\text{TEX}_{86}^{\text{H}}$ / $\text{TEX}_{86\text{-Linear}}$ SST data. Note, for the Albian–Santonian interval the different latitudinal SST gradient reconstructions overlap. The modern mean annual latitudinal SST gradient between $0\text{--}30^\circ$ and $\pm 48\text{--}54^\circ$ is also indicated (Kim et al., 2010) (d) Global benthic oxygen-isotope, $\delta^{18}\text{O}_{\text{b}}$, data (Friedrich et al., 2012); palaeotemperatures also indicated. In all cases, narrower shaded band represents 95% confidence interval for the LOESS fit, derived using a bootstrap technique. Wider shaded bands, panels (a, b, c), represent the calibration error associated with the TEX_{86} -SST estimates; $\pm 2.5^\circ\text{C}$ for the $\text{TEX}_{86}^{\text{H}}$ calibration (Kim et al., 2010) and $\pm 2.0^\circ\text{C}$ for $\text{TEX}_{86\text{-Linear}}$ calibration. The calibration error for the $\delta^{18}\text{O}_{\text{pl}}$ -SST data is not indicated but is substantially smaller, $\pm 0.7^\circ\text{C}$ (Bemis et al., 1998). Green shaded region represents the Cretaceous Thermal Maximum. (For interpretation of the references to colour in this figure legend, the reader is referred to the web version of this article.)

$\delta^{18}\text{O}_{\text{pl}}$ gradient, due to $\delta^{18}\text{O}_{\text{pl}}$ yielding cooler and more variable SSTs.

In agreement with Littler et al. (2011), our reconstruction indicates that the latitudinal SST gradient was lower in the Early Cretaceous, weakening from $\sim 10^\circ\text{C}$ (low-latitude $\text{TEX}_{86}^{\text{H}}$ minus higher mid-latitude $\text{TEX}_{86}^{\text{H}}$) in the Valanginian to $\sim 3^\circ\text{C}$ (low latitude $\text{TEX}_{86}^{\text{H}}$ minus higher mid-latitude $\text{TEX}_{86}^{\text{H}}$) in the middle–late Aptian (Fig. 9c). This reduction in the latitudinal SST gradient is steeper, $\sim 12^\circ\text{C}$ compared with $\sim 7^\circ\text{C}$, if $\text{TEX}_{86}^{\text{Linear}}$ values are used instead (Fig. 9c). For the latest Aptian (115–113 Ma) to mid-Albian (104 Ma) there is a gap in the reconstructed latitudinal SST gradient reconstruction because of a lack of SST data from low palaeolatitudes. From the mid-Albian to the Turonian our reconstruction indicates that the latitudinal SST gradient gradually increased from ~ 7 to $\sim 13^\circ\text{C}$ (low-latitude $\text{TEX}_{86}^{\text{H}}/\text{TEX}_{86}^{\text{Linear}}$ and $\delta^{18}\text{O}_{\text{pl}}$ minus higher mid-latitude $\delta^{18}\text{O}_{\text{pl}}$). This trend is almost identical if instead only low-latitude $\delta^{18}\text{O}_{\text{pl}}$ SSTs minus higher mid-latitude $\delta^{18}\text{O}_{\text{pl}}$ SSTs are considered (Supplementary Fig. 3). For the early–mid Campanian there is another gap in our ΔSST reconstruction arising from a lack of higher latitude SST data. By the late Campanian the latitudinal SST gradient was ~ 16 – 18°C (low-latitude $\text{TEX}_{86}^{\text{H}}/\text{TEX}_{86}^{\text{Linear}}$ and $\delta^{18}\text{O}_{\text{pl}}$ minus higher mid-latitude $\delta^{18}\text{O}_{\text{pl}}$) and gradually strengthened as a result of greater cooling at higher latitudes, reaching a maximum, ~ 19 – 21°C (low-latitude $\text{TEX}_{86}^{\text{H}}/\text{TEX}_{86}^{\text{Linear}}$ and $\delta^{18}\text{O}_{\text{pl}}$ minus higher mid-latitude $\delta^{18}\text{O}_{\text{pl}}$), in the late Maastrichtian.

It should be noted that our reference to ‘latitudinal SST gradient’ does not represent the full Equator–Pole temperature differential for the Cretaceous Period but the difference between our compilation of SSTs for low- and higher mid-latitude sites. Specifically, all data from ‘low-latitude’ sites encompass SST estimates for ± 5 – 30° palaeolatitude, whereas ‘higher mid-latitude’ sites included in this compilation, with the exception of the Arctic Ocean (Core FL533, $\sim 80^\circ\text{N}$ palaeolatitude) originate from sites located between ± 48 – 54° palaeolatitude in the Southern hemisphere. Nevertheless, the observed long-term shifts in the magnitude of the low- minus higher mid-latitude SST gradient, at least from the middle Cretaceous (weak) to the Late Cretaceous (less weak) likely resemble long-term trends in Equator–Pole temperature gradients.

Interestingly, the ΔSST gradient appears weakest in the Aptian, rather than at the Cretaceous Thermal Maximum during the Cenomanian–Turonian interval. This observation reflects, at least in part, the fact that the latitudinal gradient is generated from both higher mid-latitude and low-latitude TEX_{86} data for the Early Cretaceous, and from a combination of low-palaeolatitude TEX_{86} and $\delta^{18}\text{O}_{\text{pl}}$ data minus higher mid-palaeolatitude $\delta^{18}\text{O}_{\text{pl}}$ data for the middle to Late Cretaceous (Fig. 9a, b, c). This switch in the comparison of data from different proxies may influence temporal trends, particularly for the high palaeolatitudes where minimum $\delta^{18}\text{O}_{\text{pl}}$ -SST estimates are cooler than minimum TEX_{86} -SSTs (Figs. 8, 9a, b) resulting in stronger latitudinal SST contrasts. In addition, this observation may be biased by a combination of a lack of mid-Cretaceous TEX_{86} data from high palaeolatitudes ($> \pm 48^\circ$) and potential secondary influences either from cool biases in some $\delta^{18}\text{O}_{\text{pl}}$ records, inaccuracies in assumptions for conversion of $\delta^{18}\text{O}_{\text{pl}}$ values to palaeotemperature estimates, and/or warm biases in TEX_{86} -SST estimates.

The LOESS fit approach provides a broad picture of the evolution of SSTs and ΔSSTs during the Cretaceous and, within error, captures the full range of raw SST estimates when the $\text{TEX}_{86}^{\text{H}}$ calibration is applied (Fig. 9a). On shorter timescales, certain details may, however, be lost. During the Cretaceous Thermal Maximum, SSTs at higher mid-latitudes ($> \pm 48^\circ$ palaeolatitude) reached values similar to the tropics, ~ 18 – 31°C , suggesting a dramatic collapse of the latitudinal SST gradient. However, the LOESS model predicts higher mid-latitude SSTs of $\sim 25^\circ\text{C}$ and therefore does not record this potentially significant decrease in the latitudinal SST gradient at this time (Fig. 9a, b, c, Supplementary Fig. 3), suggesting that the LOESS model may overestimate the ΔSST gradient during the Turonian.

Overall, taking into account uncertainties in the LOESS model and

associated proxy errors, our latitudinal ΔSST reconstruction tentatively indicates that the latitudinal thermal gradient was higher in the Early Cretaceous and then weakened around the time of the early Aptian OAE 1a event. The ΔSST gradient was likely relatively low in the middle Cretaceous and then increased in the Late Cretaceous (Campanian–Maastrichtian). These reconstructions suggest that latitudinal temperature gradients were in general very low when global temperatures were high, in accord with similar observations made for the Eocene (Bijl et al., 2009; Hollis et al., 2012; Inglis et al., 2015). This result remains valid for the Cretaceous Period regardless of the combination of proxies used (TEX_{86} and $\delta^{18}\text{O}_{\text{pl}}$). Moreover, this weak Cretaceous latitudinal SST gradient, at least for the middle to early Late Cretaceous, offers little support for periods of large-scale ice growth.

4.5. Comparison with benthic $\delta^{18}\text{O}$ records

Comparisons between our SST compilation and global benthic foraminifer oxygen-isotope records for the middle–Late Cretaceous climate (Fig. 9d) suggest that, in general, surface and intermediate to deep-water temperatures responded similarly to changes in climate during this time interval. Friedrich et al. (2012) separate their $\delta^{18}\text{O}_{\text{b}}$ compilation into four intervals; (1) increasing temperatures from 112 to 97 Ma, Albian to mid-Cenomanian; (2) the subsequent Cenomanian–Turonian hot greenhouse interval, 97 to 91 Ma; (3) a long-lasting cooling trend between 91 and 78 Ma, late Turonian to mid-Campanian; and (4) the interval after 78 Ma, mid-Campanian to Maastrichtian, with small inter-ocean $\delta^{18}\text{O}_{\text{b}}$ values. Similar to the $\delta^{18}\text{O}_{\text{b}}$ compilation (Fig. 9d; Friedrich et al., 2012), our SST compilation also suggests increasing temperatures from the latest Aptian through Cenomanian interval, although the evidence for this trend is affected by the scarcity of SST data (particularly TEX_{86} data) during the Albian. Our SST compilation clearly demonstrates the significance of the hot Cenomanian–Turonian greenhouse, particularly at low palaeolatitudes and lower mid-palaeolatitudes (Figs. 8, 9a, b). The cooling recorded in the $\delta^{18}\text{O}_{\text{b}}$ compilation during the late Turonian to mid-Campanian is evident in SSTs from both low palaeolatitudes and lower mid-palaeolatitude locations, and likely also higher mid-palaeolatitudes, although the data again require cautious interpretation owing to their paucity. For the final interval, mid-Campanian to Maastrichtian, the $\delta^{18}\text{O}_{\text{b}}$ values of all ocean basins are similar. Such regionally similar bottom-water palaeotemperatures contrast with surface-ocean conditions, which display the strongest latitudinal differences and also the most significant cooling of the entire Cretaceous during this time. These differences likely reflect the strong influence of changes in inter-basin exchange on deep-water temperature signatures or, alternatively, changes in water-mass formation. A full connection between all ocean basins following the complete opening of the Equatorial Atlantic Gateway would have filled the North Atlantic with cool high-latitude waters, homogenizing global $\delta^{18}\text{O}_{\text{b}}$ values for the latest Cretaceous and reorganizing atmospheric circulation and the hydrological cycle both regionally and globally. Likewise, more deep- and/or intermediate-water formation at high latitudes and a reduction of the proposed formation of warm and salty water masses in the subtropics could have resulted in small $\delta^{18}\text{O}_{\text{b}}$ interbasin gradients (Barrera et al., 1997; Friedrich et al., 2004; Friedrich et al., 2009).

5. Outlook

5.1. Missing climate proxy data in time and space

Our Cretaceous SST compilation highlights several important ‘gaps’ in the data currently available that, were they to be filled, would significantly improve understanding of Cretaceous surface-ocean conditions. Temporally, there is a paucity of SST data for the Berriasian and Albian stages. For proxy comparison purposes, there are only five sites, ODP Sites 1049, 1258, 1259, 1260 and DSDP Site 511 for which both

$\delta^{18}\text{O}_{\text{pl}}$ and TEX_{86} data exist, although for DSDP 511 the $\delta^{18}\text{O}_{\text{pl}}$ and TEX_{86} data are stratigraphically non-contemporaneous. Part of the challenge is finding Cretaceous sediments with sufficient organic matter where foraminifera are still well-preserved. One suggestion would be to target coastal shelf sites – productive settings with high organic-carbon burial and shallow waters reducing dissolution of foraminiferal calcite.

Spatially, prior to ~125 Ma there are no data from the palaeo-Pacific Ocean, which constituted more than half of the world ocean during the Cretaceous (e.g., Hay et al., 1999; Scotese, 2004). The ability to sample particularly Early Cretaceous oceans is in part limited by the loss of the ancient oceanic record via subduction. Geographical coverage improves for the middle–Late Cretaceous relative to the Early Cretaceous, although there is a paucity of SST data from higher palaeolatitudes, particularly during the Cenomanian to Coniacian and during the early to middle Campanian, compounded by lack of TEX_{86} data from high-palaeolatitude locations in general. Moreover, the data from the higher palaeolatitudes typically reflect conditions between ± 48 – 54° palaeolatitude in the Southern Hemisphere, and are therefore not wholly representative of Equator–Pole temperature trends.

These palaeoclimate data ‘gaps’ are not restricted to SST proxy data; similar to planktonic foraminifera, there is a lack of benthic foraminiferal $\delta^{18}\text{O}$ data for the Early Cretaceous (Fig. 9d; Friedrich et al., 2012), and a lack of high-resolution $p\text{CO}_2$ proxy estimates, especially for the long quiet magnetic period in the middle Cretaceous, prevents a more comprehensive understanding of Cretaceous- CO_2 climate linkage (Li et al., 2014; Wang et al., 2014). A central motivation to improving our understanding of Cretaceous climate is to understand how sensitive the Earth's climate may be to much higher $p\text{CO}_2$ (e.g., PALEOSENS Project Members, 2012). Royer et al. (2012) estimate a Cretaceous Earth System Sensitivity of $\sim 3^\circ\text{C}$ but up to 6°C for the late Cenomanian–Coniacian (~95–85 Ma) based on available palaeo-reconstructions of $p\text{CO}_2$ and temperature circa 2012. Our compilation adds further constraints on (global) SST evolution during the Cretaceous. Ultimately, however, further studies are needed to elucidate the magnitude and variability of $p\text{CO}_2$, e.g., understanding episodic cyclic changes in $p\text{CO}_2$ during the middle–late Early Cretaceous (Li et al., 2014), as well as other second-order controls on climate such as palaeogeography.

5.2. Proxy data quality and interpretation

A recommendation regarding the quality of TEX_{86} data is that workers report BIT values and, perhaps more importantly for Cretaceous sediments, the maturity of the samples (biomarker sterane and hopane ratios; Schouten et al., 2004) alongside TEX_{86} values and individual GDGT relative abundances. Regarding the quality of Cretaceous planktonic $\delta^{18}\text{O}$ data, it would be beneficial to have more values from exclusively ‘glassy’ foraminifera. In addition, the development of standardized criteria for assessing foraminiferal preservation and better reporting of such preservation for each sample/sample interval would improve comparisons drawing on data generated from a variety of localities by different workers (i.e. this study). In terms of improving proxy confidence, the application of additional approaches like clumped-isotope palaeothermometry would provide independent constraints on SST and the oxygen-isotope content of seawater. Both the TEX_{86} and $\delta^{18}\text{O}$ proxies suffer from extrapolation beyond the modern calibration range, while the clumped isotopes approach does not, although such measurements present different challenges, e.g., the requirement for large amount of sample (carbonate) material (e.g., Spencer and Kim, 2015). In addition, this approach will not resolve other questions important for interpretation of $\delta^{18}\text{O}$ data, e.g., planktonic foraminiferal ecology.

5.3. Future climate modelling efforts

Our new Cretaceous SST synthesis provides an up-to-date target for future modelling studies investigating the mechanics of Cretaceous warmth. In particular, modelling of Cretaceous climate could help disentangle the relative importance of CO_2 and palaeogeography (and resulting changes in atmospheric and ocean circulation) for Cretaceous surface-ocean conditions. For example, climate modelling can be used to test hypotheses about the nature of Cretaceous latitudinal sea-surface temperature gradients under higher $p\text{CO}_2$ conditions akin to data-model comparisons already undertaken for intervals of the Late Cretaceous (Taber et al., 2016; Petersen et al., 2016). Similarly, our compiled SSTs can provide climate constraints when modelling other Cretaceous climate forcing factors including the role of clouds (Sloan and Pollard, 1998; Kirk-Davidoff et al., 2002; Abbot et al., 2012) and biological cloud feedbacks (Kump and Pollard, 2008; Upchurch et al., 2015), variations in the mixing ratios of non- CO_2 greenhouse gases (Beerling et al., 2011), long-term changes in the percentage of atmospheric oxygen (Poulsen et al., 2015), the possibility of multiple ocean steady states (Poulsen and Zhou, 2013) and polar forest vegetation-induced warming (Otto-Bliesner and Upchurch, 1997; Zhou et al., 2012) throughout the entire Cretaceous. Modelling can also be employed to explore the influence of changes in ocean-basin configuration (e.g., Poulsen et al., 2001; Zhou et al., 2008; Lunt et al., 2016), quantification of seawater $\delta^{18}\text{O}$ gradients (e.g., Roche et al., 2006; Zhou et al., 2008) with the inclusion of isotopic tracers in GCMs (cf. Speelman et al., 2010) and/or surface and intermediate- to deep-water circulation on Cretaceous SSTs. Some such studies have already been undertaken for certain Cretaceous time intervals, e.g., short-term, ~2.5 Myr, biogeochemical modelling of the carbon cycle in the Late Aptian (McAnena et al., 2013). Donnadieu et al. (2016) modelled ocean circulation modes during two Late Cretaceous time slices in order to assess the role of changes in major continental configuration, comparing simulated ocean dynamics with existing neodymium-isotope data. Changes in Cretaceous ocean chemistry, in particular neodymium-isotope patterns (e.g., Pucéat et al., 2005; Robinson et al., 2010; Le Houedec et al., 2012; Robinson and Vance, 2012; Jung et al., 2013; Murphy and Thomas, 2013; Voigt et al., 2013; Zheng et al., 2013) indicate some interesting shifts in ocean circulation modes in the Late Cretaceous that may be important for SSTs. Finally, it is likely that some of the trends in our SST proxy data compilation are due to sampling sites moving in latitude as consequence of sea-floor spreading and continental drift, e.g., northward movement of the Pacific plate (Berger and Winterer, 1974). Future analyses might include a systematic point-by-point comparison with climate model simulations to quantify this effect, as well as longitudinal SST variations, which are obscured in gradient plots.

6. Summary

Using published SST proxy data, planktonic foraminiferal oxygen isotopes and GDGT distributions, we have generated a SST compilation for the entire Cretaceous Period. Our compilation uses SSTs recalculated from raw data, allowing examination of the sensitivity of each proxy to the calculation method, including choice of calibration, and places all data on a common timescale. In addition, we have investigated secondary controls on Cretaceous GDGT distributions through application of a range of GDGT indices – BIT, MI, $f_{\text{Cren}^+/\text{Cren}^+ + \text{Cren}^-}$, and ΔRI , compared together with modern GDGT distributions. After screening the raw GDGT data for problematic samples and considering the impacts of preservation and other non-temperature influences on Cretaceous $\delta^{18}\text{O}_{\text{pl}}$ records, all robust data were then used to generate a Cretaceous SST compilation. Overall, our compilation shows many stratigraphic similarities with other records of Cretaceous climate change, including benthic foraminiferal $\delta^{18}\text{O}$ records, with both SST proxies indicating maximum warmth (SSTs $> 30^\circ\text{C}$ at low and lower mid-latitudes) in the Cenomanian–Turonian interval (97–90 Ma).

Similarly, both $\delta^{18}\text{O}_{\text{pl}}$ - and TEX_{86} -SST estimates indicate prolonged cooling of the surface ocean and possible changes in ocean heat transport in the Late Cretaceous through the Coniacian–Santonian to the end-Maastrichtian interval.

Our reconstruction of the evolution of latitudinal temperature gradients (low, $< \pm 30^\circ$, minus higher middle, $> \pm 48^\circ$, palaeolatitudes) reveals distinct temporal changes. During the Early Cretaceous the latitudinal temperature gradient, TEX_{86} minus TEX_{86} , was low (~ 10 – 17°C ; late Valanginian to early Barremian, 135–129 Ma) to very low (~ 3 – 5°C ; mid-Aptian, 123–117 Ma). During the middle Cretaceous, latitudinal temperature contrasts, TEX_{86} and $\delta^{18}\text{O}_{\text{pl}}$ minus $\delta^{18}\text{O}_{\text{pl}}$, are also inferred to have been low ($< 14^\circ\text{C}$; Cenomanian–Santonian), while, in the Late Cretaceous, latitudinal temperature gradients, TEX_{86} and $\delta^{18}\text{O}_{\text{pl}}$ minus $\delta^{18}\text{O}_{\text{pl}}$, increased significantly (~ 17 – 20°C ; mid-Campanian to end-Maastrichtian), with cooling occurring at low, lower middle and higher middle palaeolatitudes.

Supplementary data to this article can be found online at <http://dx.doi.org/10.1016/j.earscirev.2017.07.012>.

Acknowledgements

C.L.O.B., S.A.R., D.J.L., A.F. and R.D.P. were all supported by a Natural Environment Research Council Standard Grant: 'Cretaceous-Palaeocene-Eocene: Exploring Climate and Climate Sensitivity', NE/K012479/1 and NE/K014757/1. R.D.P. acknowledges the Royal Society Wolfson Research Merit Award. J.S.S.D. and S.S. were supported by the Netherlands Earth System Science Centre (NESSC), financially supported by the Ministry of Education, Culture and Science (OCW). C.L.O.B. thanks for Peter Illner for useful discussions. C.L.O.B. and R.D.P. thank Jessica Tierney for helpful discussions regarding the application of BAYSPAR. Specific acknowledgements of funding and support pertaining to the data reinterpreted in this manuscript can be found in the original publications. We thank two anonymous reviewers and the editors, Paul Wilson and André Strasser, for providing detailed comments and suggestions that helped improve this manuscript.

References

- Abbot, D.S., Voigt, A., Branson, M., Pierrehumbert, R.T., Pollard, D., Le Hir, G., Koll, D.D., 2012. Clouds and snowball earth deglaciation. *Geophys. Res. Lett.* 39, L20711. <http://dx.doi.org/10.1029/2012GL052861>.
- Alley, N.F., Frakes, L.A., 2003. First known cretaceous glaciation: Livingston tillite member of the Cadna-owie formation, South Australia. *Aust. J. Earth Sci.* 50, 139–144.
- Alsenz, H., Regnery, J., Ashkenazi-Polivoda, S., Meilijson, A., Ron-Yankovich, L., Abramovich, S., Illner, P., Almogi-Labin, A., Feinstein, S., Berner, Z., Püttmann, W., 2013. Sea surface temperature record of a Late Cretaceous tropical southern Tethys upwelling system. *Palaeogeogr. Palaeoclimatol. Palaeoecol.* 392, 350–358.
- Amiot, R., Lécuyer, C., Buffetaut, E., Fluteau, F., Legendre, S., Martineau, F., 2004. Latitudinal temperature gradient during the Cretaceous Upper Campanian–Middle Maastrichtian: $\delta^{18}\text{O}$ record of continental vertebrates. *Earth Planet. Sci. Lett.* 226, 255–272.
- Amiot, R., Wang, X., Zhou, Z., Wang, X., Buffetaut, E., Lécuyer, C., Ding, Z., Fluteau, F., Hibino, T., Kusuhashi, N., 2011. Oxygen isotopes of East Asian dinosaurs reveal exceptionally cold Early Cretaceous climates. *Proc. Natl. Acad. Sci.* 108, 5179–5183.
- Ando, A., Huber, B.T., MacLeod, K.G., Ohta, T., Kim, B.-K., 2009. Blake Nose stable isotopic evidence against the mid-Cenomanian glaciation hypothesis. *Geology* 37, 451–454.
- Ando, A., Huber, B.T., MacLeod, K.G., 2010. Depth-habitat reorganization of planktonic foraminifera across the Albian/Cenomanian boundary. *Paleobiology* 36, 357–373.
- Ando, A., Huber, B.T., MacLeod, K.G., Watkins, D.K., 2015. Early Cenomanian “hot greenhouse” revealed by oxygen isotope record of exceptionally well-preserved foraminifera from Tanzania. *Paleoceanography* 30, 1556–1572.
- Aquilina, A., Knab, N., Knittel, K., Kaur, G., Geissler, A., Kelly, S., Fossing, H., Boot, C., Parkes, R., Mills, R., 2010. Biomarker indicators for anaerobic oxidizers of methane in brackish-marine sediments with diffusive methane fluxes. *Org. Geochem.* 41, 414–426.
- Ashkenazi-Polivoda, S., Abramovich, S., Almogi-Labin, A., Schneider-Mor, A., Feinstein, S., Püttmann, W., Berner, Z., 2011. Palaeoenvironments of the latest Cretaceous oil shale sequence, Southern Tethys, Israel, as an integral part of the prevailing upwelling system. *Palaeogeogr. Palaeoclimatol. Palaeoecol.* 305, 93–108.
- Askin, R.A., 1989. Endemism and heterochrony in the Late Cretaceous (Campanian) to Paleocene palynofloras of Seymour Island, Antarctica: implications for origins, dispersal and palaeoclimates of southern floras. *Geol. Soc. Lond., Spec. Publ.* 47, 107–119.
- Barbarin, N., Bonin, A., Mattioli, E., Pucéat, E., Cappetta, H., Gréselle, B., Pittet, B., Vennin, E., Joachimski, M., 2012. Evidence for a complex Valanginian nannoconid decline in the Vocontian basin (South East France). *Mar. Micropaleontol.* 84, 37–53.
- Barclay, R.S., McElwain, J.C., Sageman, B.B., 2010. Carbon sequestration activated by a volcanic CO_2 pulse during ocean anoxic event 2. *Nat. Geosci.* 3, 205–208.
- Barrera, E., Huber, B.T., 1990. Evolution of Antarctic waters during the Maastrichtian: foraminifer oxygen and carbon isotope ratios, Leg 113. In: Barker, P.F., Kennett, J.P., O'Connell, S., Berkowitz, S., Bryant, W.R., Burckle, L.H., Egeberg, P.K., Fiitterer, D.K., Qersonde, R.E., Qolovchenko, X., Hamilton, N., Lawver, L., Lazarus, D.B., Lonsdale, M., Mohr, B., Toshiyasu Nagao, T., Pereira, C.P.Q., Pudsey, C.J., Robert, C.M., Schandl, E., Speijer, V., Stott, L.D., Thomas, E., Thompson, K.F.M., Wise, S.W. (Eds.), *Proceedings of the Ocean Drilling Program, Scientific Results*. Vol. 113 U.S. Government Printing Office, Washington, DC.
- Barrera, E., Savin, S.M., 1999. Evolution of late Campanian–Maastrichtian marine climates and oceans. In: Barrera, E., Johnson, C.C. (Eds.), *Evolution of the Cretaceous Ocean-climate System*. Geological Society of America Special Paper Vol. 332. pp. 245–282.
- Barrera, E., Savin, S.M., Thomas, E., Jones, C.E., 1997. Evidence for thermohaline-circulation reversals controlled by sea-level change in the latest Cretaceous. *Geology* 25, 715–718.
- Barron, E.J., 1983. A warm, equable Cretaceous: the nature of the problem. *Earth Sci. Rev.* 19, 305–338.
- Barron, E.J., Fawcett, P.J., Peterson, W.H., Pollard, D., Thompson, S.L., 1995. A “simulation” of Mid-Cretaceous climate. *Paleoceanography* 10, 953–962.
- Beck, W.C., Grossman, E.L., Morse, J.W., 2005. Experimental studies of oxygen isotope fractionation in the carbonic acid system at 15, 25, and 40°C . *Geochim. Cosmochim. Acta* 69, 3493–3503.
- Beerling, D.J., Fox, A., Stevenson, D.S., Valdes, P.J., 2011. Enhanced chemistry-climate feedbacks in past greenhouse worlds. *Proc. Natl. Acad. Sci.* 108, 9770–9775.
- Bemis, E., Spero, H.J., Bijma, J., Lea, D.W., 1998. Reevaluation of the oxygen isotopic composition of planktonic foraminifera: experimental results and revised paleo-temperature equations. *Paleoceanography* 13, 150–160.
- Bennett, M.R., Doyle, P., 1996. Global cooling inferred from dropstones in the Cretaceous: fact or wishful thinking? *Terra Nova* 8, 182–185.
- Berger, W.H., Winterer, E.L., 1974. Plate stratigraphy and the fluctuating carbonate line. In: Hsü, K.J., Jenkyns, H.C. (Eds.), *Pelagic Sediments: On Land and Under the Sea*. Blackwell Publishing Ltd., Oxford, UK.
- Bernasconi, S.M., Schmid, T.W., Grauel, A.-L., Mutterlose, J., 2011. Clumped-isotope geochemistry of carbonates: a new tool for the reconstruction of temperature and oxygen isotope composition of seawater. *Appl. Geochem.* 26, S279–S280.
- Bice, K.L., Norris, R.D., 2002. Possible atmospheric CO_2 extremes of the Middle Cretaceous (late Albian–Turonian). *Paleoceanography* 17, 1070. <http://dx.doi.org/10.1029/2002PA000778>.
- Bice, K.L., Norris, R.D., 2005. Data report: stable isotope ratios of foraminifera from ODP Leg 207, Sites 1257, 1258, and 1260 and a cleaning procedure for foraminifera in organic-rich shales. In: Mosher, D.C., Erbacher, J., Malone, M.J. (Eds.), *Proceedings of the Ocean Drilling Program, Scientific Results*. Vol. 207.
- Bice, K.L., Huber, B.T., Norris, R.D., 2003. Extreme polar warmth during the Cretaceous greenhouse? Paradox of the late Turonian $\delta^{18}\text{O}$ record at Deep Sea Drilling Project Site 511. *Paleoceanography* 18, 1031. <http://dx.doi.org/10.1029/2002PA000848>.
- Bice, K.L., Birgel, D., Meyers, P.A., Dahl, K.A., Hinrichs, K.U., Norris, R.D., 2006. A multiple proxy and model study of Cretaceous upper ocean temperatures and atmospheric CO_2 concentrations. *Paleoceanography* 21, PA2002. <http://dx.doi.org/10.1029/2005PA001203>.
- Bijl, P.K., Schouten, S., Sluijs, A., Reichert, G.-J., Zachos, J.C., Brinkhuis, H., 2009. Early Palaeogene temperature evolution of the southwest Pacific Ocean. *Nature* 461, 776–779.
- Bijl, P.K., Bendle, J.A.P., Bohaty, S.M., Pross, J., Schouten, S., Tauxe, L., Stickley, C.E., McKay, R.M., Röhl, U., Olney, M., 2013. Eocene cooling linked to early flow across the Tasmanian Gateway. *Proc. Natl. Acad. Sci.* 110, 9645–9650.
- Bijma, J., Hemleben, C., 1994. Population dynamics of the planktic foraminifer *Globigerinoides sacculifer* (Brady) from the central Red Sea. *Deep-Sea Res. I Oceanogr. Res. Pap.* 41, 485–510.
- Blaga, C.I., Reichert, G.-J., Heiri, O., Sinninghe Damsté, J.S., 2009. Tetraether membrane lipid distributions in water-column particulate matter and sediments: a study of 47 European lakes along a north–south transect. *J. Paleolimnol.* 41, 523–540.
- Blumenberg, M., Seifert, R., Reitner, J., Pape, T., Michaelis, W., 2004. Membrane lipid patterns typify distinct anaerobic methanotrophic consortia. *Proc. Natl. Acad. Sci. U. S. A.* 101, 11111–11116.
- Bodin, S., Meissner, P., Janssen, N.M., Steuber, T., Mutterlose, J., 2015. Large igneous provinces and organic carbon burial: controls on global temperature and continental weathering during the Early Cretaceous. *Glob. Planet. Chang.* 133, 238–253.
- Bornemann, A., Norris, R.D., 2007. Size-related stable isotope changes in Late Cretaceous planktic foraminifera: implications for paleoecology and photosymbiosis. *Mar. Micropaleontol.* 65, 32–42.
- Bornemann, A., Norris, R.D., Friedrich, O., Beckmann, B., Schouten, S., Sinninghe Damsté, J.S., Vogel, J., Hofmann, P., Wagner, T., 2008. Isotopic evidence for glaciation during the Cretaceous supergreenhouse. *Science* 319, 189–192.
- Botini, C., Erba, E., Tiraboschi, D., Jenkyns, H.C., Schouten, S., Sinninghe Damsté, J.S., 2015. Climate variability and ocean fertility during the Aptian Stage. *Clim. Past* 11, 383–402.
- Brassell, S.C., 2009. Steryl ethers in a Valanginian claystone: molecular evidence for cooler waters in the central Pacific during the Early Cretaceous? *Palaeogeogr. Palaeoclimatol. Palaeoecol.* 282, 45–57.

- Clarke, L.J., Jenkyns, H.C., 1999. New oxygen isotope evidence for long-term Cretaceous climatic change in the southern hemisphere. *Geology* 27, 699–702.
- Cramer, B., Toggweiler, J., Wright, J., Katz, M., Miller, K., 2009. Ocean overturning since the Late Cretaceous: inferences from a new benthic foraminiferal isotope compilation. *Paleoceanography* 24, PA4216. <http://dx.doi.org/10.1029/2008PA001683>.
- Cramer, B., Miller, K., Barrett, P., Wright, J., 2011. Late Cretaceous–Neogene trends in deep ocean temperature and continental ice volume: reconciling records of benthic foraminiferal geochemistry ($\delta^{18}\text{O}$ and Mg/Ca) with sea level history. *J. Geophys. Res. Oceans* (1978–2012), 116. C12023. <http://dx.doi.org/10.1029/2011JC007255>.
- Crowley, T.J., Zachos, J.C., 2000. Comparison of zonal temperature profiles for past warm time periods. *Warm Clim. Earth Hist.* 50–76.
- De Lurio, J.L., Frakes, L., 1999. Glendonites as a paleoenvironmental tool: implications for early Cretaceous high latitude climates in Australia. *Geochim. Cosmochim. Acta* 63, 1039–1048.
- De Nooijer, L.J., Toyofuku, T., Kitazato, H., 2009. Foraminifera promote calcification by elevating their intracellular pH. *Proc. Natl. Acad. Sci.* 106, 15374–15378.
- Dennis, K.J., Cochran, J.K., Landman, N.H., Schrag, D.P., 2013. The climate of the Late Cretaceous: new insights from the application of the carbonate clumped isotope thermometer to Western Interior Seaway macrofossil. *Earth Planet. Sci. Lett.* 362, 51–65.
- D'Hondt, S., Arthur, M.A., 1996. Late Cretaceous oceans and the cool tropic paradox. *Science* 271, 1838–1841.
- Donnadieu, Y., Pucéat, E., Moiroud, M., Guillocheau, F., Deconinck, J.F., 2016. A better-ventilated ocean triggered by Late Cretaceous changes in continental configuration. *Nat. Commun.* 7, 10316. <http://dx.doi.org/10.1038/ncomms10316>.
- van Duin, A.C., Sinninghe Damsté, J.S., Kodpman, M.P., van De Graaf, B., De Leeuw, J.W., 1997. A kinetic calculation method of homohopane maturation: applications in the reconstruction of burial histories of sedimentary basins. *Geochim. Cosmochim. Acta* 61, 2409–2429.
- Dumitrescu, M., Brassell, S.C., Schouten, S., Hopmans, E.C., Sinninghe Damsté, J.S., 2006. Instability in tropical Pacific sea-surface temperatures during the early Aptian. *Geology* 34, 833–836.
- Edelman-Furstenberg, Y., 2009. Cyclic upwelling facies along the Late Cretaceous southern Tethys (Israel): taphonomic and ichnofacies evidence of a high-productivity mosaic. *Cretac. Res.* 30, 847–863.
- Elling, F.J., Könneke, M., Lipp, J.S., Becker, K.W., Gagen, E.J., Hinrichs, K.-U., 2014. Effects of growth phase on the membrane lipid composition of the thaumarchaeon *Nitrosopumilus maritimus* and their implications for archaeal lipid distributions in the marine environment. *Geochim. Cosmochim. Acta* 141, 579–597.
- Elling, F.J., Könneke, M., Mußmann, M., Greve, A., Hinrichs, K.-U., 2015. Influence of temperature, pH, and salinity on membrane lipid composition and TEX₈₆ of marine planktonic thaumarchaeal isolates. *Geochim. Cosmochim. Acta* 171, 238–255.
- Erba, E., Duncan, R.A., Bottini, C., Tiraboschi, D., Weissert, H., Jenkyns, H.C., Malinverno, A., 2015. Environmental consequences of Ontong Java Plateau and Kerguelen Plateau volcanism. In: Neal, C.R., Sager, W.W., Sano, T., Erba, E. (Eds.), *The Origin, Evolution, and Environmental Impact of Oceanic Large Igneous Provinces*. Geological Society of America Special Paper Vol. 511. pp. 271–303.
- Erbacher, J., Huber, B.T., Norris, R.D., Markey, M., 2001. Increased thermohaline stratification as a possible cause for an ocean anoxic event in the Cretaceous period. *Nature* 409, 325–327.
- Erbacher, J., Friedrich, O., Wilson, P.A., Lehmann, J., Weiss, W., 2011. Short-term warming events during the boreal Albian (mid-Cretaceous). *Geology* 39, 223–226.
- Erez, J., Luz, B., 1983. Experimental paleotemperature equation for planktonic foraminifera. *Geochim. Cosmochim. Acta* 47, 1025–1031.
- Falzone, F., Petrizzo, M.R., Clarke, L.J., MacLeod, K.G., Jenkyns, H.C., 2016. Long-term Late Cretaceous oxygen and carbon-isotope trends and planktonic foraminiferal turnover: a new record from the southern midlatitudes. *Geol. Soc. Am. Bull.* 128, 1725–1735.
- Fassell, M.L., Bralower, T.J., 1999. Warm, equable mid-Cretaceous: stable isotope evidence. In: BARRERA, E., JOHNSON, C.C. (Eds.), *Evolution of the Cretaceous Ocean-climate System*. Geological Society of America Special Paper Vol. 332. pp. 121–142.
- Ferguson, K.M., Gregory, R.T., Constantine, A., 1999. Lower Cretaceous (Aptian-Albian) secular changes in the oxygen and carbon isotope record from high paleolatitude, fluvial sediments, southeast Australia: comparisons to the marine record. In: Barrera, E., Johnson, C.C. (Eds.), *Evolution of the Cretaceous Ocean-climate System*. Geological Society of America Special Paper Vol. 332. pp. 59–72.
- Flögel, S., Wallmann, K., Kuhnt, W., 2011. Cool episodes in the Cretaceous—exploring the effects of physical forcings on Antarctic snow accumulation. *Earth Planet. Sci. Lett.* 307, 279–288.
- Forster, A., Schouten, S., Baas, M., Sinninghe Damsté, J.S., 2007a. Mid-Cretaceous (Albian–Santonian) sea surface temperature record of the tropical Atlantic Ocean. *Geology* 35, 919–922.
- Forster, A., Schouten, S., Moriya, K., Wilson, P.A., Sinninghe Damsté, J.S., 2007b. Tropical warming and intermittent cooling during the Cenomanian/Turonian oceanic anoxic event 2: sea surface temperature records from the equatorial Atlantic. *Paleoceanography* 22, PA1219. <http://dx.doi.org/10.1029/2006PA001349>.
- Frakes, L., Francis, J., 1988. A guide to Phanerozoic cold polar climates from high-latitude ice-rafting in the Cretaceous. *Nature* 333, 547–549.
- Frakes, L., Francis, J., Syktus, J., 1992. Climate Modes of the Phanerozoic: The History of the Earth's Climate Over the Past 600 Million Years. Cambridge University Press, Cambridge.
- Frakes, L., Alley, N., Deynoux, M., 1995. Early Cretaceous ice rafting and climate zonation in Australia. *Int. Geol. Rev.* 37, 567–583.
- Francis, J.E., Frakes, L., 1993. Cretaceous climates. In: Wright, V.P. (Ed.), *Sedimentology Review 1*. Blackwell Publishing Ltd., Oxford, UK.
- Freeman, K.H., Hayes, J., 1992. Fractionation of carbon isotopes by phytoplankton and estimates of ancient CO₂ levels. *Glob. Biogeochem. Cycles* 6, 185–198.
- Friedrich, O., Erbacher, J., 2006. Benthic foraminiferal assemblages from Demerara Rise (ODP Leg 207, western tropical Atlantic): possible evidence for a progressive opening of the Equatorial Atlantic Gateway. *Cretac. Res.* 27, 377–397.
- Friedrich, O., Herrle, J.O., Köhler, P., Hemleben, C., 2004. Early Maastrichtian stable isotopes: changing deep water sources in the North Atlantic? *Paleoceanogr. Palaeoclimatol. Palaeoecol.* 211, 171–184.
- Friedrich, O., Erbacher, J., Moriya, K., Wilson, P.A., Kuhnert, H., 2008. Warm saline intermediate waters in the Cretaceous tropical Atlantic Ocean. *Nat. Geosci.* 1, 453–457.
- Friedrich, O., Herrle, J.O., Wilson, P.A., Cooper, M.J., Erbacher, J., Hemleben, C., 2009. Early Maastrichtian carbon cycle perturbation and cooling event: implications from the South Atlantic Ocean. *Paleoceanography* 24, PA2211. <http://dx.doi.org/10.1029/2008PA001654>.
- Friedrich, O., Norris, R.D., Erbacher, J., 2012. Evolution of middle to Late Cretaceous oceans—a 55 my record of Earth's temperature and carbon cycle. *Geology* 40, 107–110.
- Galeotti, S., Rusciadelli, G., Sprovieri, M., Lanci, L., Gaudio, A., Pekar, S., 2009. Sea-level control on facies architecture in the Cenomanian–Coniacian Apulian margin (Western Tethys): a record of glacio-eustatic fluctuations during the Cretaceous greenhouse? *Paleoceanogr. Palaeoclimatol. Palaeoecol.* 276, 196–205.
- Gradstein, F.M., Ogg, J.G., Smith, A.G. (Eds.), 2004. *Geologic Time Scale*. Cambridge University Press.
- Gradstein, F.M., Ogg, J.G., Schmitz, M., Ogg, G., 2012. *The Geological Time Scale 2012*. Volume Set. Elsevier.
- Grasby, S.E., McCune, G.E., Beauchamp, B., Galloway, J.M., 2017. Lower Cretaceous cold snaps led to widespread glendonite occurrences in the Sverdrup Basin, Canadian High Arctic. *Geol. Soc. Am. Bull.* 129, 771–787. <http://dx.doi.org/10.1130/B31600.1>.
- Hammer, Ø., Harper, D., Ryan, P., 2001. *PAST—Paleontological Statistics*. www.uv.es/~pardomv/pe/2001_1/past/pastprog/past.pdf (accessed on 25, 2009).
- Hag, B.U., 2014. Cretaceous eustasy revisited. *Glob. Planet. Chang.* 113, 44–58.
- Hay, W.W., Floegge, S., 2012. New thoughts about the Cretaceous climate and oceans. *Earth Sci. Rev.* 115, 262–272.
- Hay, W.W., Deconto, R.M., Wold, C.N., Wilson, K.M., Voigt, S., Schulz, M., Wold, A.R., Dullo, W.-C., Ronov, A.B., Balukhovskiy, A.N., Soding, E., 1999. Alternative global Cretaceous paleogeography. In: Barrera, E., Johnson, C.C. (Eds.), *Evolution of the Cretaceous Ocean-climate System*. Geological Society of America Special Paper Vol. 332. pp. 1–47.
- van Helmond, N.A.G.M., Sluijs, A., Reichert, G.-J., Sinninghe Damsté, J.S., Slomp, C.P., Brinkhuis, H., 2014. A perturbed hydrological cycle during Oceanic Anoxic Event 2. *Geology* 42, 123–126.
- van Helmond, N.A.G.M., Sluijs, A., Sinninghe Damsté, J.S., Reichert, G.-J., Voigt, S., Erbacher, J., Pross, J., Brinkhuis, H., 2015. Freshwater discharge controlled deposition of Cenomanian–Turonian black shales on the NW European epicontinental shelf (Wunstorf, northern Germany). *Clim. Past* 11, 495–508.
- Hemleben, C., Spindler, M., Erson, O., 1989. *Modern Planktonic Foraminifera*. Springer, New York.
- Herman, A.B., Spicer, R.A., 1996. Palaeobotanical evidence for a warm Cretaceous Arctic Ocean. *Nature* 380, 330–333.
- Hernández-Sánchez, M.T., Woodward, E.M.S., Taylor, K.W.R., Henderson, G.M., Pancost, R.D., 2014. Variations in GDGT distributions through the water column in the South East Atlantic Ocean. *Geochim. Cosmochim. Acta* 132, 337–348.
- Herrle, J.O., Schröder-Adams, C.J., Davis, W., Pugh, A.T., Galloway, J.M., Fath, J., 2015. Mid-Cretaceous high Arctic stratigraphy, climate, and oceanic anoxic events. *Geology* 43, 403–406.
- van Hinsbergen, D.J., De Groot, L.V., van Schaik, S.J., Spakman, W., Bijl, P.K., Sluijs, A., Langereis, C.G., Brinkhuis, H., 2015. A Paleolatitude Calculator for Paleoclimate Studies. *PLoS One* 10, e0126946.
- Ho, S.L., Laepple, T., 2016. Flat meridional temperature gradient in the early Eocene in the subsurface rather than surface ocean. *Nat. Geosci.* 9, 606–610.
- Ho, S.L., Mollenhauer, G., Fietz, S., Martínez-García, A., Lamy, F., Rueda, G., Schipper, K., Méheust, M., Rosell-Melé, A., Stein, R., 2014. Appraisal of TEX₈₆ and thermometries in subpolar and polar regions. *Geochim. Cosmochim. Acta* 131, 213–226.
- Hofmann, P., Stüsser, I., Wagner, T., Schouten, S., Sinninghe Damsté, J.S., 2008. Climate–ocean coupling off North-West Africa during the lower Albian: the oceanic anoxic event 1b. *Paleoceanogr. Palaeoclimatol. Palaeoecol.* 262, 157–165.
- Hollis, C.J., Taylor, K.W.R., Handley, L., Pancost, R.D., Huber, M., Creech, J.B., Hines, B.R., Crouch, E.M., Morgans, H.E., Crampton, J.S., 2012. Early Paleogene temperature history of the Southwest Pacific Ocean: reconciling proxies and models. *Earth Planet. Sci. Lett.* 349, 53–66.
- Hönisch, B., Allen, K.A., Lea, D.W., Spero, H.J., Eggins, S.M., Arbuszewski, J., Dumenil, P., Rosenthal, Y., Russell, A.D., Elderfield, H., 2013. The influence of salinity on Mg/Ca in planktic foraminifera – evidence from cultures, core-top sediments and complementary $\delta^{18}\text{O}$. *Geochim. Cosmochim. Acta* 121, 196–213.
- Hopmans, E.C., Weijers, J.W.H., Schefuß, E., Herfort, L., Sinninghe Damsté, J.S., Schouten, S., 2004. A novel proxy for terrestrial organic matter in sediments based on branched and isoprenoid tetraether lipids. *Earth Planet. Sci. Lett.* 224, 107–116.
- Houston, R.M., Huber, B.T., Spero, H.J., 1999. Size-related isotopic trends in some Maastrichtian planktic foraminifera: methodological comparisons, intraspecific variability, and evidence for photosymbiosis. *Mar. Micropaleontol.* 36, 169–188.
- Huber, B.T., Hodell, D.A., Hamilton, C.P., 1995. Middle–Late Cretaceous climate of the southern high latitudes: stable isotopic evidence for minimal equator-to-pole thermal gradients. *Geol. Soc. Am. Bull.* 107, 1164–1191.
- Huber, B.T., Norris, R.D., MacLeod, K.G., 2002. Deep-sea paleotemperature record of extreme warmth during the Cretaceous. *Geology* 30, 123–126.
- Huber, B.T., MacLeod, K.G., Gröcke, D.R., Kucera, M., 2011. Paleotemperature and paleosalinity inferences and chemostratigraphy across the Aptian/Albian boundary in

- the subtropical North Atlantic. *Paleoceanography* 26, PA4221. <http://dx.doi.org/10.1029/2011PA002178>.
- Huguet, C., Schimmelmann, A., Thunell, R., Lourens, L.J., Sinninghe Damsté, J.S., Schouten, S., 2007. A study of the TEX₈₆ paleothermometer in the water column and sediments of the Santa Barbara Basin, California. *Paleoceanography* 22, PA3203.
- Huguet, C., De Lange, G.J., Gustafsson, Ö., Middelburg, J.J., Sinninghe Damsté, J.S., Schouten, S., 2008. Selective preservation of soil organic matter in oxidized marine sediments (Madeira Abyssal Plain). *Geochim. Cosmochim. Acta* 72, 6061–6068.
- Huguet, C., Kim, J.-H., De Lange, G.J., Sinninghe Damsté, J.S., Schouten, S., 2009. Effects of long term oxic degradation on the TEX₈₆ and BIT organic proxies. *Org. Geochem.* 40, 1188–1194.
- Hurley, S.J., Elling, F.J., Könneke, M., Buchwald, C., Wankel, S.D., Santoro, A.E., Lipp, J.S., Hinrichs, K.-U., Pearson, A., 2016. Influence of ammonia oxidation rate on thaumarchaeal lipid composition and the TEX₈₆ temperature proxy. *Proc. Natl. Acad. Sci.* 113, 7762–7767.
- Hut, G., 1987. Consultants' Group Meeting on Stable Isotope Reference Samples for Geochemical and Hydrological Investigations. International Atomic Energy Agency, Vienna, pp. 42.
- Inglis, G.N., Farnsworth, A., Lunt, D., Foster, G.L., Hollis, C.J., Pagani, M., Jardine, P.E., Pearson, P.N., Markwick, P., Galsworthy, A.M.J., Raynham, L., Taylor, K.W.R., Pancost, R.D., 2015. Descent towards the icehouse: Eocene sea surface cooling inferred from GDGT distributions. *Paleoceanography* 29, 1000–1020. <http://dx.doi.org/10.1002/2014PA002723>.
- Jarvis, I., Lignum, J.S., Gröcke, D.R., Jenkyns, H.C., Pearce, M.A., 2011. Black shale deposition, atmospheric CO₂ drawdown, and cooling during the Cenomanian–Turonian Oceanic Anoxic Event. *Paleoceanography* 26, PA3201. <http://dx.doi.org/10.1029/2010PA002081>.
- Jenkyns, H.C., 2010. Geochemistry of oceanic anoxic events. *Geochim. Geophys. Geosyst.* 11, Q03004. <http://dx.doi.org/10.1029/2009GC002788>.
- Jenkyns, H.C., Gale, A.S., Corfield, R.M., 1994. Carbon and oxygen isotope stratigraphy of the English Chalk and Italian Scaglia and its palaeoclimatic significance. *Geol. Mag.* 131, 1–34.
- Jenkyns, H.C., Forster, A., Schouten, S., Sinninghe Damsté, J.S., 2004. High temperatures in the late Cretaceous Arctic Ocean. *Nature* 432, 888–892.
- Jenkyns, H.C., Schouten-Huibers, L., Schouten, S., Sinninghe Damsté, J.S., 2012. Warm Middle Jurassic–Early Cretaceous high-latitude sea-surface temperatures from the Southern Ocean. *Clim. Past* 8, 215–226.
- Jenkyns, H.C., Dickson, A.J., Ruhl, M., Boorn, S.H.J.M., 2017. Basalt–seawater interaction, the Plenus Cold Event, enhanced weathering and geochemical change: deconstructing Oceanic Anoxic Event 2 (Cenomanian–Turonian, Late Cretaceous). *Sedimentology* 64, 16–43.
- Jung, C., Voigt, S., Friedrich, O., Koch, M.C., Frank, M., 2013. Campanian–Maastrichtian ocean circulation in the tropical Pacific. *Paleoceanography* 28, 562–573.
- Kemper, E., 1987. Das Klima der Kreide-Zeit. *Geologisches Jahrbuch, Reihe-A* 96, 5–185.
- Kemper, E., Schmitz, H.H., 1981. Glendonite—Indikatoren des polarmarinen Ablagerungsmilieus. *Geol. Rundsch.* 70, 759–773.
- Kim, S.-T., O'Neil, J.R., 1997. Equilibrium and nonequilibrium oxygen isotope effects in synthetic carbonates. *Geochim. Cosmochim. Acta* 61, 3461–3475.
- Kim, J.H., Schouten, S., Hopmans, E.C., Donner, B., Sinninghe Damsté, J.S., 2008. Global sediment core-top calibration of the TEX₈₆ paleothermometer in the ocean. *Geochim. Cosmochim. Acta* 72, 1154–1173.
- Kim, J.-H., Huguet, C., Zonneveld, K.A., Versteegh, G.J., Roeder, W., Sinninghe Damsté, J.S., Schouten, S., 2009. An experimental field study to test the stability of lipids used for the TEX₈₆ and U₃₇^K paleothermometers. *Geochim. Cosmochim. Acta* 73, 2888–2898.
- Kim, J.H., van der Meer, J., Schouten, S., Helmke, P., Willmott, V., Sangiorgi, F., Koç, N., Hopmans, E.C., Sinninghe Damsté, J.S., 2010. New indices and calibrations derived from the distribution of crenarchaeal isoprenoid tetraether lipids: implications for past sea surface temperature reconstructions. *Geochim. Cosmochim. Acta* 74, 4639–4654.
- Kim, J.-H., Schouten, S., Rodrigo-Gámiz, M., Rampen, S., Marino, G., Huguet, C., Helmke, P., Buscail, R., Hopmans, E.C., Pross, J., Sangiorgi, F., Middelburg, J.B.M., Sinninghe Damsté, J.S., 2015. Influence of deep-water derived isoprenoid tetraether lipids on the paleothermometer in the Mediterranean Sea. *Geochim. Cosmochim. Acta* 150, 125–141.
- Kim, J.-H., Villanueva, L., Zell, C., Sinninghe Damsté, J.S., 2016. Biological source and provenance of deep-water derived isoprenoid tetraether lipids along the Portuguese continental margin. *Geochim. Cosmochim. Acta* 172, 177–204.
- Kirk-Davidoff, D.B., Schrag, D.P., Anderson, J.G., 2002. On the feedback of stratospheric clouds on polar climate. *Geophys. Res. Lett.* 29.
- Koga, Y., Akagawa-Matsushita, M., Ohga, M., Nishihara, M., 1993. Taxonomic significance of the distribution of component parts of polar ether lipids in methanogens. *Syst. Appl. Microbiol.* 16, 342–351.
- Kump, L.R., Pollard, D., 2008. Amplification of Cretaceous warmth by biological cloud feedbacks. *Science* 320, 195.
- Ladant, J.-B., Donnadieu, Y., 2016. Palaeogeographic regulation of glacial events during the Cretaceous supergreenhouse. *Nat. Commun.* 7.
- Le Houedec, S., Meynadier, L., Cogné, J.P., Allègre, C.J., Gourel, A.T., 2012. Oceanwide imprint of large tectonic and oceanic events on seawater Nd isotope composition in the Indian Ocean from 90 to 40 Ma. *Geochim. Geophys. Geosyst.* 13, Q06008. <http://dx.doi.org/10.1029/2011GC003963>.
- Lee, K.E., Kim, J.H., Wilke, I., Helmke, P., Schouten, S., 2008. A study of the alkenone, TEX₈₆, and planktonic foraminifera in the Benguela upwelling system: implications for past sea surface temperature estimates. *Geochim. Geophys. Geosyst.* 9, Q10019. <http://dx.doi.org/10.1029/2008GC002056>.
- Lengger, S.K., Kraaij, M., Tjallingii, R., Baas, M., Stuut, J.-B., Hopmans, E.C., Sinninghe Damsté, J.S., Schouten, S., 2013. Differential degradation of intact polar and core glycerol dialkyl glycerol tetraether lipids upon post-depositional oxidation. *Org. Geochem.* 65, 83–93.
- Lhomme, N., Clarke, G.K., Ritz, C., 2005. Global budget of water isotopes inferred from polar ice sheets. *Geophys. Res. Lett.* 32, L20502. <http://dx.doi.org/10.1029/2005GL023774>.
- Li, X., Jenkyns, H.C., Zhang, C., Wang, Y., Liu, L., Cao, K., 2014. Carbon isotope signatures of pedogenic carbonates from SE China: rapid atmospheric pCO₂ changes during middle–late Early Cretaceous time. *Geol. Mag.* 151, 830–849.
- Linnert, C., Robinson, S.A., Lees, J.A., Bown, P.R., Pérez-Rodríguez, I., Petrizzo, M.R., Falzoni, F., Littler, K., Arz, J.A., Russell, E.E., 2014. Evidence for global cooling in the Late Cretaceous. *Nat. Commun.* 5, 4194. <http://dx.doi.org/10.1038/ncomms5194>.
- Littler, K., Robinson, S.A., Bown, P.R., Nederbragt, A.J., Pancost, R.D., 2011. High sea-surface temperatures during the Early Cretaceous Epoch. *Nat. Geosci.* 4, 169–172.
- Littler, K., Robinson, S.A., Bown, P.R., 2014. An offset in TEX₈₆ values between interbedded lithologies: implications for sea-surface temperature reconstructions. *Palaeogeogr. Palaeoclimatol. Palaeoecol.* 399, 42–51.
- Liu, Z., Pagani, M., Zinniker, D., Deconto, R., Huber, M., Brinkhuis, H., Shah, S.R., Leckie, R.M., Pearson, A., 2009. Global cooling during the Eocene–Oligocene climate transition. *Science* 323, 1187–1190.
- Lunt, D.J., Farnsworth, A., Loftson, C., Foster, G.L., Markwick, P., O'Brien, C.L., Pancost, R.D., Robinson, S.A., Wrobel, N., 2016. Palaeogeographic controls on climate and proxy interpretation. *Clim. Past* 12, 1181–1198.
- MacLeod, K.G., Huber, B.T., Berrocoso, Á.J., Wendler, I., 2013. A stable and hot Turonian without glacial ^δ18O excursions is indicated by exquisitely preserved Tanzanian foraminifera. *Geology* 41, 1083–1086.
- McAnena, A., Flögel, S., Hofmann, P., Herrle, J., Griesand, A., Pross, J., Talbot, H., Rethemeyer, J., Wallmann, K., Wagner, T., 2013. Atlantic cooling associated with a marine biotic crisis during the mid-Cretaceous period. *Nat. Geosci.* 6, 558–561.
- McArthur, J., Janssen, N., Reboulet, S., Leng, M., Thirwall, M., van de Schootbrugge, B., 2007. Palaeotemperatures, polar ice-volume, and isotope stratigraphy (Mg/Ca, ^δ18O, ^δ13C, ⁸⁷Sr/⁸⁶Sr): the Early Cretaceous (Berriasian, Valanginian, Hauterivian). *Palaeogeogr. Palaeoclimatol. Palaeoecol.* 248, 391–430.
- Miller, K.G., Barrera, E., Olsson, R.K., Sugarman, P.J., Savin, S.M., 1999. Does ice drive early Maastrichtian eustasy? *Geology* 27, 783–786.
- Miller, K.G., Sugarman, P.J., Browning, J.V., Komiz, M.A., Olsson, R.K., Feigenson, M.D., Hernández, J.C., 2004. Upper Cretaceous sequences and sea-level history, New Jersey coastal plain. *Geol. Soc. Am. Bull.* 116, 368–393.
- Miller, K.G., Komiz, M.A., Browning, J.V., Wright, J.D., Mountain, G.S., Katz, M.E., Sugarman, P.J., Cramer, B.S., Christie-Blick, N., Pekar, S.F., 2005. The Phanerozoic record of global sea-level change. *Science* 310, 1293–1298.
- Mohtadi, M., Oppo, D.W., Lückge, A., Depol-Holz, R., Steinke, S., Groeneveld, J., Hemme, N., Hebbeln, D., 2011. Reconstructing the thermal structure of the upper ocean: insights from planktic foraminifera shell chemistry and alkenones in modern sediments of the tropical eastern Indian Ocean. *Paleoceanography* 26, PA3219. <http://dx.doi.org/10.1029/2011PA002132>.
- Moriya, K., Wilson, P.A., Friedrich, O., Erbacher, J., Kawahata, H., 2007. Testing for ice sheets during the mid-Cretaceous greenhouse using glassy foraminiferal calcite from the mid-Cenomanian tropics on Demerara Rise. *Geology* 35, 615–618.
- Multza, S., Donner, B., Fischer, G., Paul, A., Pätzold, J., Rühlemann, C., Segl, M., 2004. The South Atlantic oxygen isotope record of planktic foraminifera. In: *The South Atlantic in the Late Quaternary*. Springer, pp. 121–142.
- Murphy, D.P., Thomas, D.J., 2013. The evolution of Late Cretaceous deep-ocean circulation in the Atlantic basins: neodymium isotope evidence from South Atlantic drill sites for tectonic controls. *Geochim. Geophys. Geosyst.* 14, 5323–5340.
- Mutterlose, J., Brumsack, H., Flögel, S., Hay, W., Klein, C., Langrock, U., Lipinski, M., Ricken, W., Söding, E., Stein, R., 2003. The Greenland–Norwegian Seaway: a key area for understanding Late Jurassic to Early Cretaceous paleoenvironments. *Paleoceanography* 18, 1010. <http://dx.doi.org/10.1029/2001PA000625>.
- Mutterlose, J., Bornemann, A., Herrle, J., 2009. The Aptian–Albian cold snap: evidence for “mid” Cretaceous icehouse interludes. *Neues Jahrbuch für Geologie und Paläontologie-Abhandlungen* 252, 217–225.
- Mutterlose, J., Malkoc, M., Schouten, S., Sinninghe Damsté, J.S., Forster, A., 2010. TEX₈₆ and stable ^δ18O paleothermometry of early Cretaceous sediments: implications for belemnite ecology and paleotemperature proxy application. *Earth Planet. Sci. Lett.* 298, 286–298.
- Mutterlose, J., Malkoc, M., Schouten, S., Sinninghe Damsté, J.S., 2012. Reconstruction of vertical temperature gradients in past oceans—proxy data from the Hauterivian–early Barremian (Early Cretaceous) of the Boreal Realm. *Palaeogeogr. Palaeoclimatol. Palaeoecol.* 363, 135–143.
- Mutterlose, J., Bottini, C., Schouten, S., Sinninghe Damsté, J.S., 2014. High sea-surface temperatures during the early Aptian Oceanic Anoxic Event 1a in the Boreal Realm. *Geology* 42, 439–442.
- Naafs, B.D.A., Pancost, R.D., 2016. Sea-surface temperature evolution across Aptian Oceanic Anoxic Event 1a. *Geology* 44, 959–962.
- Nathorst, A.G., 1890. Ueber die Reste eines Broffruchtbaums *Artocarpus Dicksoni* n. sp., aus den cenomanen Kreideablagerungen Grönlands. *Kongl. Svenska Vetenskaps-Akad. Hand.* 24, 2–9.
- Niebler, H.-S., Hubberten, H.-W., Gersonde, R., 1999. Oxygen isotope values of planktic foraminifera: a tool for the reconstruction of surface water stratification. In: Fischer, G., Wefer, G. (Eds.), *Use of Proxies in Paleoclimatology*. Springer, pp. 165–189.
- Norris, R.D., Wilson, P.A., 1998. Low-latitude sea-surface temperatures for the mid-Cretaceous and the evolution of planktic foraminifera. *Geology* 26, 823–826.
- Norris, R.D., Bice, K.L., Magno, E.A., Wilson, P.A., 2002. Jiggling the tropical thermostat in the Cretaceous hothouse. *Geology* 30, 299–302.
- Otto-Bliesner, B.L., Upchurch Jr., G.R., 1997. Vegetation-induced warming of high-

- latitude regions during the Late Cretaceous period. *Nature* 385, 804–807.
- PALEOSENS Project Members, 2012. Making sense of palaeoclimate sensitivity. *Nature* 491, 683–691.
- Pancost, R.D., Hopmans, E.C., Sinninghe Damsté, J.S., 2001. Archaeal lipids in Mediterranean cold seeps: molecular proxies for anaerobic methane oxidation. *Geochim. Cosmochim. Acta* 65, 1611–1627.
- Pearson, P.N., 2012. Oxygen isotopes in foraminifera: overview and historical review. *Paleontol. Soc. Pap.* 18, 1–38.
- Pearson, A., Ingalls, A.E., 2013. Assessing the use of archaeal lipids as marine environmental proxies. *Annu. Rev. Earth Planet. Sci.* 41, 359–384.
- Pearson, P.N., Ditchfield, P.W., Singano, J., Harcourt-Brown, K.G., Nicholas, C.J., Olsson, R.K., Shackleton, N.J., Hall, M.A., 2001. Warm tropical sea surface temperatures in the Late Cretaceous and Eocene epochs. *Nature* 413, 481–487.
- Pearson, P.N., van Dongen, B.E., Nicholas, C.J., Pancost, R.D., Schouten, S., Singano, J.M., Wade, B.S., 2007. Stable warm tropical climate through the Eocene Epoch. *Geology* 35, 211–214.
- Peterse, F., Kim, J.-H., Schouten, S., Kristensen, D.K., Koç, N., Sinninghe Damsté, J.S., 2009. Constraints on the application of the MBT/CBT palaeothermometer at high latitude environments (Svalbard, Norway). *Org. Geochem.* 40, 692–699.
- Petersen, S.V., Tabor, C.R., Lohmann, K.C., Poulsen, C.J., Meyer, K.W., Carpenter, S.J., Erickson, J.M., Matsunaga, K.K., Smith, S.Y., Sheldon, N.D., 2016. Temperature and salinity of the Late Cretaceous Western Interior Seaway. *Geology* 44, 903–906.
- Petrizzo, M.R., Huber, B.T., Wilson, P.A., MacLeod, K.G., 2008. Late Albian paleoceanography of the western subtropical North Atlantic. *Paleoceanography* 23, PA1213. <http://dx.doi.org/10.1029/2007PA001517>.
- Pirrie, D., Doyle, P., Marshall, J., Ellis, G., 1995. Cool Cretaceous climates: new data from the Albian of Western Australia. *J. Geol. Soc.* 152, 739–742.
- Pirrie, D., Marshall, J., Doyle, P., Riccardi, A., 2004. Cool early Albian climates; new data from Argentina. *Cretac. Res.* 25, 27–33.
- Pitcher, A., Rychlik, N., Hopmans, E.C., Spieck, E., Rijpstra, W.I.C., Ossebaer, J., Schouten, S., Wagner, M., Sinninghe Damsté, J.S., 2010. Crenarchaeol dominates the membrane lipids of *Candidatus Nitrososphaera gargensis*, a thermophilic Group I.1b Archaeon. *ISME J.* 4, 542–552.
- Poole, I., Cantrill, D., Utescher, T., 2005. A multi-proxy approach to determine Antarctic terrestrial palaeoclimate during the Late Cretaceous and Early Tertiary. *Palaeogeogr. Palaeoclimatol. Palaeoecol.* 222, 95–121.
- Poulsen, C.J., Zhou, J., 2013. Sensitivity of Arctic climate variability to mean state: insights from the Cretaceous. *J. Clim.* 26, 7003–7022.
- Poulsen, C.J., Barron, E.J., Peterson, W.H., Wilson, P.A., 1999. A reinterpretation of Mid-Cretaceous shallow marine temperatures through model-data comparison. *Paleoceanography* 14, 679–697.
- Poulsen, C.J., Barron, E.J., Arthur, M.A., Peterson, W.H., 2001. Response of the mid-Cretaceous global oceanic circulation to tectonic and CO₂ forcings. *Paleoceanography* 16, 576–592.
- Poulsen, C.J., Gendaszek, A.S., Jacob, R.L., 2003. Did the rifting of the Atlantic Ocean cause the Cretaceous thermal maximum? *Geology* 31, 115–118.
- Poulsen, C.J., Tabor, C., White, J.D., 2015. Long-term climate forcing by atmospheric oxygen concentrations. *Science* 348, 1238–1241.
- Powers, L., Werne, J.P., Vanderwoude, A.J., Sinninghe Damsté, J.S., Schouten, S., 2010. Applicability and calibration of the TEX₈₆ paleothermometer in lakes. *Org. Geochem.* 41, 404–413.
- Price, G.D., 1999. The evidence and implications of polar ice during the Mesozoic. *Earth Sci. Rev.* 48, 183–210.
- Price, G., Mutterlose, J., 2004. Isotopic signals from late Jurassic–early Cretaceous (Volgian–Valanginian) sub-Arctic belemnites, Yatria River, Western Siberia. *J. Geol. Soc.* 161, 959–968.
- Price, G.D., Nunn, E.V., 2010. Valanginian isotope variation in glendonites and belemnites from Arctic Svalbard: transient glacial temperatures during the Cretaceous greenhouse. *Geology* 38, 251–254.
- Price, G.D., Passey, B.H., 2013. Dynamic polar climates in a greenhouse world: evidence from clumped isotope thermometry of Early Cretaceous belemnites. *Geology* 41, 923–926.
- Pucéat, E., Lécuyer, C., Sheppard, S.M., Dromart, G., Reboulet, S., Grandjean, P., 2003. Thermal evolution of Cretaceous Tethyan marine waters inferred from oxygen isotope composition of fish tooth enamels. *Paleoceanography* 18, 1029. <http://dx.doi.org/10.1029/2002PA000823>.
- Pucéat, E., Lécuyer, C., Reisberg, L., 2005. Neodymium isotope evolution of NW Tethyan upper ocean waters throughout the Cretaceous. *Earth Planet. Sci. Lett.* 236, 705–720.
- Qin, W., Carlson, L.T., Armbrust, E.V., Devol, A.H., Moffett, J.W., Stahl, D.A., Ingalls, A.E., 2015. Confounding effects of oxygen and temperature on the TEX₈₆ signature of marine Thaumarchaeota. *Proc. Natl. Acad. Sci.* 112, 10979–10984.
- Ravelo, A.C., Hillaire-Marcel, C., 2007. The use of oxygen and carbon isotopes of foraminifera in paleoceanography. In: Hillaire-Marcel, C., De Vernal, A. (Eds.), *Developments in Marine Geology*. Elsevier, pp. 735–764.
- Robinson, S.A., Vance, D., 2012. Widespread and synchronous change in deep-ocean circulation in the North and South Atlantic during the Late Cretaceous. *Paleoceanography* 27, PA1102. <http://dx.doi.org/10.1029/2011PA002240>.
- Robinson, S.A., Murphy, D.P., Vance, D., Thomas, D.J., 2010. Formation of “southern component water” in the Late Cretaceous: evidence from Nd-isotopes. *Geology* 38, 871–874.
- Roche, D., Donnadiou, Y., Pucéat, E., Paillard, D., 2006. Effect of changes in $\delta^{18}\text{O}$ content of the surface ocean on estimated sea surface temperatures in past warm climate. *Paleoceanography* 21, PA2023. <http://dx.doi.org/10.1029/2005PA001220>.
- Rogov, M., Zakharov, V., 2010. Jurassic and Lower Cretaceous glendonite occurrences and their implication for Arctic paleoclimate reconstructions and stratigraphy. *Earth Sci. Front.* 17, 345–346.
- Royer, D.L., Berner, R.A., Montañez, I.P., Tabor, N.J., Beerling, D.J., 2004. CO₂ as a primary driver of Phanerozoic climate. *GSA Today* 14, 4–10.
- Royer, D.L., Pagani, M., Beerling, D., 2012. Geobiological constraints on Earth system sensitivity to CO₂ during the Cretaceous and Cenozoic. *Geobiology* 10, 298–310.
- Rudnicki, M.D., Wilson, P.A., Anderson, W.T., 2001. Numerical models of diagenesis, sediment properties, and pore fluid chemistry on a paleoceanographic transect: Blake Nose, Ocean Drilling Program Leg 171B. *Paleoceanography* 16, 563–575.
- Schiebel, R., Hemleben, C., 2005. Modern planktic foraminifera. *Paläontol. Z.* 79, 135–148.
- Schlanger, S.O., Jenkyns, H.C., 1976. Cretaceous oceanic anoxic events: cause and consequence. *Geol. Mijnb.* 55, 179–184.
- Schlanger, S., Arthur, M., Jenkyns, H., Scholle, P., 1987. The Cenomanian-Turonian Oceanic Anoxic Event, I. Stratigraphy and distribution of organic carbon-rich beds and the marine $\delta^{13}\text{C}$ excursion. *Geol. Soc. Lond. Spec. Publ.* 26, 371–399.
- Schneider-Mor, A., Alsenz, H., Ashkenazi-Polivoda, S., Illner, P., Abramovich, S., Feinstein, S., Almogi-Labin, A., Berner, Z., Püttmann, W., 2012. Paleocyanographic reconstruction of the late Cretaceous oil shale of the Negev, Israel: integration of geochemical, and stable isotope records of the organic matter. *Palaeogeogr. Palaeoclimatol. Palaeoecol.* 319, 46–57.
- Schouten, S., Hopmans, E.C., Schefuß, E., Sinninghe Damsté, J.S., 2002. Distributional variations in marine crenarchaeal membrane lipids: a new tool for reconstructing ancient sea water temperatures? *Earth Planet. Sci. Lett.* 204, 265–274.
- Schouten, S., Hopmans, E.C., Forster, A., van Breugel, Y., Kuypers, M.M., Sinninghe Damsté, J.S., 2003. Extremely high sea-surface temperatures at low latitudes during the middle Cretaceous as revealed by archaeal membrane lipids. *Geology* 31, 1069–1072.
- Schouten, S., Hopmans, E.C., Sinninghe Damsté, J.S., 2004. The effect of maturity and depositional redox conditions on archaeal tetraether lipid palaeothermometry. *Org. Geochem.* 35, 567–571.
- Schouten, S., Forster, A., Panoto, F.E., Sinninghe Damsté, J.S., 2007. Towards calibration of the TEX₈₆ palaeothermometer for tropical sea surface temperatures in ancient greenhouse worlds. *Org. Geochem.* 38, 1537–1546.
- Schouten, S., Hopmans, E.C., van der Meer, J., Mets, A., Bard, E., Bianchi, T.S., Diefendorf, A., Escala, M., Freeman, K.H., Furukawa, Y., 2009. An interlaboratory study of TEX₈₆ and BIT analysis using high-performance liquid chromatography–mass spectrometry. An interlaboratory study of TEX₈₆ and BIT analysis using high-performance liquid chromatography–mass spectrometry. *Geochim. Geophys. Geosyst.* 10, Q03012. <http://dx.doi.org/10.1029/2008GC002221>.
- Schouten, S., Hopmans, E.C., Rosell-Melé, A., Pearson, A., Adam, P., Bauersachs, T., Bard, E., Bernasconi, S.M., Bianchi, T.S., Brooks, J.J., 2013a. An interlaboratory study of TEX₈₆ and BIT analysis of sediments, extracts, and standard mixtures. *Geochim. Geophys. Geosyst.* 14, 5263–5285.
- Schouten, S., Hopmans, E.C., Sinninghe Damsté, J.S., 2013b. The organic geochemistry of glycerol dialkyl glycerol tetraether lipids: a review. *Org. Geochem.* 54, 19–61.
- Schrag, D.P., Depaolo, D.J., Richter, F.M., 1995. Reconstructing past sea surface temperatures: correcting for diagenesis of bulk marine carbonate. *Geochim. Cosmochim. Acta* 59, 2265–2278.
- Scotese, C.R., 2004. A continental drift flipbook. *J. Geol.* 112, 729–741.
- Seki, O., Schmidt, D.N., Schouten, S., Hopmans, E.C., Sinninghe Damsté, J.S., Pancost, R.D., 2012. Paleocyanographic changes in the eastern equatorial Pacific over the last 10 Myr. *Paleoceanography* 27, PA3224. <http://dx.doi.org/10.1029/2011PA002158>.
- Sellwood, B.W., Price, G.D., Valdes, P.J., 1994. Cooler estimates of Cretaceous temperatures. *Nature* 370, 453–455.
- Sexton, P.F., Wilson, P.A., Pearson, P.N., 2006. Microstructural and geochemical perspectives on planktic foraminiferal preservation: “glassy” versus “frosty”. *Geochim. Geophys. Geosyst.* 7, Q12P19. <http://dx.doi.org/10.1029/2006GC001291>.
- Shackleton, N.J., Kennett, J.P., 1975. Paleotemperature history of the Cenozoic and the initiation of Antarctic glaciation: oxygen and carbon isotope analyses in DSDP Sites 277, 279, and 281. Initial Rep. Deep Sea Drill. Proj. 29, 743–755.
- Shipboard Science Party, 1998. In: Norris, R.D., Kroon, D., Klaus, A., et al. (Eds.), 171B: Site 1049. Proc. ODP, Init. Repts. Ocean Drilling Program, College Station, TX, pp. 47–92. <http://dx.doi.org/10.2973/odp.proc.ir.171B.103.1998>.
- Shipboard Scientific Party, 2004. In: Erbacher, J., Mosher, D.C., Malone, M.J., Al, E. (Eds.), Site 1257. Proc. ODP, Init. Repts. Ocean Drilling Program, College Station, TX, pp. 1–111. <http://dx.doi.org/10.2973/odp.proc.ir.207.104.2004>.
- Sinninghe Damsté, J.S., Kuypers, M.M., Pancost, R.D., Schouten, S., 2008. The carbon isotopic response of algae, (cyano)bacteria, archaea and higher plants to the late Cenomanian perturbation of the global carbon cycle: insights from biomarkers in black shales from the Cape Verde Basin (DSDP Site 367). *Org. Geochem.* 39, 1703–1718.
- Sinninghe Damsté, J.S., van Bentum, E.C., Reichart, G.-J., Pross, J., Schouten, S., 2010. A CO₂ decrease-driven cooling and increased latitudinal temperature gradient during the mid-Cretaceous oceanic anoxic event 2. *Earth Planet. Sci. Lett.* 293, 97–103.
- Sinninghe Damsté, J.S., Schouten, S., Verschuren, D., 2012. Distribution of tetraether lipids in the 25-ka sedimentary record of Lake Challa: extracting reliable TEX₈₆ and MBT/CBT palaeotemperatures from an equatorial African lake. *Quat. Sci. Rev.* 50, 43–54.
- Sloan, L.C., Pollard, D., 1998. Polar stratospheric clouds: a high latitude warming mechanism in an ancient greenhouse world. *Geophys. Res. Lett.* 25, 3517–3520.
- Sluijs, A., van Rooij, L., Harrington, G., Schouten, S., Sessa, J., Levay, L., Reichart, G.-J., Slomp, C., 2014. Warming, euxinia and sea level rise during the Paleocene–Eocene Thermal Maximum on the Gulf Coastal Plain: implications for ocean oxygenation and nutrient cycling. *Clim. Past* 10, 1421–1439.
- Speelmann, E.N., Sewall, J.O., Noone, D., Huber, M., Von Der Heydt, A., Sinninghe Damsté, J.S., Reichart, G.-J., 2010. Modeling the influence of a reduced equator-to-pole sea surface temperature gradient on the distribution of water isotopes in the Early/

- Middle Eocene. *Earth Planet. Sci. Lett.* 298, 57–65.
- Spencer, C., Kim, S.-T., 2015. Carbonate clumped isotope paleothermometry: a review of recent advances in CO₂ gas evolution, purification, measurement and standardization techniques. *Geosci. J.* 19, 357–374.
- Spero, H.J., Bijma, J., Lea, D.W., Bemis, B.E., 1997. Effect of seawater carbonate concentration on foraminiferal carbon and oxygen isotopes. *Nature* 390, 497–500.
- Stoll, H.M., Schrag, D.P., 1996. Evidence for glacial control of rapid sea level changes in the Early Cretaceous. *Science* 272, 1771.
- Stoll, H.M., Schrag, D.P., 2000. High-resolution stable isotope records from the Upper Cretaceous rocks of Italy and Spain: glacial episodes in a greenhouse planet? *Geol. Soc. Am. Bull.* 112, 308–319.
- Tabor, C.R., Poulsen, C.J., Lunt, D.J., Rosenbloom, N.A., Otto-Bliesner, B.L., Markwick, P.J., Brady, E.C., Farnsworth, A., Feng, R., 2016. The cause of Late Cretaceous cooling: a multimodel-proxy comparison. *Geology* 44, 963–966.
- Tarduno, J., Brinkman, D., Renne, P., Cottrell, R., Scher, H., Castillo, P., 1998. Evidence for extreme climatic warmth from Late Cretaceous Arctic vertebrates. *Science* 282, 2241–2243.
- Taylor, K.W., Huber, M., Hollis, C.J., Hernandez-Sanchez, M.T., Pancost, R.D., 2013. Re-evaluating modern and Palaeogene GDGT distributions: implications for SST reconstructions. *Glob. Planet. Chang.* 108, 158–174.
- Teichert, B., Luppold, F., 2013. Glendonites from an Early Jurassic methane seep—climate or methane indicators? *Palaeogeogr. Palaeoclimatol. Palaeoecol.* 390, 81–93.
- Tierney, J., 2014. Biomarker-based inferences of past climate: the TEX₈₆ paleo-temperature proxy. *Treatise Geochem.* 12, 379–393.
- Tierney, J.E., Tingley, M.P., 2014. A Bayesian, spatially-varying calibration model for the TEX₈₆ proxy. *Geochim. Cosmochim. Acta* 127, 83–106.
- Tierney, J.E., Tingley, M.P., 2015. A TEX₈₆ surface sediment database and extended Bayesian calibration. *Sci. Data* 2, 150029. <http://dx.doi.org/10.1038/sdata.2015.29>.
- Tierney, J.E., Sinninghe Damsté, J.S., Pancost, R.D., Sluijs, A., Zachos, J.C., 2017. Eocene temperature gradients. *Nat. Geosci.* 10, 538–539.
- Trommer, G., Siccha, M., van der Meer, M.T., Schouten, S., Sinninghe Damsté, J.S., Schulz, H., Hemleben, C., Kucera, M., 2009. Distribution of Crenarchaeota tetraether membrane lipids in surface sediments from the Red Sea. *Org. Geochem.* 40, 724–731.
- Tyrell, T., Zeebe, R.E., 2004. History of carbonate ion concentration over the last 100 million years. *Geochim. Cosmochim. Acta* 68, 3521–3530.
- Uchikawa, J., Zeebe, R.E., 2010. Examining possible effects of seawater pH decline on foraminiferal stable isotopes during the Paleocene-Eocene thermal maximum. *Paleoceanography* 25, PA2216. <http://dx.doi.org/10.1029/2009PA001864>.
- Ufnar, D., González, L., Ludvigson, G., Brenner, R., Witzke, B., 2004. Evidence for increased latent heat transport during the Cretaceous (Albian) greenhouse warming. *Geology* 32, 1049–1052.
- Upchurch, G.R., Kiehl, J., Shields, C., Scherer, C., 2015. Latitudinal temperature gradients and high-latitude temperatures during the latest Cretaceous: congruence of geologic data and climate models. *Geology* 43, 683–686.
- Vellekoop, J., Sluijs, A., Smit, J., Schouten, S., Weijers, J.W.H., Sinninghe Damsté, J.S., Brinkhuis, H., 2014. Rapid short-term cooling following the Chicxulub impact at the Cretaceous–Paleogene boundary. *Proc. Natl. Acad. Sci.* 111, 7537–7541.
- Vellekoop, J., Esmeray-Senlet, S., Miller, K.G., Browning, J.V., Sluijs, A., van de Schootbrugge, B., Sinninghe Damsté, J.S., Brinkhuis, H., 2016. Evidence for Cretaceous–Paleogene boundary bolide “impact winter” conditions from New Jersey, USA. *Geology* 44, 619–622.
- Villanueva, L., Schouten, S., Sinninghe Damsté, J.S., 2014. Depth-related distribution of a key gene of the tetraether lipid biosynthetic pathway in marine Thaumarchaeota. *Environ. Microbiol.* 12, 438–448.
- Voigt, S., Gale, A.S., Flögel, S., 2004. Midlatitude shelf seas in the Cenomanian–Turonian greenhouse world: temperature evolution and North Atlantic circulation. *Paleoceanography* 19, PA4020. <http://dx.doi.org/10.1029/2004PA001015>.
- Voigt, S., Jung, C., Friedrich, O., Frank, M., Teschner, C., Hoffmann, J., 2013. Tectonically restricted deep-ocean circulation at the end of the Cretaceous greenhouse. *Earth Planet. Sci. Lett.* 369, 169–177.
- Wagner, T., Pletsch, T., 1999. Tectono-sedimentary controls on Cretaceous black shale deposition along the opening Equatorial Atlantic Gateway (ODP Leg 159). In: Cameron, N.R., Bate, R.H., Clure, V.S. (Eds.), *The Oil and Gas Habitats of the South Atlantic*. Geological Society, London, Special Publications Vol. 153. pp. 241–265.
- Wagner, T., Herrle, J.O., Sinninghe Damsté, J.S., Schouten, S., Stüßler, I., Hofmann, P., 2008. Rapid warming and salinity changes of Cretaceous surface waters in the sub-tropical North Atlantic. *Geology* 36, 203–206.
- Wakeham, S.G., Lewis, C.M., Hopmans, E.C., Schouten, S., Sinninghe Damsté, J.S., 2003. Archaea mediate anaerobic oxidation of methane in deep euxinic waters of the Black Sea. *Geochim. Cosmochim. Acta* 67, 1359–1374.
- Wang, Y., Huang, C., Sun, B., Quan, C., Wu, J., Lin, Z., 2014. Paleo-CO₂ variation trends and the Cretaceous greenhouse climate. *Earth Sci. Rev.* 129, 136–147.
- Weijers, J.W.H., Schouten, S., Spaargaren, O.C., Sinninghe Damsté, J.S., 2006. Occurrence and distribution of tetraether membrane lipids in soils: implications for the use of the TEX₈₆ proxy and the BIT index. *Org. Geochem.* 37, 1680–1693.
- Weijers, J.W.H., Lim, K.L.H., Aquilina, A., Sinninghe Damsté, J.S., Pancost, R.D., 2011. Biogeochemical controls on glycerol dialkyl glycerol tetraether lipid distributions in sediments characterized by diffusive methane flux. *Geochim. Geophys. Geosyst.* 12, Q10010. <http://dx.doi.org/10.1029/2011GC003724>.
- Wilf, P., Johnson, K.R., Huber, B.T., 2003. Correlated terrestrial and marine evidence for global climate changes before mass extinction at the Cretaceous–Paleogene boundary. *Proc. Natl. Acad. Sci.* 100, 599–604.
- Wilson, P.A., Norris, R.D., 2001. Warm tropical ocean surface and global anoxia during the mid-Cretaceous period. *Nature* 412, 425–429.
- Wilson, P.A., Opdyke, B.N., 1996. Equatorial sea-surface temperatures for the Maastrichtian revealed through remarkable preservation of metastable carbonate. *Geology* 24, 555–558.
- Wilson, P.A., Norris, R.D., Cooper, M.J., 2002. Testing the Cretaceous greenhouse hypothesis using glassy foraminiferal calcite from the core of the Turonian tropics on Demerara Rise. *Geology* 30, 607–610.
- Wolf, J.A., 1990. Palaeobotanical evidence for a marked temperature increase following the Cretaceous/Tertiary boundary. *Nature* 343, 153–156.
- Wuchter, C., Schouten, S., Coolen, M.J.L., Sinninghe Damsté, J.S., 2004. Temperature-dependent variation in the distribution of tetraether membrane lipids of marine Crenarchaeota: implications for TEX₈₆ paleothermometry. *Paleoceanography* 19, PA4028. <http://dx.doi.org/10.1029/2004PA001041>.
- Wuchter, C., Schouten, S., Wakeham, S.G., Sinninghe Damsté, J.S., 2005. Temporal and spatial variation in tetraether membrane lipids of marine Crenarchaeota in particulate organic matter: implications for TEX₈₆ paleothermometry. *Paleoceanography* 20, PA3013. <http://dx.doi.org/10.1029/2004PA001110>.
- Yang, W.-B., Niu, H.-C., Sun, W.-D., Shan, Q., Zheng, Y.-F., Li, N.-B., Li, C.-Y., Arndt, N.T., Xu, X., Jiang, Y.-H., 2013. Isotopic evidence for continental ice sheet in mid-latitude region in the supergreenhouse Early Cretaceous. *Sci Rep* 3, 2732. <http://dx.doi.org/10.1038/srep02732>.
- Zachos, J.C., Stott, L.D., Lohmann, K.C., 1994. Evolution of early Cenozoic marine temperatures. *Paleoceanography* 9, 353–387.
- Zachos, J.C., Schouten, S., Bohaty, S., Quattlebaum, T., Sluijs, A., Brinkhuis, H., Gibbs, S., Bralower, T., 2006. Extreme warming of mid-latitude coastal ocean during the Paleocene-Eocene Thermal Maximum: inferences from TEX₈₆ and isotope data. *Geology* 34, 737–740.
- Zeebe, R.E., 1999. An explanation of the effect of seawater carbonate concentration on foraminiferal oxygen isotopes. *Geochim. Cosmochim. Acta* 63, 2001–2007.
- Zeebe, R.E., 2001. Seawater pH and isotopic paleotemperatures of Cretaceous oceans. *Palaeogeogr. Palaeoclimatol. Palaeoecol.* 170, 49–57.
- Zhang, Y.G., Zhang, C.L., Liu, X.-L., Li, L., Hinrichs, K.-U., Noakes, J.E., 2011. Methane index: a tetraether archaeal lipid biomarker indicator for detecting the instability of marine gas hydrates. *Earth Planet. Sci. Lett.* 307, 525–534.
- Zhang, Y.G., Pagani, M., Wang, Z., 2016. Ring index: a new strategy to evaluate the integrity of TEX₈₆ paleothermometry. *Paleoceanography* 31, 220–232. <http://dx.doi.org/10.1002/2015PA002848>.
- Zheng, X.-Y., Jenkyns, H.C., Gale, A.S., Ward, D.J., Henderson, G.M., 2013. Changing ocean circulation and hydrothermal inputs during Ocean Anoxic Event 2 (Cenomanian–Turonian): evidence from Nd-isotopes in the European shelf sea. *Earth Planet. Sci. Lett.* 375, 338–348.
- Zhou, J., Poulsen, C.J., Pollard, D., White, T.S., 2008. Simulation of modern and middle Cretaceous marine ⁸¹⁸O with an ocean-atmosphere general circulation model. *Paleoceanography* 23, PA3223. <http://dx.doi.org/10.1029/2008PA001596>.
- Zhou, J., Poulsen, C., Rosenbloom, N., Shields, C., Briegleb, B., 2012. Vegetation-climate interactions in the warm mid-Cretaceous. *Clim. Past* 8, 565–576.